# UNIVERSITY OF CALIFORNIA, SAN DIEGO

Generation, coordination, and re-afferent signaling of
rhythmic whisking in rodents

A dissertation submitted in partial satisfaction of the requirements for the
degree Doctor of Philosophy
in
Neurosciences, Specialization in Computational Neuroscience

by

Jeffrey D. Moore

Committee in charge:

Professor David Kleinfeld, Chair
Professor Sascha du Lac
Professor Harvey J. Karten
Professor Takaki Komiyama
Professor William B. Kristan

2013

The Dissertation of Jeffrey D. Moore is approved, and it is acceptable in quality and form for publication on microfilm and electronically:

_____

_____

_____

_____

_____

Chair

University of California, San Diego

2013

# Table of Contents

# List of Figures

# Acknowledgements

I would first like to thank the members of my thesis committee, Profs. Sascha du Lac, Harvey Karten, Takaki Komiyama, and William B. Kristan, as well as outside collaborators, Profs. Fan Wang (Duke) and Jack Feldman (UCLA), for their excellent advice, guidance, and generous contributions of laboratory resources in support of this dissertation. I would also like to thank my colleagues in the Kleinfeld lab for their technical assistance and for discussions that contributed to the dissertation, in particular Drs. Daniel N. Hill, David W. Matthews, Patrick J. Drew, and the late Dr. John C. Curtis.

I would especially like to thank my thesis advisor, supervisor, and mentor, Prof. David Kleinfeld, for his continued dedication and support. Throughout the course of my graduate career he has always gone above and beyond his role as an advisor and worked tirelessly to ensure that I had the resources I needed, and to promote a rigorous scholarly atmosphere for everything we do as scientists. Beyond excellent technical training in neuroscience, he continues to teach me how to be an effective and engaged member of the scientific community.

Finally I would like to thank my close collaborator, mentor, and role model, Prof. Martin Deschênes (Laval), for all the time he spent teaching me

and working with me, as well as for his contribution of laboratory resources. This work would not have been possible without his guidance, insight, and expertise in experimental technique. I am grateful for the many months he spent as a sabbatical visitor in our laboratory, imparting many years of experience and wisdom each winter. I admire his dedication to working directly at the laboratory bench, his close attention to detail, as well as his ability to foresee the most critically relevant and tractable scientific questions. I am very lucky to have had the opportunity to work with him.

Chapters 2 and 3 of this dissertation follow from work that is currently published in:

Deschênes M, Moore JD, Kleinfeld D. Sniffing and whisking in rodents. Current Opinion in Neurobiology. 22(2): 243-250 (2012)

Moore JD*, Deschênes M*, Furuta T, Huber D, Smear MC, Demers M, Kleinfeld D.Hierarchy of orofaical rhythms revealed through whisking and breathing. Nature. 497(7448): 205-210 (2013)

This material is included with the generous consent of all authors and permission of the journals. The content of chapter 4 is a manuscript that is currently in preparation for submission and will include Profs. Martin Deschênes and David Kleinfeld as authors. I am a primary researcher on these works, and I am grateful for the contributions of all of the aforementioned authors.

# Vita

2013 Ph.D., Neurosciences, Specialization in Computational Neuroscience, University of California, San Diego

2007 Sc.B. Electrical Science and Engineering, Massachusetts Institute of Technology

2007 Sc.B. Brain and Cognitive Sciences, Massachusetts Institute of Technology

2006 Summer Associate, Cardiac Rhythm Management Division, Medtronic Inc.

2005 Summer Undergraduate Research Fellow, Bio-Inspired Technologies, Jet Propulsion Laboratory

## Publications


Moore, J. D.*, Deschênes, M.*, Furuta, T., Huber, D., Smear, M. C., Demers, M., & Kleinfeld, D. (2013). Hierarchy of orofacial rhythms revealed through whisking and breathing. *Nature*, *497*(7448), 205-210.

Deschênes, M., Moore, J., & Kleinfeld, D. (2012). Sniffing and whisking in rodents. *Current opinion in neurobiology*, *22*(2), 243-250.

Hill, D. N., Curtis, J. C., Moore, J. D., & Kleinfeld, D. (2011). Primary motor cortex reports efferent control of vibrissa motion on multiple timescales. *Neuron*,*72*(2), 344-356.


## Awards

2013 UCSD Leon Thal Award for Graduate Research
2009 NIH / NRSA Individual Predoctoral Fellowship
2007 MIT Hans-Lukas Teuber Award for Academic Achievement
2007 Phi Beta Kappa
2006 MIT MASLab Robotics Contest – 1st Place
2006 Tau Beta Pi Engineering Honor Society
2006 Eta Kappa Nu EECS Honor Society

# ABSTRACT OF THE DISSERTATION

Generation, coordination, and re-afferent signaling of
rhythmic whisking in rodents

by

Jeffrey D. Moore

Doctor of Philosophy in Neurosciences,

Specialization in Computational Neuroscience

University of California, San Diego, 2013

Professor David Kleinfeld, Chair

Exploratory “whisking” is a rhythmic motor activity that enables rodents to locate objects in their environment through physical contact with their mystacial vibrissae. How the nervous system generates this rhythmic movement, and how the resulting movement enables these animals to determine the position of objects remain unknown. There are ethological similarities between whisking and sniffing, which may suggest that these two exploratory activities have related underlying neural control circuits. We discuss the similar dynamics of these two active sensory behaviors, and how they shape their respective sensory inputs. We demonstrate that the motor patterns for these behaviors are coordinated by respiratory centers in the

ventral medulla. Specifically, we identify a region in the ventral medulla that provides rhythmic input to the facial motoneurons to drive coordinated vibrissa protraction, and we show that this region is under direct control of the respiratory patterning circuitry. Because vibrissa-based object localization may require sensory signals of this self-generated movement, we consider the representation of whisking in the brainstem trigeminal sensory nuclei and their respective target thalamic nuclei. Specifically, there are two major parallel anatomical pathways from these nuclei to primary somatosensory cortex. We demonstrate that a single pathway simultaneously conveys sensory signals of whisking and touch. Neurons in this pathway are diversely tuned to these two sources of sensory input.

# Chapter 1 – Introduction

Biological sensors in animals are typically under active motor control, and perception of objects in the world therefore depends on self-generated movement. Descartes realized this, and provided as an example the case of a blind man walking with sticks (Descartes, 1637). In reference to an accompanying diagram (**Fig 1.1**), he writes:

> …when the blind man… turns his hand A towards E, or again his hand C towards E, the nerves embedded in that hand cause a certain change in his brain, and through this change his soul can know not only the place A or C but also all the other places located on the straight line AE or CE; in this way his soul can turn its attention to the objects B and D, and determine the places they occupy without in any way knowing or thinking of those which his hands occupy. Similarly, when our eye or head is turned in some direction, our soul is informed of this by the change in the brain which is caused by the nerves embedded in the muscles used for these movements.

Like the sticks in Descartes' example, rodents and other mammals are endowed with exquisite arrays of sinus hairs, or vibrissae, which transduce tactile stimuli through mechanoreceptors in their follicles (**Fig 1.2**) (Rice et al., 1993; Vincent, 1913). In rodents the mystacial pad on the snout, which houses the vibrissae, contains specialized muscles that allow them to control these tactile sensors (**Fig 1.3**) (Dorfl, 1982). In a behavior known as "whisking", rodents generate a rhythmic sweeping motion of the vibrissae in order to scan their immediate surroundings for tactile sensory information (Welker, 1964). These are some of the fastest movements made by

mammals (Jin et al., 2004) and constitute a prominent exploratory activity among species that whisk. Despite substantial efforts to determine the neurophysiological underpinnings and neuroanatomical architecture of vibrissa-based tactile sensation (Bosman et al., 2011; Kleinfeld and Deschênes, 2011), our understanding of how the central nervous system generates rhythmic whisking has been limited. Initial observations that whisking seemed to be related to another prominent active exploratory activity, sniffing (Welker, 1964), have been quantified only very recently (Cao et al., 2012; Deschênes et al., 2012; Lu et al., 2013; Moore et al., 2013; Ranade et al., 2013).

The relationship between sniffing and whisking, as well as the associated olfactory and tactile sensory perceptions that they produce in the nervous system, are reviewed in Chapter 2. The coordination of these active sensory behaviors and their shared motor plant suggest the possibility that their underlying neural patterning circuits are linked. Chapter 3 presents evidence of a central pattern generator for whisking, located in the ventral portion of the intermediate reticular formation of the medulla, that is under the direct control of a separate pattern generator for breathing. This hierarchical control structure coordinates the muscles used for protraction of the vibrissae, which are controlled by the whisking oscillator, with the muscles used for retraction of the vibrissae and dilation of the naris during breathing. More

generally, this work may bear on the nature of coordination among other rhythmic orofacial behaviors, such as chewing, licking/lapping, and suckling, all of which are central to mammalian life. The work further provides evidence for the primacy of the breathing rhythm in orofacial control.

With the knowledge of how rhythmic whisking is generated and coordinated within the brainstem, we return in Chapter 4 to Descartes' problem of how the nervous system can compute the locations of objects in the external world based on inputs from mobile sensors. The problem was later formalized by von Holst, who pointed out that the same physical sensors could be activated both by stimuli in the outside world, which he termed "ex-afference", as well as by self-generated movement, which he termed "re-afference" (von Holst, 1954). In von Holst's formulation, the re-afferent signal could be precisely cancelled out by a copy of the centrally generated motor command, which he called an "efference copy", if the movement were executed as planned (**Fig 1.4**). In Chapter 4 we examine the potential roles of interacting ex-afferent and re-afferent signals in vibrissa-based object localization.

Much is known about the architecture and connectivity of sensory brain regions that process inputs from the vibrissa follicle (Bosman et al., 2011; Deschenes and Urbain, 2009; Lefort et al., 2009), and various neuronal

computations could determine the position of an external object relative to the face. Some recently proposed hypotheses make use of a re-afferent signal related to vibrissa position during whisking (Curtis and Kleinfeld, 2009; Kleinfeld and Deschênes, 2011; Szwed et al., 2003), while others emphasize the role of efference copy signals and an adaptive motor strategy (O'Connor et al., 2010a; O'Connor et al., 2013; Petreanu et al., 2012). In Chapter 4 we constrain the possible mechanisms for how the vibrissa system computes object location, by measuring and comparing the nature of whisking re-afferent signals in somatosensory regions of the brainstem and thalamus with established connectivity patterns. Our results suggest a mixed representation of re-afferent and ex-afferent signals along a single anatomical pathway. Neurons in this pathway have the highest acuity ex-afferent signals of touch as well as diversely tuned re-afferent signals of whisking, and are likely the source of related signals in primary somatosensory cortex. We discuss the implications of this finding with respect to object localization.

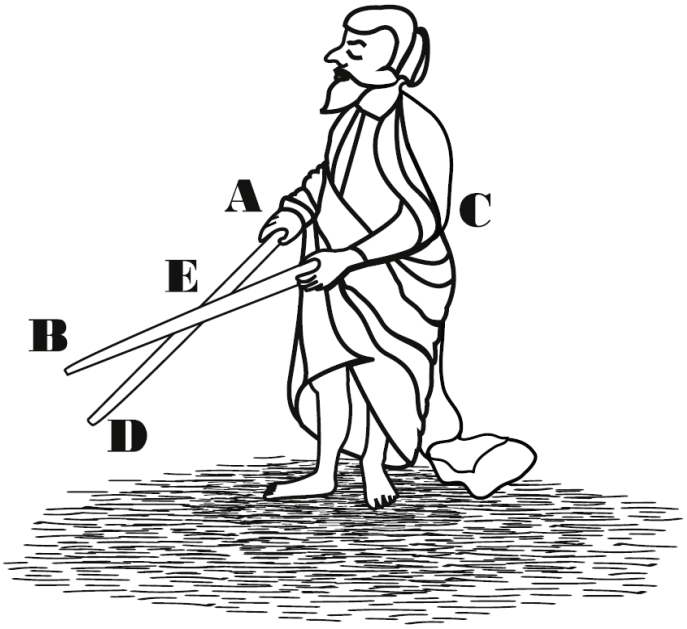


**Figure 1.1. Descartes' blind man walking with sticks**

Points A-E are described in the text. From (Descartes, 1637). Adapted from (Kleinfeld and Deschênes, 2011).

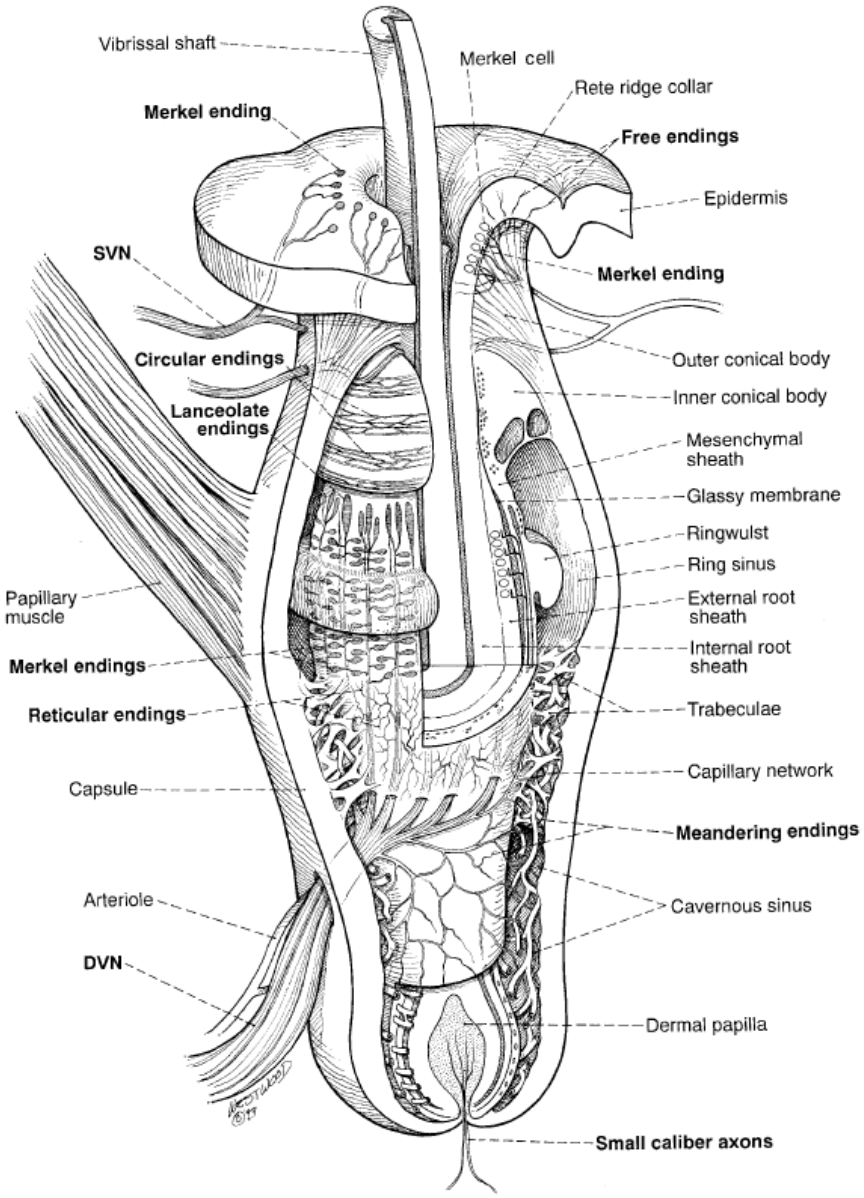


**Figure 1.2. The vibrissa follicle**

Sensory endings (bold) with different types of mechanoreceptors innervate the follicle, and include merkel cells, lanceolate endings, and free endings. The superficial vibrissal nerves (SVN) and deep vibrissal nerves (DVN) merge with the infraorbital branch of the trigeminal nerve. Adapted from (Rice et al., 1993).

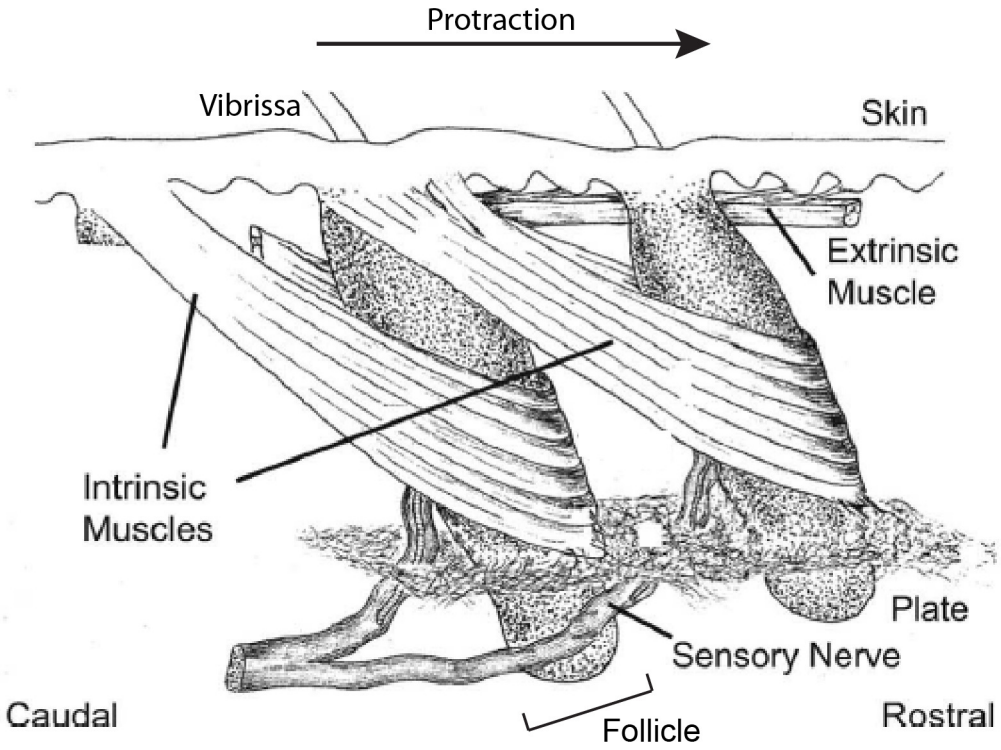


**Figure 1.3. The vibrissa musculature**

"Intrinsic" papillary muscles wrap around each individual follicle. Their contraction protracts the vibrissa. Additional "extrinsic" muscles are responsible for both protraction and retraction of the mystacial pad (Dorfl, 1982; Haidarliu et al., 2010; Hill et al., 2008). Adapted from (Dorfl, 1982).

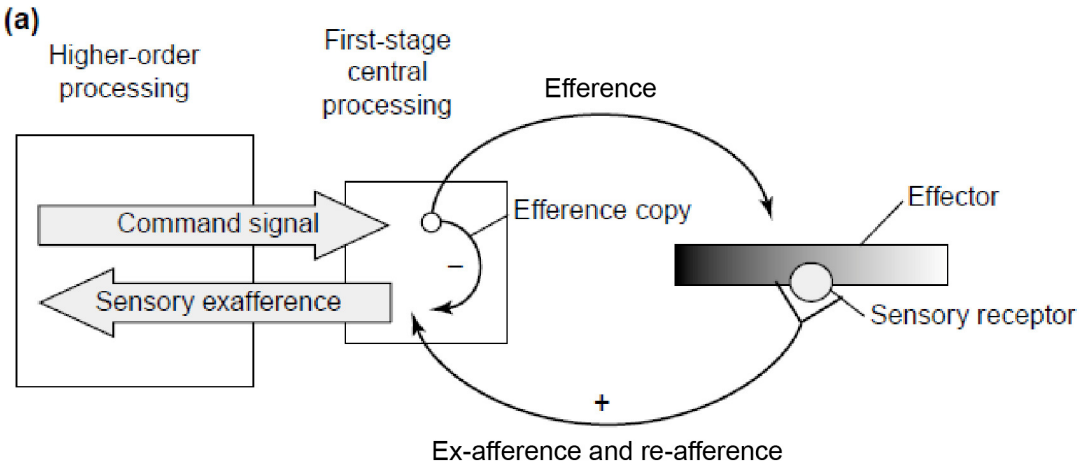


**Figure 1.4. The re-afference principle**

A motor command signal (efference) triggers the movement of an effector, which results in a signal originating from a sensory receptor in the effector (re-afference) that is combined with stimuli from the external world (ex-afference). A copy of the command signal (efference copy) is subtracted from the re-afferent signal, and the resulting ex-afferent signal is transmitted to higher-order central nervous structures. From (von Holst and Mittelstaedt, 1950). Adapted from (Cullen, 2004).

# Chapter 2 – Sniffing and whisking in rodents

Sniffing and whisking are two rhythmic orofacial motor activities that enable rodents to localize and track objects in their environment. They have related temporal dynamics, possibly as a result of both shared musculature and shared sensory tasks. Sniffing and whisking also constitute the overt expression of an animal's anticipation of a reward. Yet, the neuronal mechanisms that underlie the control of these behaviors have not been established. Here, we review the similarities between sniffing and whisking and suggest that such similarities indicate a mechanistic link between these two rhythmic exploratory behaviors.

## *2.1 Introduction*

When one observes rodents introduced in a new environment, one immediately notices that they are extremely curious (Benjamini et al., 2011). They run about, stand up on their hind legs, crane their necks forward, and repeatedly explore the whole environment by sniffing and whisking vigorously. Psychologists have described curiosity as a drive like hunger and thirst, which implies that gathering information is rewarding. In experimental studies, sniffing and whisking are commonly considered as motor strategies

for rapidly gathering detailed information about the location, texture, and scent of objects. Yet, it is intriguing that decorticated rats, or rats deprived of olfactory and vibrissa afferents, continue to sniff and whisk in a relatively normal manner. Therefore, beyond the obvious intuition that vibrissae are 'for touch' and noses 'for smell', it is not clear why rhythmic activity is associated with the use of these sensors. Here, we examine the dynamics of rhythmic sniffing and whisking, and how they shape olfactory and tactile sensations in rodents. We place special emphasis on the behavioral significance of the apparent coordination of these patterned activities.

## *2.2 A link between sniffing and whisking*

In a now classic paper published in 1964, Welker (Welker, 1964) provided the first descriptive account of the sniffing behavior in rats. Using cinematographic technique, he reported that sniffing consists of an integrated movement sequence involving: (1) bursts of polypnea, (2) recurrent protraction and retraction of mystacial vibrissae, (3) repetitive retraction and protraction of the tip of the snout, and (4) a rapid series of head movements and fixations. These four components occur at rates between 5 and 11 Hz, in bursts of various durations, and "exhibit a fixed temporal relationship to one another" (**Fig. 2.1b**). Welker further made the little noticed remark that

”Polypnea and nose movements together may occur independently of vibrissae and head movements, but rapid vibrissae or head movements were never observed to occur independently of polypnea and nose movements”. In short, Welker noted that whisking was always coupled to sniffing. This temporal relationship is illustrated in **Figure 2.1c,d**, where whisking and sniffing were recorded as a rat explores the exit of a tunnel (**Fig. 2.1a**).

Welker’s seminal observations did not raise immediate interest in the sensorimotor community as the rodent vibrissa (barrel) cortex had yet to be discovered (Woolsey and Van Der Loos, 1970), and most sensorimotor work at that time was focused on primates. Later studies in the field of respiratory physiology alluded to Welker’s findings in reporting instances of facial nerve, muscle, or motoneuron activity that were time-locked to different phases of the respiratory cycle (Huangfu et al., 1993; Hwang and St John, 1988; Sherrey and Megirian, 1977). Interestingly, the nasolabial muscle, which contributes to flare of the naris during sniffing, also acts as a retractor muscle during whisking (Berg and Kleinfeld, 2003; Hill et al., 2008). This dual role suggests an obligate neuromuscular coupling between whisking and sniffing that requires coordinated control to ensure that these behaviors do not interfere with each other.

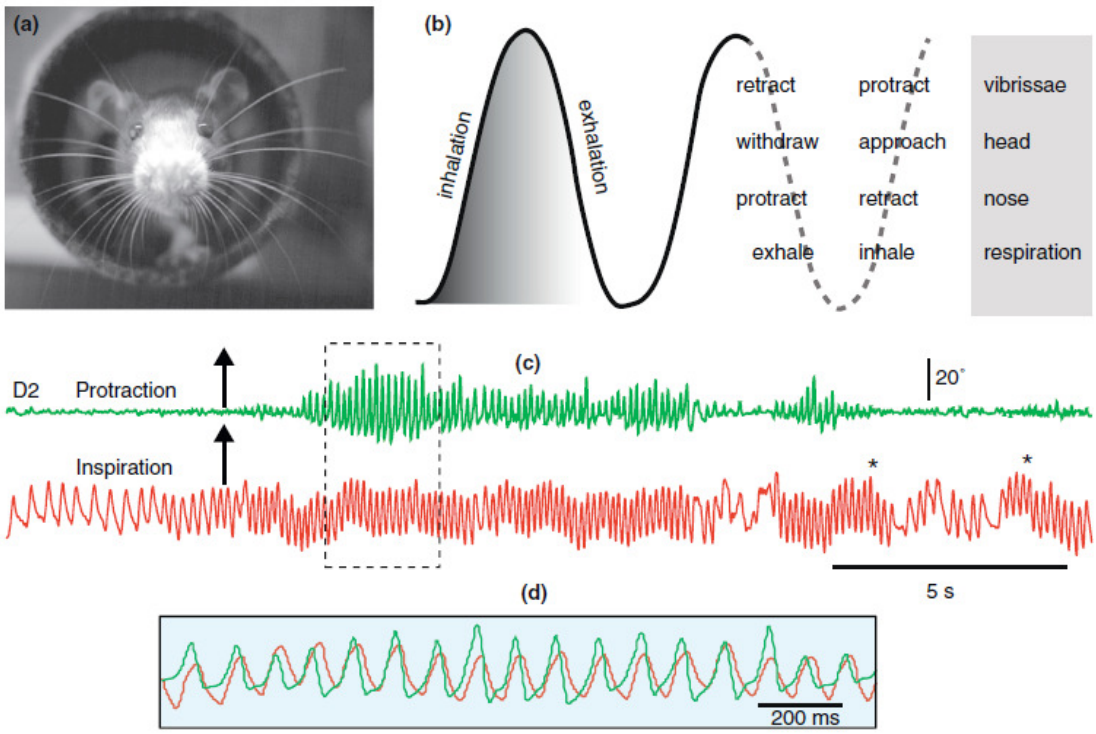


**Figure 2.1. Co-occurrence of sniffing and whisking in rodents.**

**(a)** Photograph of a rat whisking at the exit of a tunnel. Image was obtained in the dark under near infrared illumination. **(b)** Sniff and whisk cycles are coordinated with nose and head movements. Adapted from Welker (Welker, 1964). **(c)** Whisking occurs in phase with sniffing, but sniffing can occur without whisking; asterisks denote sniffing bouts without whisking. Overlapping traces in **(d)** show the framed area in **(c)**. The motion of vibrissa D2 was monitored by high-speed videography (250 frames per second), and sniffing was recorded by means of a thermocouple implanted in the nasal cavity (unpublished data).

## *2.3 Rythmogenesis of sniffing and whisking*

Sniffing in rats is usually defined as rapid, rhythmic respiration (Welker, 1964; Youngentob et al., 1987). Rats, unlike humans, always breathe nasally, so lower frequencies (1-3 Hz) correspond to basal respiration while higher frequencies (4-12 Hz) correspond to "sniffing" *per se*. Although rats and mice are commonly used in studies of respiratory rhythmogenesis, the neural mechanisms underlying the generation of sniffing remain unknown. One possibility is that sniffing relies on an increased rate of bursts in the central pattern generator (CPG) that controls breathing, *e.g.*, the Bötzinger/pre-Bötzinger complex and the parafacial group (Feldman and Del Negro, 2006; Smith et al., 2009). Yet, a mechanism for generating rhythmic sniffing remains to be demonstrated.

As with respiration, it has long been postulated that whisking is driven by a CPG located in the brainstem. This hypothesis is derived from the observation that whisking persists after decortication (Semba and Komisaruk, 1984; Welker, 1964), and that bilateral section of the infraorbital branch of the trigeminal nerve, *i.e.*, sensory denervation, has only little effect on the generation, kinematics, and bilateral coordination of the normal whisking pattern (Berg and Kleinfeld, 2003; Gao et al., 2001; Welker, 1964). Attempts

to identify neurons that form the core of the whisking CPG have so far yielded unconvincing results. Beyond the obvious participation of facial motoneurons as downstream command neurons, the premotor whisking circuitry remains elusive. It has been proposed that facial motoneurons themselves generate whisking in response to modulatory input from serotonergic pre-motoneurons (Hattox et al., 2003). Yet, this hypothesis does not explain the synchrony of motoneuron discharges, nor how different pools of facial motoneurons are activated both bilaterally, and in a multiphasic manner, to generate the protraction/retraction cycle (Berg and Kleinfeld, 2003; Hill et al., 2008). Alternatively, and on the basis of Welker's description of the close phase relationship between sniffing and whisking (Welker, 1964), one might speculate that both rhythmic activities share a common neural circuitry.

## *2.4 The function of the vibrissae in sensation*

It is necessary to first consider the anatomical organization and function of the vibrissa sensorimotor plant itself to understand the behavioral significance of whisking. Rats and mice are nocturnal animals with poor visual acuity. They have laterally-placed eyes, which allows very little overlap of the visual fields. Panoramic vision gives them a wide field of view, which likely helps them detect predators but provides poor depth discrimination. At close range they rely on sniffing and whisking to sense objects and move about,

search for food and shelter, and interact with conspecifics (Wolfe et al., 2011). They are equipped with two sets of vibrissae (**Fig. 2.2**); one set is the large macrovibrissae that form a matrix of approximately 25 motile sensors on each side of the face, while the other is a dense array of shorter vibrissae, or microvibrissae, around the mouth, chin and nose. Each of the macrovibrissae has a corresponding “intrinsic” papillary muscle responsible for the protraction phase of the whisk cycle (Haidarliu et al., 2010). Microvibrissae do not have intrinsic muscles and do not protract, but they are distinguished from the surrounding pelagic fur by a thick shaft that is housed within a follicle-blood sinus complex. The entire mystacial pad, including the microvibrissae, is under active control of three major “extrinsic” muscles that are responsible for pad translation (Haidarliu et al., 2010; Hill et al., 2008).

Though both macro and microvibrissae are capable of detecting tactile features such as texture and shape, there appears to be specialization and complementarity of function. Macrovibrissae serve principally to locate objects in space (**Fig. 2.2c**), whereas the microvibrissa array is primarily used for close examination of shape and surface properties (Brecht et al., 1997) (**Fig. 2.2d**). The functional importance of both sets of vibrissae is reflected by their extensive representation in the primary somatosensory cortical area (**Fig. 2.2b**). However, very little is known about the psychophysics and physiology of tactile sensation mediated by the microvibrissae nor about the

anatomical organization of pathways that convey microvibrissa information from the trigeminus to cortical stations.

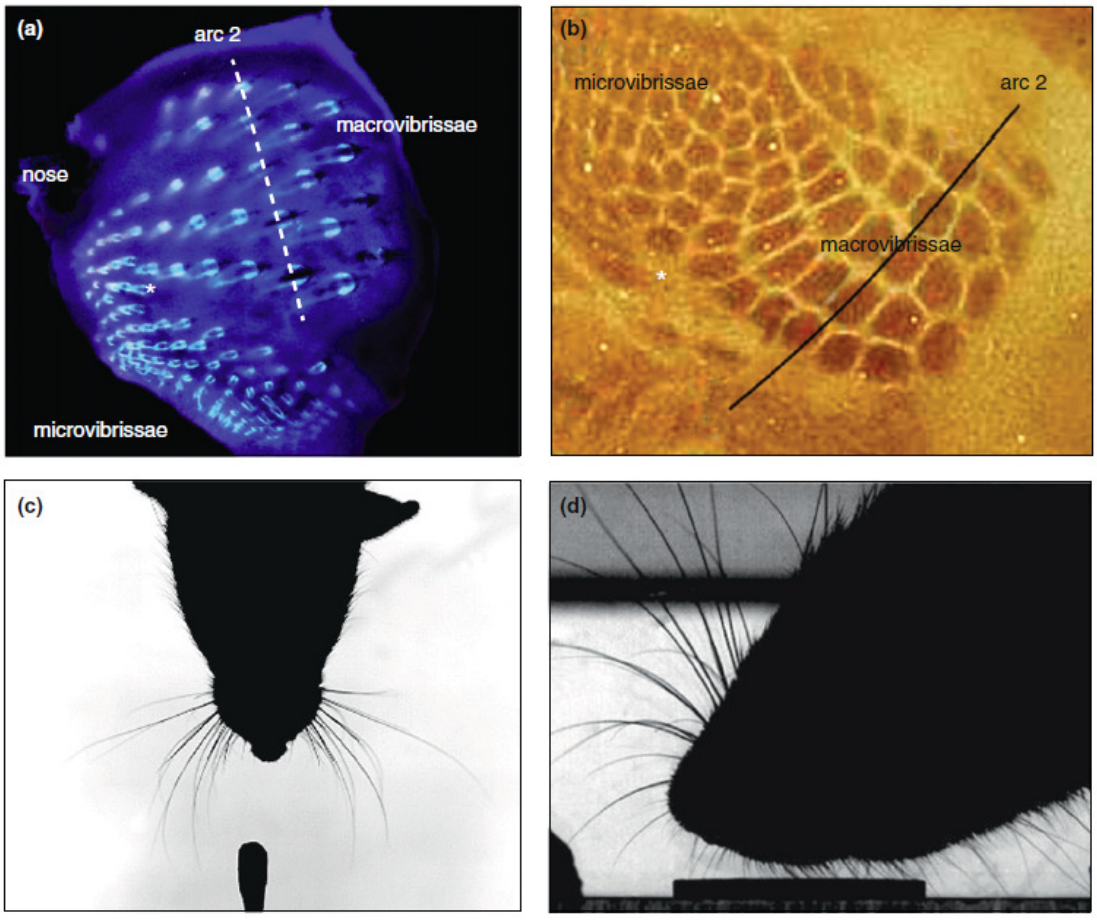


**Figure 2.2. Rodents have two sets of vibrissae.**

**(a)** Vibrissa follicles on the mystacial pad and perioral region. **(b)** The follicles are mapped in a one-to-one manner in layer 4 of the primary somatosensory cortex. Note the presence of small-sized follicles, *i.e.*, microvibrissae, that are represented by smaller sized barrels in cortex. Asterisks indicate the transition point between macro- and microvibrissae and their representation in cortex. **(c)** Photograph of a rat whisking upon presentation of a new odor on the cotton swab in the lower part of the image (unpublished data)**. (d)** Photograph of a rat sampling a coin with its microvibrissae. Adapted from Fox et al. (Fox et al., 2009).

## *2.5 Sniffing and whisking shape sensory inputs*

Sniffing and whisking affect both the encoding and central processing of sensory inputs. Sniffing and whisking *per se*, in the absence of odor or touch, modulate the activity of mitral cells and first-order vibrissa afferents respectively (Cury and Uchida, 2010; Khatri et al., 2009; Leiser and Moxon, 2007; Shusterman et al., 2011) (**Fig. 2.3a**). Though air flow varies in amplitude, velocity and frequency, individual mitral cells preferentially discharge at a specific phase of the sniffing cycle (Shusterman et al., 2011), such that odor evoked responses are normalized to the duration of the sniff cycle (**Fig. 2.3b**). Similarly, there is analogous coding of touch information in terms of normalized parameters of whisking in the vibrissa system, where neuronal activity locks to the phase in the whisk cycle in primary somatosensory cortex (Crochet and Petersen, 2006; Curtis and Kleinfeld, 2009; de Kock and Sakmann, 2009; Fee et al., 1997) (**Fig. 2.3c**). This is thought to provide a phase reference signal for decoding object location independently of the amplitude, midpoint, and frequency of whisking (Curtis and Kleinfeld, 2009; Kleinfeld and Deschênes, 2011). The encoding of sensory inputs in a manner that is pegged to the rhythmic motor control of the sensory organs demonstrates the fundamental link of motor control of behavior to sensation for both somatosensation (Curtis and Kleinfeld, 2009) and olfaction (Smear et al., 2011).

The modulation of touch sensation by motor activity has precedents from other studies as well. Whisking gates touch along afferent pathways of the vibrissa system (Fanselow and Nicolelis, 1999; Ferezou et al., 2006; Hentschke et al., 2006; Lee et al., 2008). The study of Ferezou et al. (Ferezou et al., 2006) is particularly interesting in this regard (**Fig. 2.4**). Using voltage-sensitive dyes in freely moving mice, the authors find that in awake but otherwise sessile mice, an unexpected vibrissa deflection produces a large response in barrel cortex. When the same stimulus is delivered unexpectedly during a whisking bout, the evoked response is markedly attenuated. Finally, 'expected' contact of the vibrissae with an object during exploratory whisking leads to a pronounced cortical response. These results are clear indication that both the state of arousal and the behavioral context impact on the transfer of sensory messages along the vibrissa-to-barrel pathway. The results of anatomical and physiological studies indicate that gating occurs at the first relay station in brainstem, via inhibitory projections from the spinal trigeminal complex to the principal trigeminal nucleus (Furuta et al., 2008; Kleinfeld and Deschênes, 2011). In the olfactory system, however, there is no clear evidence that a central signal related to sniffing gates sensory inputs (Wachowiak, 2011).

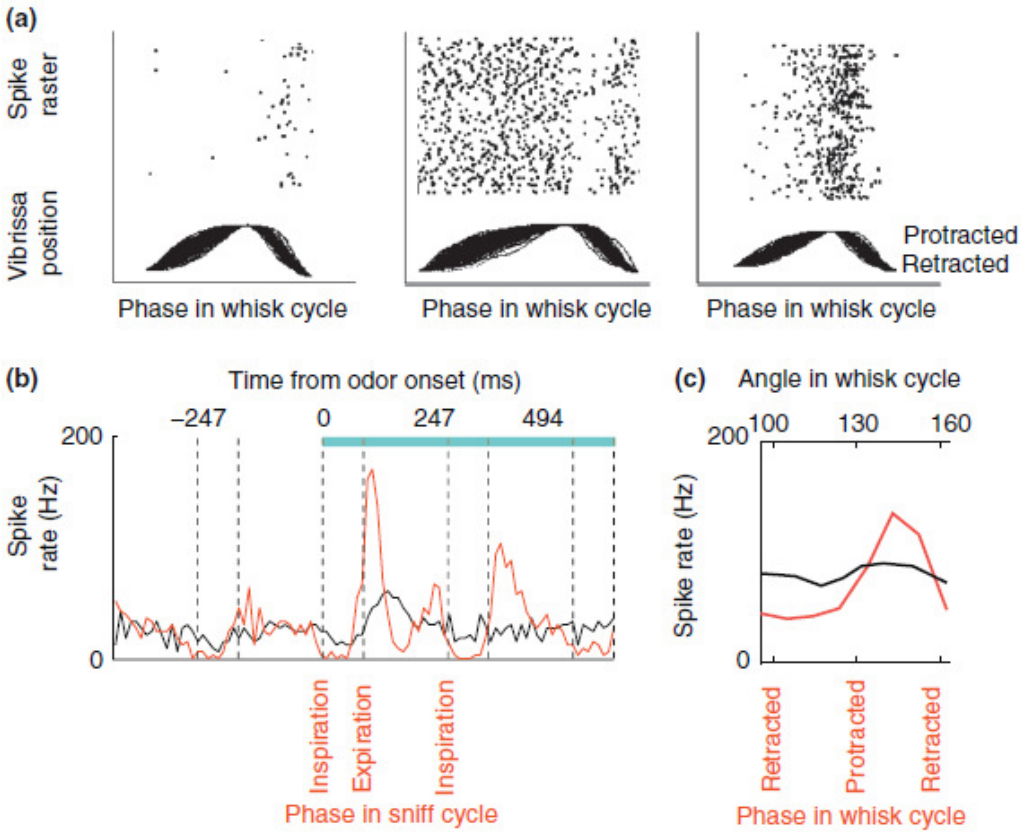


**Figure 2.3. Encoding of odorants and vibrissa contact during the sniffing and whisking cycles.**

**(a)** Whisking solely in air modulates the activity of trigeminal ganglion cells. Unit recordings were obtained from a head-fixed rat together with simultaneous optical tracking of vibrissa position. Vibrissa movements are aligned to protraction onset, retraction onset, and end. Raster plots the spike times above the movements. Adapted from Khatri et al. (Khatri et al., 2009). **(b)** Peristimulus time histograms for a mitral/tufted cell in response to an odor stimulus (blue bar, stimulus duration): synchronized by odor onset (black), and temporally warped to the phase in the sniff cycle (red). Note that mitral cell activity is modulated by sniffing before the odor presentation, and that odor-induced responses are more tightly time-locked to the sniff phase than to the time after odor onset. Vertical dashed lines indicate the beginning and end of inhalation intervals. Adapted from Shusterman et al. (Shusterman et al., 2011). **(c)** Touch response in vibrissa sensory cortex is strongly modulated by the phase in the whisk cycle. The red trace shows the spike rate of a neuron in response to object contact parsed according to the phase in the whisk cycle at which the contact occurred. The black line is the same data parsed according to the angular position of the vibrissa where the contact occurred. Unlike the case for phase, there is no significant tuning for angle. Adapted from Curtis and Kleinfeld (Curtis and Kleinfeld, 2009).

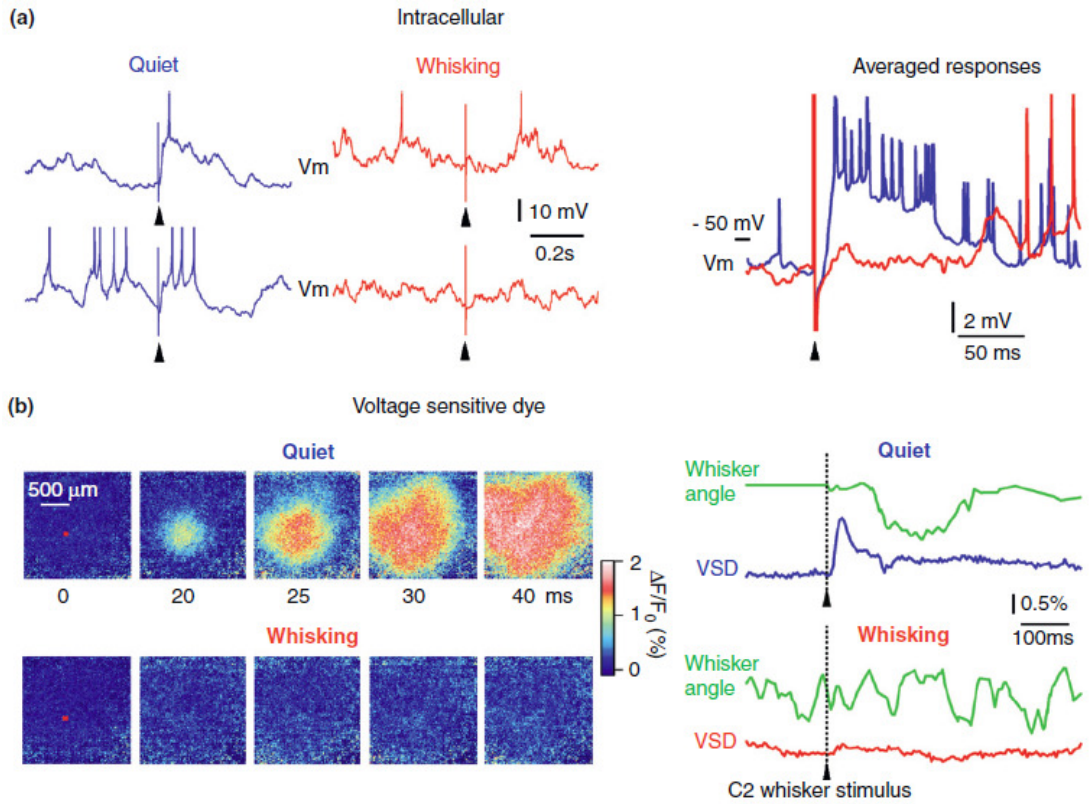


**Figure 2.4. State-dependent gating of vibrissa responses in barrel cortex**.

**(a)** Vibrissa stimuli (arrowheads) were delivered randomly during recording from a layer 4 barrel neuron. Whole-cell recordings show that the depolarizing sensory response is strongly reduced during active whisking (red) compared to during quiescent wakefulness (blue). Adapted from Ferezou et al. (Ferezou et al., 2006). **(b)** The above state-dependent reduction in sensory processing can be imaged with voltage-sensitive dye. Passively evoked sensory responses during quiescent wakefulness have large amplitude and spread across large cortical areas, whereas the response is almost suppressed during whisking. The red square on the images at 0 ms indicates the region of interest centered on the C2 cortical column from which voltage-sensitive dye fluorescence changes are quantified in the adjacent traces (lower right). Adapted from Crochet and Petersen (Crochet and Petersen, 2006).

## *2.6 Context- and state-dependent sniffing and whisking modes*

There is evidence to suggest that the expression of both whisking and sniffing is dependent on the motivational state and behavioral goals of the animal. Analysis of sniffing in rats performing a go-nogo odor discrimination task reveal two modes of sniffing: a 7 to 8 Hz sniffing mode associated with odor sampling, and a 10 to 12 Hz sniffing mode in anticipation of reward delivery (Kepecs et al., 2005). Correspondingly, several other studies report that sniffing is associated with reward anticipation. For example, sniffing becomes part of the conditioned response as rats learn to predict the occurrence of a reward based on a sensory cue (Bindra and Campbell, 1967; Clarke and Trowill, 1971). Electrical stimulation of brain regions whose activation is intrinsically rewarding, such as the lateral hypothalamus, elicits exploratory behaviors as well as high-frequency sniffing (Ikemoto and Panksepp, 1994). Although whisking was not quantified in these latter studies, the authors incidentally report that whisking was associated with sniffing. Further, in a situation where rewarding brain stimulation is repeatedly delivered at fixed intervals, regardless of response, rats eventually exhibit vigorous sniffing just prior to the delivery of the stimulation (Richard Waranch and Terman, 1975).

The context of exploratory behavior can shape how sensory input is processed in the nervous system. In a study in which rats whisked in air either spontaneously or for a reward, oscillations in the local field potential in primary sensory cortex showed drastically increased coherence with the whisking rhythm when the rats were motivated by the reward (Ganguly and Kleinfeld, 2004). This occurred without an increase in field potential amplitude and thus implies a decrease in the variability of the cortical response under conditions of a near-term reward, possibly as a result of increased attention to salient features in the environment.

As with sniffing, different whisking frequencies could subserve different behavioral goals. First, a wide range of whisking frequencies, *i.e.*, 2 to 20 Hz, was reported in an early study of texture discrimination (Carvell and Simons, 1990). Later work showed that whisking could be divided into two overall frequency ranges, each with a different pattern and associated behavior (Berg and Kleinfeld, 2003). Large amplitude whisks at 8 to 9 Hz are associated with exploration, while a second pattern of whisking, termed foveal whisking, occurs when the animal is perched and the vibrissae are thrust forward and stretched toward an object of interest. This latter pattern consists of relatively low-amplitude whisks in the frequency range of 15 to 25 Hz (Berg and Kleinfeld, 2003), and are reminiscent of 25 Hz oscillatory muscle activity that occurs during the hold period of a precision grip task in monkey (Baker et

al., 1997). For the moment it is unresolved whether fast whisks are part of a scanning motor strategy, or whether they are rhythmic events related to a strategy of maintaining vibrissae in a protracted position.

The above observations suggest that sniffing and whisking not only serve odor sampling and touch, but they also constitute activity patterns that are the overt expression of reward expectation, and thus serve to automatically sample and identify objects of potential interest. This motivates the question of whether there are specific behavioral contexts in which whisking and sniffing are related. When whisking and sniffing occur together, they appear to be synchronous (Welker, 1964) (asterisk in **Fig. 2.1c**), yet no study has examined the precise conditions under which the two rhythms couple. Casual observations suggest that rats sniff without whisking when the object of interest is near the nose, and can be inspected with the microvibrissae in conjunction with head and forepaw movements. Beyond behavioral contexts, it is of theoretical interest to understand how two CPGs phase lock and decouple in a dynamic manner that depends on their synaptic interactions and the action of modulators that control emotional and motivational states(Grannan et al., 1993). Such an understanding of these mechanisms could provide insight into the nature of coupling of other rhythmic behaviors to respiration (Travers et al., 1997).

## *2.7 Why do rodents sniff and whisk?*

Although sniffing clearly subserves olfaction and strongly patterns olfactory processing, several studies reported that basal respiratory rhythm is sufficient for delivering odorants to olfactory receptors, and that rats and mice can perform simple odor discrimination after a single sniff (Kepecs et al., 2007; Uchida and Mainen, 2003; Wachowiak, 2011). Likewise, rodents can locate objects and gauge aperture widths with a single whisk and, rather dramatically, severing the facial nerve to block whisking does not affect performance (Krupa et al., 2001; O'Connor et al., 2010b). Lastly, rodents can perform many tactile tasks without whisking *per se*, either by using head and body movements to move the vibrissae or by maintaining their vibrissae still in a region of interest where contact or stimulation is expected (Hutson and Masterton, 1986; O'Connor et al., 2010b).

Given the above evidence that smelling can occur without sniffing and vibrissa touch can be effective without whisking, the questions remain as to why rodents sniff and why they whisk. There are likely to be multiple answers. First, since rodents have relatively limited visual capabilities and are the targets of predators, fast sampling of the immediate environment has clear survival value (Wesson et al., 2009). The few extra hundreds of milliseconds of warning that are gained by scanning the environment may be sufficient for

escape. Second, since rodents live in burrows and locomote in a bumpy, cluttered environment, they must rely on tactile inputs to look ahead and avoid obstacles. The speed of locomotion could account for variability in the whisking frequency given the monotonic relation between whisking frequency and the speed of locomotion across species that whisk (Mitchinson et al., 2011). Finally, sniffing and whisking not only serve odor sampling and touch, but also represent the overt expression of an animal's interest in its environment. In this regard, casual observation suggests a marked difference in behavior between strains of rats, with Long Evans rats being much more enthusiastic sniffers and whiskers than their Sprague Dawley congeners. The use of transgenic mice, in which the effects of neuromodulators are up or down regulated, might be useful models to understand the neural basis of the drive to sniff and whisk.

## *2.8 Conclusions*

Many rhythmic behaviors in rodents have been reported to alternately couple and decouple to breathing. These include whisking and head movements (Welker, 1964), licking, mastication, and swallowing (Travers et al., 1997). These rhythmic activities are all generated by pattern generators located in the brainstem. The case of sniffing and whisking is of particular

interest as these behaviors often occur spontaneously, are phase locked, and are related to the sensory exploration of the immediate environment. From a practical standpoint, they can be controlled by classical and operant conditioning. The accessibility of the vibrissa system for electrophysiological studies and the use of high-speed videography and indwelling sensors for electromyography, air flow, and related measurements make the rodent an ideal system to understand the neural mechanisms that underlie the generation of these rhythms. Such studies may further provide a framework for the nature of the circuitry, the modulation of sensory inputs, and the computations that underlie coupling between other brainstem-controlled rhythmic behaviors.

Beyond sensory coding, sniffing and whisking constitute overt expression of the emotional and motivational state of rodents. A detailed knowledge of these behaviors could provide simple metrics for assessing the animal's subjective valuation of objects and experiences. Such metrics would be of particular interest, for instance, to assess motor and motivational deficits in animal models of neuropsychiatric disorders.

## *2.9 Acknowledgements*

We thank Adam Kepecs and Dima Rindberg for discussions that shaped this review, and the Canadian Institutes of Health Research (grant MT-5877), the National Institutes of Health (grants NS058668 and NS066664), and the US-Israeli Binational Foundation (grant 2003222) for their support.

This chapter follows from work that is currently published in:

Deschênes M, Moore JD, Kleinfeld D. Sniffing and whisking in rodents. Current Opinion in Neurobiology. 22(2): 243-250 (2012)

This material is included with the generous consent of all authors and permission of the journal. The dissertation author is a primary researcher on this work.

# Chapter 3 – Hierarchy of orofacial rhythms revealed through whisking and breathing

Whisking and sniffing are predominant aspects of exploratory behavior in rodents, yet the neural mechanisms that generate their motor patterns remain largely uncharacterized. We use anatomical, behavioral, electrophysiological, and pharmacological tools to demonstrate that these patterns are coordinated by respiratory centers in the ventral medulla. We delineate a distinct region in the ventral medulla that provides rhythmic input to the facial motoneurons that drive protraction of the vibrissae. Neuronal output from this region is reset at each inspiration by direct input from the preBötzinger complex, such that high frequency sniffing has a one-to-one coordination with whisking while basal respiration is accompanied by intervening whisks that occur between breaths. We conjecture that the respiratory nuclei, which project to other premotor regions for oral and facial control, function as a master clock for behaviors that coordinate with breathing.

## *3.1 Introduction*

Active sensing is an essential component of orofacial behavior. Animals rhythmically sniff to smell, lick to taste, and whisk to touch. The muscles involved in these patterned sensory behaviors overlap with those involved with the ingestive behaviors of chewing, swallowing, and suckling. Of critical importance, all of these behaviors share the motor plant involved in respiration and control of the upper airway. Given the essential nature of breathing and the biomechanical constraints that link the different behaviors, the coordination among orofacial behaviors constitutes a computational aspect of homeostatic control with little margin for error (Alheid and McCrimmon, 2008; Feldman et al., 2013; Garcia et al., 2011; Nakamura and Katakura, 1995; Smith et al., 2009; Travers et al., 1997).

Here we investigate the issue of coordination of orofacial behaviors in the context of sniffing and whisking in rodents. These closely associated rhythmic behaviors constitute the animals' predominant activities during exploration and social interactions (Brecht and Freiwald, 2012; Vincent, 1912; Welker, 1964). The cycle of rhythmic breathing is driven by neurons in the preBötzinger complex, which generates the inspiratory rhythm (Smith et al., 1991; Tan et al., 2008), the Bötzinger complex and parafacial respiratory groups, which shape the expiratory rhythm (Feldman et al., 2013), the ventral respiratory groups, which drive the respiratory pump muscles (Dobbins and

Feldman, 1994), and several pools of cranial motoneurons that control the upper airway valve muscles (Bieger and Hopkins, 1987). The drive for rhythmic whisking remains to be identified. Yet whisking persists after decortication (Semba and Komisaruk, 1984; Welker, 1964) and sensory deafferentation (Berg and Kleinfeld, 2003; Gao et al., 2001; Welker, 1964), which suggests that it too involves a rhythmic generator in the brainstem. Further, the facial motoneurons that drive the muscles involved in whisking are located immediately rostral to nuclei within the ventral medulla that generate breathing, and activity within these facial motoneurons and muscles is time-locked to breathing (Huangfu et al., 1993; Onimaru et al., 2006). These prior results support a common neural circuitry for the rhythmic control of both breathing and whisking.

## *3.2 Methods*

### Animals

Thirty-seven female Long Evans rats (250 to 350 g, Charles River) were used for behavioral and electrophysiological experiments, an additional 25 rats of mixed sex were used solely for lesion studies, and 13 female rats were used for purely anatomical studies. Four adult mice, two male C57BL/6J

and two female ChR2-MBD (Lewis Jr. et al., 2009) were used for behavioral studies. Experimental protocols were carried out in accordance with federally prescribed animal care and use guidelines and were approved by the Institutional Animal Care and Use Committees at the University of California in San Diego, Laval University, and Janelia Farms Research Center.

## Preparation

Head-fixed rats were habituated to body restraint for 5 days, then implanted with a custom-built head restraining mount (Kleinfeld et al., 2002) and a thermocouple (K-type; Omega Engineering, CT) in the nasal cavity (Uchida and Mainen, 2003). Surgical procedures were carried out in animals anesthetized with ketamine (90 mg/kg) / xylazine (5 mg/kg). In brief, a craniotomy was performed over the cerebellum, and a plastic chamber was centered over the opening and secured with acrylic cement. The craniotomy was filled with silicone gel (no. 3-4689; Dow Corning, MI). In two animals, Teflon-coated tungsten wires were inserted in the vibrissa pad to record activity of the intrinsic muscles and of the nasolabialis muscle (Berg and Kleinfeld, 2003; Hill et al., 2008). Rats were allowed to recover for two days before the onset of behavioral experiments. During the recording sessions, rats were placed inside a body-restraining cloth sack and rigid tube, and the animals were head-restrained (Kleinfeld et al., 2002). All vibrissae except

numbers C2 or D2 were cut at the base and movement of the intact vibrissa was recorded with videography. Rats were coaxed to whisk by presenting food or bedding from the home cage (Ganguly and Kleinfeld, 2004). Lastly, in some experiments, a tube was placed in front of the snout to deliver one or two two-second puffs of air saturated with ammonia while the animal whisked.

Head-fixed mice were implanted with a titanium bar for head fixation (O'Connor et al., 2010a) and with a stainless steel cannula to measure breathing as previously described (Shusterman et al., 2011). The mice were allowed to recover for 10 days prior to behavioral experiments.

## Recording and analysis

To measure whisking, vibrissa motion in head-fixed rats was monitored one of several ways with a Basler A602f camera at a spatial resolution of 120 µm/pixel or an NMOS linear sensor (S3904-2048Q; Hamamatsu, PA). For behavioral measurements, 360x250 pixel planar images were acquired at 250 Hz with a white light emitting diode backlight for trials of 10 s each. Vibrissa angle was tracked by fitting a line to the spatially contiguous pixels comprising the initial 5 mm segment of the vibrissa base. For measurements in conjunction with extracellular recording from brainstem, we used either the

Basler A602f camera in line-scan mode with a 1 kHz scan rate or the NMOS linear sensor and imaged motion along a line that was 5 to 10 mm from the edge of the mystacial pad. Pixel intensity along the line was thresholded and the centroid of the detected vibrissa was converted to a voltage proportional to pixel position in real time.

Vibrissa motion in freely moving rats with one or more vibrissae in the C or D-row was monitored with a HiSpec 2G Mono camera (Fastec Imaging, CA) at a 250 Hz frame rate, or a Powershot SX260HS camera at a 120 Hz frame rate (Canon, NY). Rats were placed in a raised, clear plastic box with a passageway that allowed them to perch in search of their home cage, located 20 cm away. Trained animals craned across the gap and sniffed and whisked vigorously (Ganguly and Kleinfeld, 2004). Vibrissa motion was tracked with commercial software (ProAnalyst, Xcitex Inc., MA), and previously described algorithms (Knutsen et al., 2005).

Vibrissa motion in head-fixed mice with vibrissae in the C-row was recorded with a high-speed CMOS camera (EOSENS CL; Mikrotron) through a telecentric lens (0.36X; Edmund Optics; NJ). Streampix 3 software (Norpix, Quebec) was used to acquire the images, 640x352 pixels at a spatial resolution of 24 µm per pixel. The vibrissae were illuminated from below with collimated infrared light from a high-power light emitting diode (640nm;

Roithner, Vienna). Vibrissa motion was tracked with automated procedures (O'Connor et al., 2010a).

The extracted vibrissa movements for all cases were separated into single whisks by band-pass filtering the position traces between 3 and 25 Hz with a 3-pole Butterworth filter run in forwards and backwards directions and applying the Hilbert transform (Hill et al., 2011a). Individual candidate whisks were identified by phase resets of the Hilbert transform, and were accepted only if the minimum-to-maximum amplitude exceeded 5° and the whisk lasted less than 250 ms. The onset time of each whisk was defined as the time at which the vibrissa angle exceeded 10 % of the minimum-to-maximum amplitude.

For electromyography, muscular activity was monitored in different muscle groups, and the integrated envelope of the EMG activity, denoted $|\nabla EMG|$, was computed as previously described (Berg and Kleinfeld, 2003; Hill et al., 2008). We then computed the cross-correlation between protraction onset times and the $|\nabla EMG|$. The 95 % confidence intervals were obtained by re-sampling with replacement 1000 times from the set of protraction onset times and computing the cross-correlation with the re- sampled dataset.

To measure breathing, respiration-related changes in temperature or pressure sensors were digitized and band pass filtered between 1 and 15 Hz with a 3-pole Butterworth filter run backwards and forwards in time. Onset times for inspiratory events were defined as described above for whisking.

In rats, respiration-related changes in temperature were verified to be synchronous with chest expansion, which are presumed to track diaphragm movements, as measured with a piezoelectric strap around the abdomen in separate experiments.

To examine neuronal signaling in awake, behaving rats, multiunit neuronal activity was recorded in the ventral medulla with quartz micropipettes, 10 to 25 μm tip diameter, filled with 2 % (w/v) Chicago sky blue (Sigma, MO) in artificial cerebral spinal saline, or with tungsten microelectrodes (1 MΩ impedance; Microprobes, MD). Electrode position was controlled by a motorized manipulator (model MP-285, Sutter, CA). Units were held for one to twenty minutes. Signals were amplified, band-pass filtered between 300 Hz and 6 kHz and sampled at 20 or 40 kHz. The noise level, σ, was defined as the standard deviation of the voltages recorded over the entire time the electrode was maintained at a recording site. Multiunit spike events were defined as voltage fluctuations that exceeded 3.5-times σ.

One or more recording sites in each session were marked with an extracellular deposit of Chicago sky blue by electrophoresis; - 10 to - 50 µA with 10 s pulses spaced every 20 s for five minutes, or by electrolytic lesion with 40 to 80 µA applied for three intervals of 2 to 5 s. Rats were deeply anesthetized at the end of the session and perfused with phosphate buffered saline (PBS), followed by perfusion with 4 % (w/v) paraformaldehyde in PBS. Brains were post-fixed overnight in 4 % paraformaldehyde in PBS, cryoprotected in 30 % (w/v) sucrose in PBS, and sectioned along the sagittal or coronal plane at a thickness of 60 µm with a freezing microtome. Sections were stained with either Neutral red, Neurotrace™ blue (fluorescent Nissl; Invitrogen, CA), or cytochrome oxidase (Deschênes et al., 2003).

To investigate kainic acid-induced whisking, microinjections of kainic acid were made through quartz or glass micropipettes, 10 to 15 µm in diameter, in rats anesthetized with ketamine/xylazine as described above. Injections were targeted to the approximate vibrissa region of the intermediate band of the reticular formation (vIRt) as defined in our anatomical studies (**Fig. 3.17**) using stereotaxic coordinates. Kainic acid was prepared as 1 % (w/v) in Tris buffer, pH 8.2 and delivered by iontophoresis with -500 nA, 250 ms pulses spaced every 500 ms for 600 s. In several

experiments, biotinylated dextran amine (MW 3000; Invitrogen) prepared as 2 % (w/v), was added to the solution to facilitate labeling of the injection site.

Rats were secured with a head-fixed mount and their vibrissae were monitored with a camera in linescan mode (Basler A602f). Coordinated, rhythmic vibrissa movements typically began 15 to 30 minutes after the kainic acid injection, at which point all vibrissae except number C2 or D2 were trimmed. Individual whisks were detected, as described above, with the exception that the threshold for detecting a whisk was set to 1 °.

Single and multiunit recordings in the vicinity of the site of the kainic acid injections were made in a subset of rats using glass microelectrodes with 2 to 3 µm tips back-filled with Neurobiotin™ (Vector Labs, CA), prepared as a 2 % (w/v) solution in 500 mM potassium acetate. These pipettes served for both recording and labeling of the recording site. The centroid of injection sites that induced whisking varied by up to 1 mm relative to the actual anatomical location of the vIRt, consistent with variability in stereotaxic coordinates between rats (Paxinos et al., 1985) and the rapid diffusion of kainic acid. We thus made multiple penetrations offset by at most 100 µm of each other to locate units whose spiking was locked to whisking following the kainic acid injection. The depth of each unit along a penetration was noted, and at the end of a subset of the experiments the recording site was labeled

via iontophoresis; + 50 to 100 nA, 2 s pulses spaced every 4 s for 1000 s. The animals were perfused two hours after the injection.

For coherence and correlation analysis, we assessed the degree and statistical significance of correlation between whisking and breathing events (**Fig. 3.1d**) by computing the cross correlation between whisk onset times and breath onset times separately for basal respiration, with rates < 3 Hz, and sniffing, with rates > 5 Hz. The maximum lag for the cross-correlation computed in each case was bounded by the minimum breathing period. Statistical significance was assessed by performing a one sample Kolmogorov-Smirnov test versus the uniform distribution expected by chance. Correspondingly, we define the modulation depth of the cross correlation as the corresponding Kolmogorov-Smirnov test statistic.

Additional analyses were performed in the frequency domain to assess the spectral content and synchrony between whisking, breathing, and spiking activity. For experiments in awake animals, whose behavior exhibited interleaved bouts of basal respiration, sniffing and whisking, our data was segmented as follows. First, “inspiratory” whisks were defined as those whisks whose onset occurred within 100 ms of an inspiration, while intervening whisks were defined as whisks that did not occur within 100 ms of the closest onset of inspiration. Next, behavioral epochs were classified as

“basal respiration” when the instantaneous respiratory frequency was less than 3 Hz, “sniffing” for periods when the instantaneous respiratory frequency was greater than 5 Hz, “inspiratory whisking” for periods of successive inspiratory whisks, and “intervening whisking” for periods of successive intervening whisks during “basal respiration”. Bouts of these behaviors were divided into non-overlapping segments of a pre-determined length, *i.e.*, 1 s for basal respiration, 500 ms for sniffing and inspiratory whisking, and 300ms for intervening whisking. For each segment we extracted the relevant behavioral signal, *i.e.*, inspiration onset times for basal respiration and sniffing and vibrissa position for inspiratory and intervening whisking, and the relevant physiological signal, *i.e.*, the $|\nabla EMG|$ or the multiunit spike times.

The Chronux toolbox (www.chronux.org) was used to compute the spectral coherence between these respective behavioral and physiological signals, averaged over all segments with a time-bandwidth product of one. We report the magnitude and phase of the coherence at the peak frequency of the behavior (**Fig. 3.1c**), *i.e.*, 2 Hz for basal respiration, 6 Hz for sniffing and inspiratory whisking, and 8 Hz for intervening whisking. The whisking and breathing analyses are normalized so that a phase of zero corresponds to the onsets of protraction and inspiration, respectively, as defined above.

For experiments in anesthetized animals with pharmacologically induced whisking, we computed the spectral coherence between vibrissa position and either spike times or |∇EMG| irrespective of breathing, averaged over all 2 s segments with a time-bandwidth product of 2. We report the magnitude and phase of the coherence at the peak frequency whisking, which varied between experiments. The analysis is normalized as above, where phase zero corresponds to the onset of protraction.

## Medullary lesions and whisking

Electrolytic lesions were made with metal microelectrodes (0.5 MΩ; FHC Inc., ME) by passing direct current of + 40 to 80 µA for 5 s at multiple nearby spatial locations. In select cases the lesions were performed with glass pipettes in head-fixed animals immediately after unit recordings in the vIRt. Ibotenic acid lesions were made by pressure injection of approximately 300 nL of ibotenic acid, prepared as 1 % (w/v) in physiological saline. Sindbis virus lesions were made by pressure injection of approximately 100 to 300 nL of viral vector (Ghosh et al., 2011) (~$3x10^3$ infectious particles/µL) using glass micropipettes with 30 µm diameter tips. After the animal was allowed to recovery from surgery, high speed videography of vibrissa motion on both sides of the face in both head-fixed and freely-moving animals was

performed. Vibrissae were tracked and individual whisks were identified based on the motion on the contralateral side, as described above. The mean amplitude of the Hilbert transform over the period of each whisk was calculated for both the ipsilateral and contralateral sides.

## Anatomy

For anterograde and retrograde labeling, all tracer injections were made under ketamine/xylazine anesthesia, as above, with concurrent monitoring of respiration. Cells in the Bötzinger/parafacial complex were labeled with Neurobiotin™ (Vector Labs, CA), prepared as a 2 % (w/v) solution in 500 mM potassium acetate. Glass microelectrodes with 4 to 5 µm tips served for both recording and injection. Bötzinger cells were identified by their expiratory-related activity and Neurobiotin™ was delivered by iontophoresis; + 50 to 100 nA, 2 s pulses spaced every 4 s for 1000 s. The animals were perfused after 90 minutes of recovery.

Cells in the preBötzinger complex were similarly identified by their inspiratory-related activity and labeled with biotinylated dextran amine (10 kD MW; Invitrogen), prepared as a 2 % (w/v) solution in 500 mM potassium acetate. Biotinylated dextran amine was delivered by iontophoresis using

glass microelectrodes with 8 to 10 µm tips; + 200 nA, 2 s pulses spaced every 4 s for 1000 s. The animals were perfused after 2 days of recovery.

Cells that projected to the facial motor nucleus were labeled retrogradely with Neurobiotin™, prepared as a 2 % (w/v) solution in 10 mM sodium citrate buffer at pH 3.0 using glass microelectrodes with 20 µm diameter tips. The location was confirmed by microstimulation, +5 to 10 µA pulses, 100 µs in width, delivered at 100 Hz, that led to ~ 2º movements of one or more vibrissae. Neurobiotin™ was delivered by iontophoresis; + 300 nA, 2 s pulses spaced every 4 s for 1000 s. The animals were perfused after three hours of recovery. Complementary studies involved the use of Fluoro-Gold™ (Fluorochrome, Denver), prepared as a 1 % (w/v) in 0.1 M cacodylate buffer at pH 7.0, delivered as above but with the animals perfused after two days.

After perfusion, brains were post-fixed for two hours and cryoprotected in 30 % (w/v) sucrose for 12 hours. Then the brainstems were isolated and cut in the coronal or sagittal plane at a thickness of 50 µm on a freezing microtome. Neurobiotin™ and BDA were revealed with ABC Elite and SG kits (Vector Labs) or with streptavidin-Alexa 488 (1:200 dilution; Invitrogen). Fluoro-Gold™ was revealed by immunohistochemistry (1:5000 dilution; Millipore, CA). Sections were then counterstained with either Neutral red,

immunostained for choline acetyltransferase (1:1000 dilution of α-ChAt; Millipore), or reacted for cytochrome oxidase.

To examine lesion anatomy, animals lesioned with the Sindbis viral vector, in which we observed a severe deficit in whisking, were perfused immediately after video recordings; this corresponded to 50 to 75 hours after injection of the virus. Animals that did not exhibit a deficit were perfused after 4 to 6 days. Animals lesioned electrolytically or with ibotenic acid were perfused 2 to 10 days after the procedure. For electrolytic lesions, 60 µm coronal or sagittal sections were stained for neutral red. For ibotenic acid and Sindbis viral lesions, 30 µm coronal or sagittal sections were immunostained for neuronal nuclear protein (1:200 dilution of α-NeuN; Millipore). For Sindbis viral lesions, alternate sections were stained for myelin (Luxol fast blue; Sigma) and cell bodies (neutral red).

For mapping, histological sections were scanned at 1 µm spatial resolution using a Nanozoomer (Hamamatsu) digital slide scanner. The stereotaxic recording sites were superimposed on the scans according to their distance to the nearest labeled site. Sections containing Chicago sky blue deposits and associated recording sites were aligned by manual rotation and translation with an atlas of sagittal Nissl sections (brainmaps.org). The

outlines of prominent medullary structures including the facial nucleus, lateral reticular nucleus, *ambiguus* nucleus and inferior olive were traced with Neurolucida™ (Microbrightfield, VT) software, and sections were aligned based on these anatomical borders to yield a three-dimensional reconstruction of the medulla. The extents of brainstem lesions were similarly mapped onto standard frontal sections (Paxinos and Watson, 1986).

## Combined anatomy and in-situ hybridization

For retrograde labeling and in-situ hybridization, tracer injections were made under ketamine/xylazine anesthesia. Fluoro-Gold™, 4 % (w/v) in saline, was injected into the lateral part of the facial nucleus by passing 500 nA current pulses, 7 s in duration, every 14 s for 300 s using glass microelectrodes with 20 µm diameters tips. After a survival periods of 48 hours, rats were perfused as described above. After fixation, brains were removed, the brainstem isolated, cryoprotected with diethylpyrocarbonate-treated sucrose, and cut into 30-µm-thick sagittal sections on a freezing microtome for *in situ* hybridization (Ito and Oliver, 2010).

To count cells, retrogradely labeled cells in sections processed for *in situ* hybridization were counted under confocal microscopy with a 40X objective,

as described (Furuta et al., 2008). Approximately ten fields were scanned in a grid-like manner across the vIRt, as defined in our other anatomical tracing experiments **Fig. 3.18**). For each field, a stack of 5 to 10 optical sections were acquired, and counts were made from the stacked images.

## *3.3 Results*

### Obligatory phase-locking of whisking and breathing

Concurrent measurements of breathing and whisking in head-fixed rats reveal key aspects of their coordination (**Fig. 3.1a,b)**. First, breathing over a wide range of rates can occur without substantial whisking (**top and middle, Fig. 3.1b**). To test whether whisking can also occur without breathing, we applied a puff of ammonia to the snout, which inactivates the central inspiratory drive (Lawson et al., 1991) (**Fig. 3.2**) and temporarily inhibits respiration. Critically, rats can whisk during such a disruption in breathing (**middle, Fig. 3.1b**), which implies that the oscillator(s) for breathing and whisking are separately gated.

Exploratory behavior typically consists of bouts of simultaneous whisking and fast breathing, or “sniffing” (Welker, 1964). Under such

circumstances, fast breathing is always accompanied by a one-to-one relation with whisking (**top, Fig. 3.1b**), which is strikingly evident as the rat begins to breathe again after apnea (**middle, Fig. 3.1b**). In contrast, basal breathing is accompanied by whisks that are coincident with an inspiration, denoted "inspiratory-locked whisks", plus decrementing "intervening whisks" that occur between successive breaths (**bottom, Fig 3.1b**). This leads to an incommensurate many-to-one relation between whisking and breathing. These data imply that there are separate, or separable, oscillators for breathing and whisking, and that the breathing rhythm may reset the whisking rhythm.

The temporal relation between whisking and breathing was quantified across the complete data set (5 rats) (**Fig. 3.1c-d**). We observe that breathing occurs over a broad range of frequencies, yet has two modes (top, **Fig. 3.1c**). We define “basal respiration" as epochs with a breathing rate below 3 Hz and “sniffing” as epochs with rates above 5 Hz (top, **Fig. 3.1c**). Whisking has a broad, high frequency spectral content during both basal respiration and sniffing (bottom, **Fig. 3.1c**). The detailed timing between whisking and breathing is revealed though a frequency-ordered plot of the correlation of whisking with breathing (**Fig. 3.1d**). Vibrissa protractions are time-locked to the onset of inspiration across the entire range of breathing frequencies; the green arrow in **Figure 3.1d** accounts for the delay between inspiratory drive

to diaphragm relative to that of the upper airway (Fukuda and Honda, 1982). Basal respiration cycles are accompanied by multiple whisks per breath, with an instantaneous whisking frequency of ~ 8 Hz for the intervening whisks (**Figs. 3.1d** & **3.3**). Analogous results, but with an instantaneous whisking frequency of ~ 13 Hz for the intervening whisks, are observed with mice (n = 4) (**Fig. 3.4**). Lastly, phase-sensitivity analysis (Ermentrout and Kleinfeld, 2001) shows that inspirations late in the whisk cycle elicit a new protraction earlier than expected (**Fig. 3.5**) and that breathing drives whisking but not *vice versa* (**Fig. 3.6**). Collectively, these data imply a unidirectional connection from the breathing oscillator (Feldman et al., 2013; Garcia et al., 2011; Smith et al., 1991) to a still hypothetical oscillator that generates whisking.

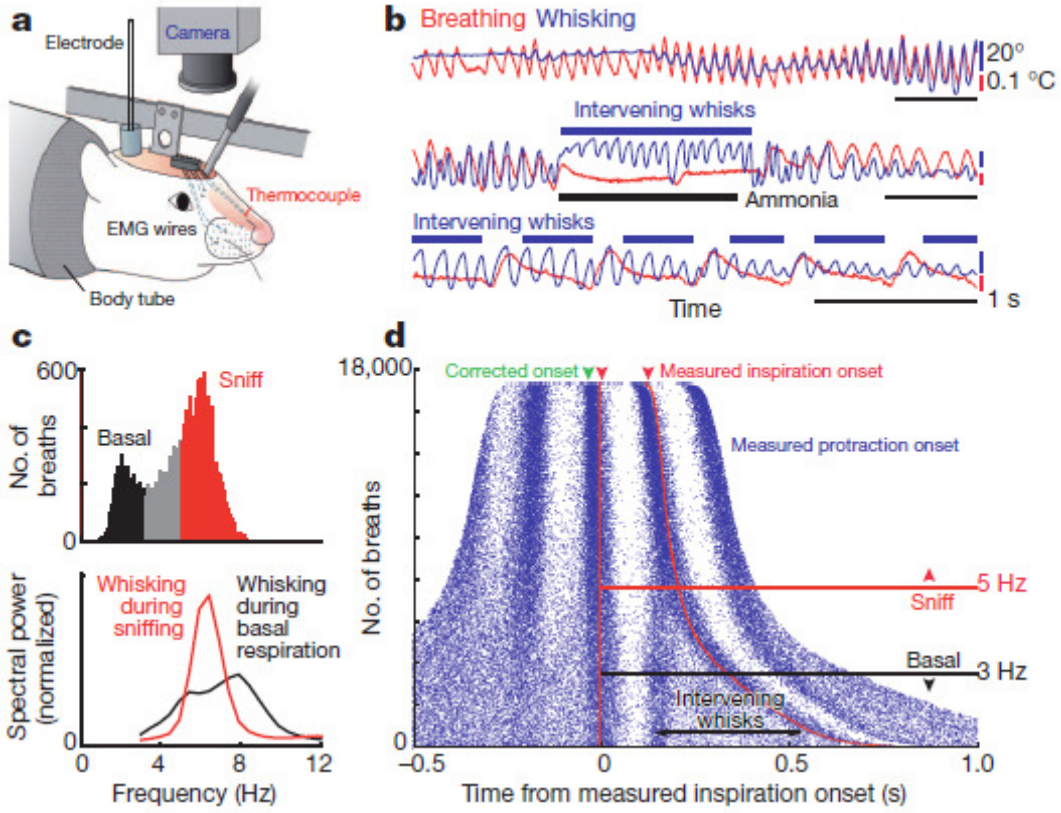


**Figure 3.1 Coordination of whisking and breathing.**

**(a)** Procedures to measure whisking, breathing, and associated electrophysiology in head-restrained rats. **(b)** Simultaneous measurement of vibrissa position (blue) and breathing (red). Protraction and inspiration are upward. **(c)** Histogram of instantaneous breathing frequencies (top) delineates the classification of breaths below 3 Hz as basal respiration and those above 5 Hz as sniffs. The spectral power of whisking (bottom) is plotted during periods of basal respiration (black) as well as sniffing (red). **(d)** Rasters of inspiration onset times (red) and protraction onset times (blue) relative to the onset of inspiration for individual breaths are ordered by the duration of the breath; green arrow represents the 30 ms lead of inspiratory drive to facial muscles as opposed to the measured inspiration. Whisks and inspiration onset times are significantly correlated during both sniffing and basal respiration ($p < 0.01$).

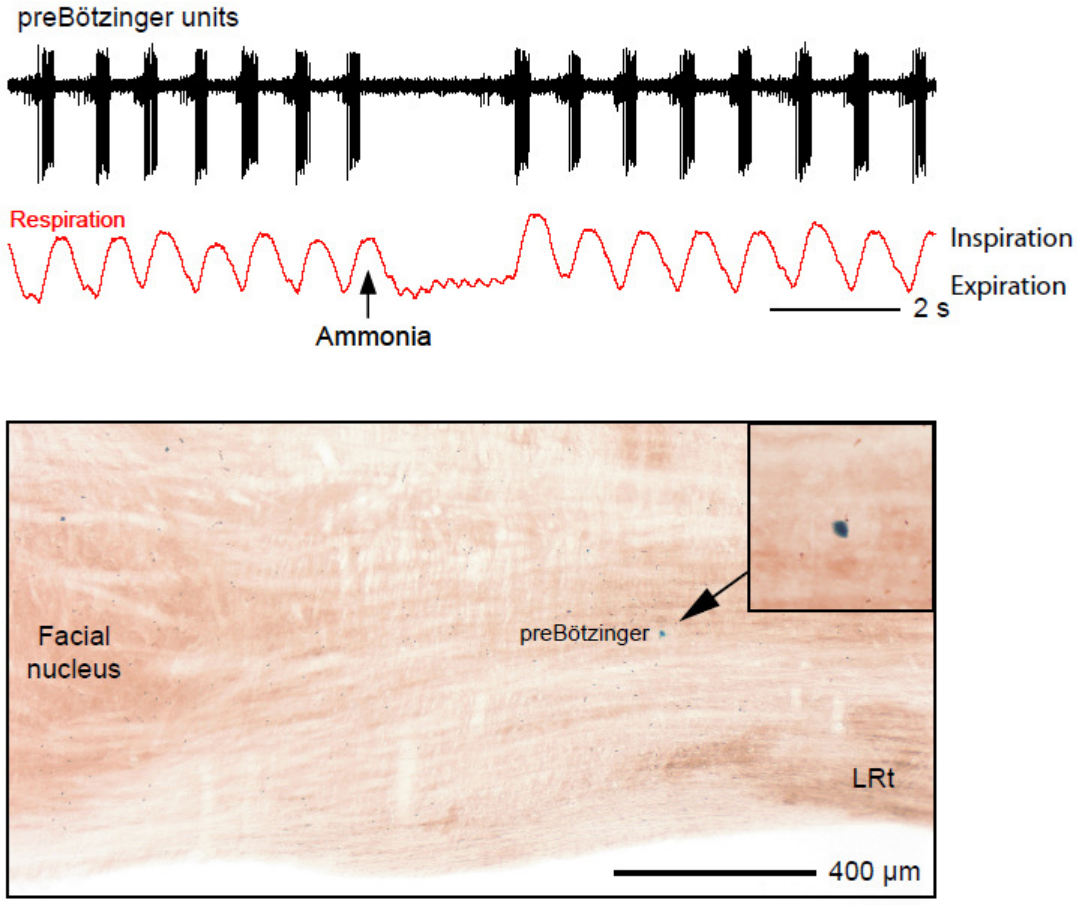


**Figure 3.2. Transient exposure to ammonia inhibits activity in the preBötzinger complex in the anesthetized rat.**

A puff of ammonia suppresses rhythmic bursts in preBötzinger cells, which constitute the core of the inspiratory central pattern generator for breathing. The recording site in the preBötzinger is labeled by a deposit of the dye Chicago sky blue.

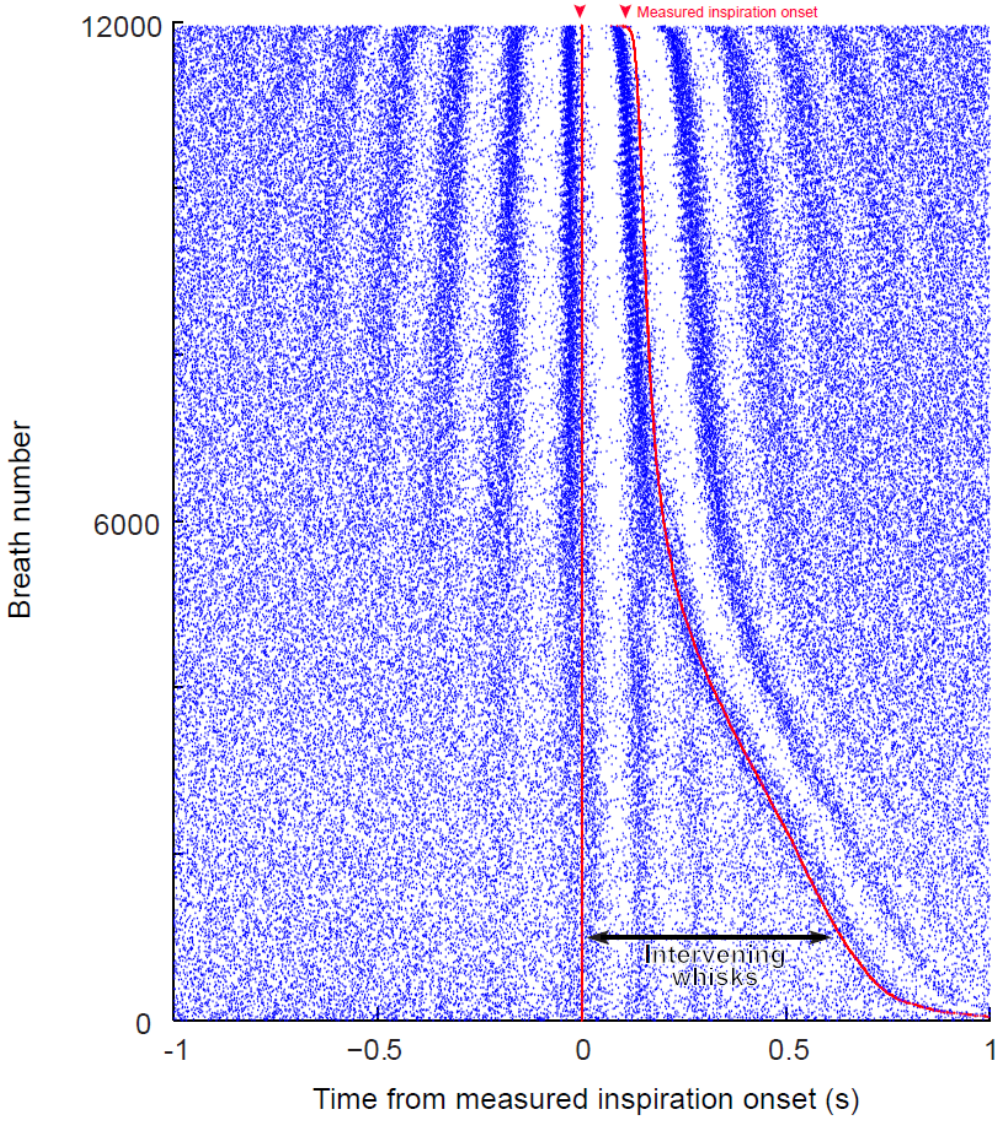


**Figure 3.3. Coordination of whisking and breathing in one rat.**

Temporal relationship between whisking and breathing events. Raster plots of inspiration and protraction onset times relative to each breath are sorted by the duration of the breath. In an individual animal, the intrinsic whisking oscillation frequency is stable and locked to the measured breathing onset time at both basal respiratory frequencies as well as sniffing frequencies. During basal respiration, the first, second, and third whisks following inspiratory drive occur at stereotypic times relative to breathing.

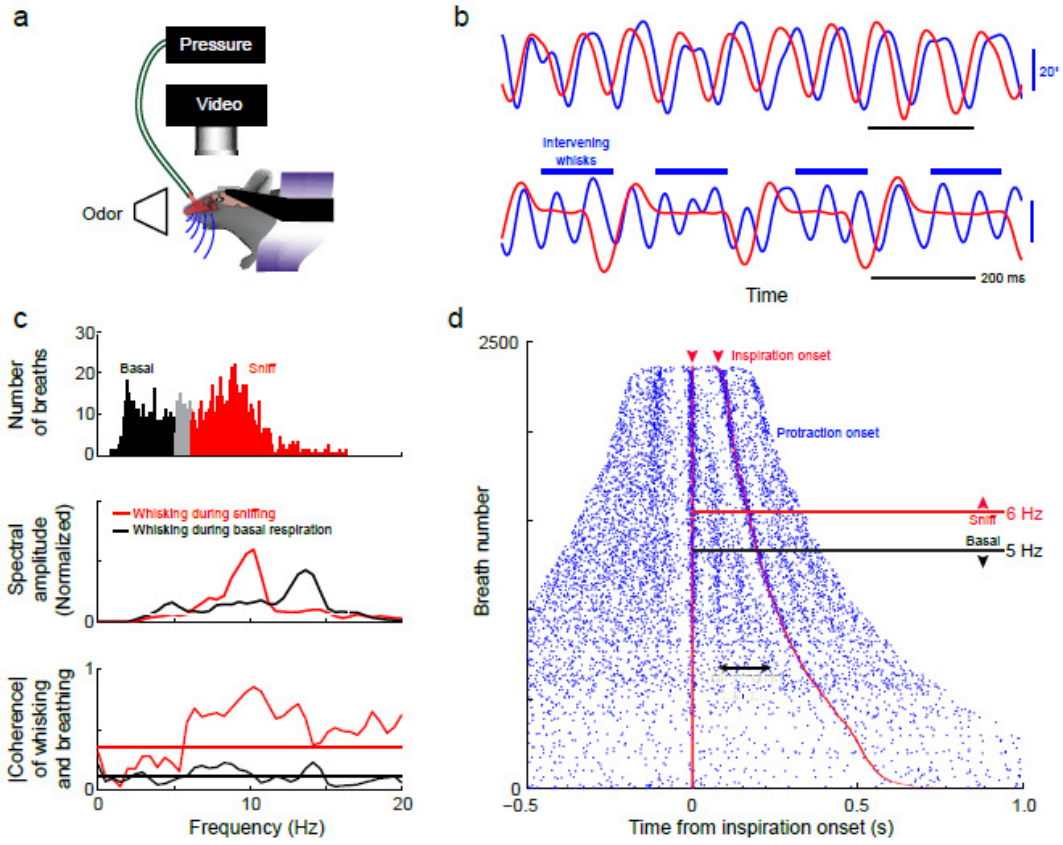


**Figure 3.4. Coordination of whisking and breathing in mice.**

**(a)** Experimental procedures to measure whisking and breathing. Head-restrained mice were implanted with a pressure transducer in the nasal cavity1, and vibrissae were monitored with high speed videography. **(b)** Simultaneous measurement of whisking and breathing. Vibrissa C2 position is in blue and pressure is in red. Protraction and inspiration are upward. During sniffing, inspiration is synchronous with vibrissa protraction on each cycle (top). During basal respiration, whisking is faster than breathing but inspiration remains synchronous with protraction (bottom). **(c)** Spectral relationship between whisking and breathing. Histogram of instantaneous breathing frequency for each breath (top). Breathing rates above 6 Hz are classified as sniffing, and below 5 Hz are classified as basal respiration. Whisking spectra are plotted for periods of sniffing (red) and periods of basal respiration (black). Coherence between whisking and breathing for periods of sniffing and periods of basal respiration. Dashed lines represent thresholds for statistical significance ($p < 0.05$). **(d)** Temporal relationship between whisking and breathing events. Raster plots of inspiration and protraction onset times relative to each breath are sorted by the duration of the breath, as in Figure 1. At high respiratory rates, whisking and breathing show a 1:1 relationship, but at lower frequencies there are intervening whisks between breaths. These data refute the claims of Cao, Roy, Sachdev and Heck (Cao et al., 2012).

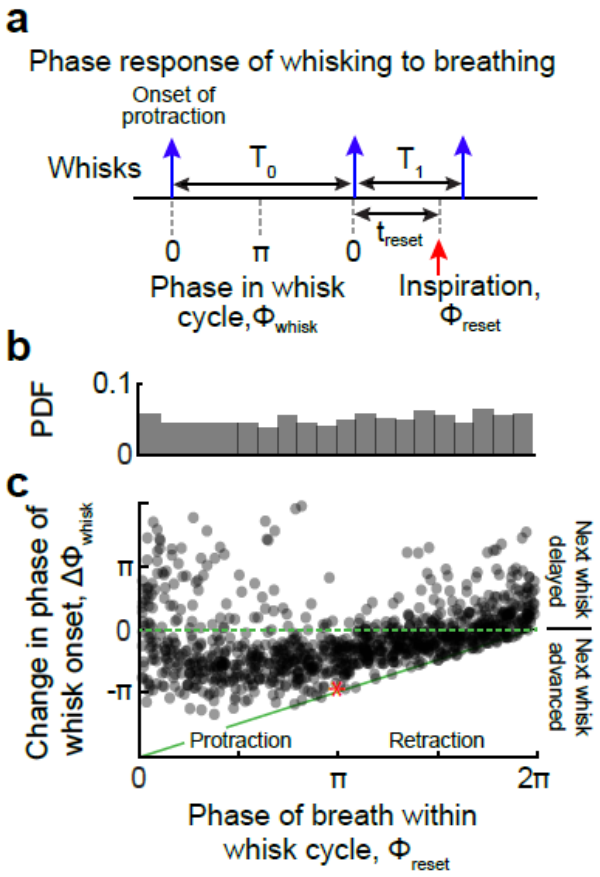


**Figure 3.5. Phase resetting of whisking by breathing**

**(a)** Schematic describing the phase-response of whisking relative to the onset of inspiration. For each whisk, the time at which inspiration occurs after the onset of protraction is defined as treset; in this analysis inspiration plays the role of an external perturbation. The expected duration of the whisk is denoted by T0 and, as the whisking frequency is stable throughout a bout, is taken as the duration of the preceding whisk. The duration of the perturbed whisk is denoted by T1. These times are normalized as the phase of the breath within the whisk cycle, defined by

$$\Phi_{reset} = 2\pi(t_{reset}/T_0)$$

along with the resultant change in whisking phase, defined by

$$\Delta\Phi_{whisk} = 2\pi(T_1 - T_0) / T_0$$

**(b)** Probability density of fresett during basal respiration. Inspiration occurs at all phases of the whisking rhythm during basal respiration**. (c)** Phase response of whisking to the onset of inspiratory drive during basal respiration. Onset times are adjusted as shown in Figure 1d. Symbols are defined above. The red asterisk represents the calculated perturbation for the example in the time-line in panel a.

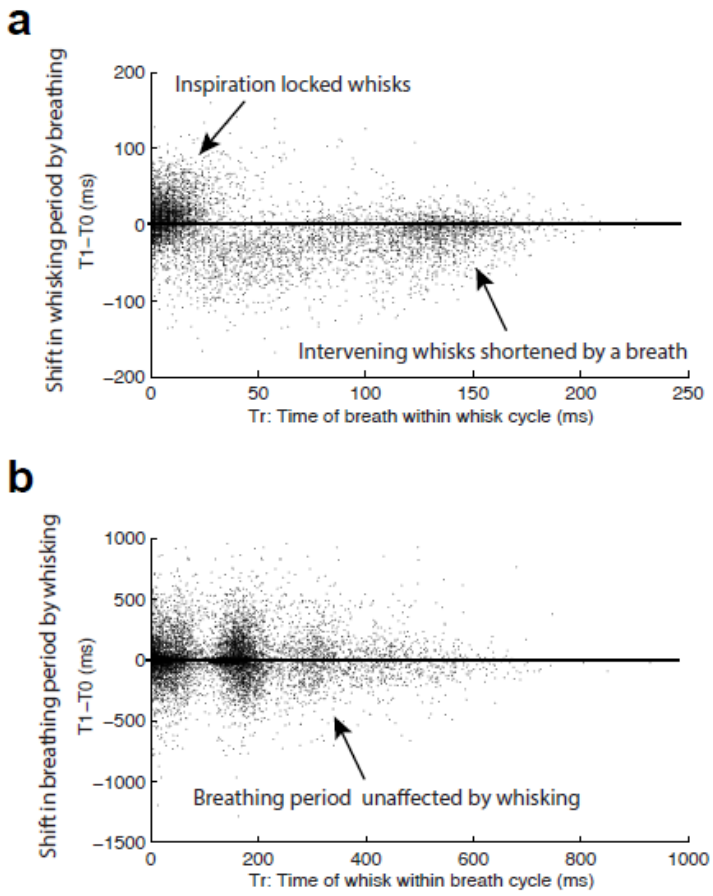


**Figure 3.6. Response of the whisking rhythm to breathing versus the breathing rhythm to whisking**

To emphasize the asymmetric interaction between whisking and breathing, we plot the shift in period (T1 -T0) of each behavior as a function of the time within the cycle when the other behavior occurs (treset). As in Figure S4, T0 represents the expected period of the perturbed behavior, taken as the period of the cycle prior to that which contains an interrupting event, and T1 represents the interrupted period. Unlike Figure S4, both sniffing and basal respiratory frequencies are included in the analysis to permit a symmetric comparison between the response of whisking to breathing and the response of breathing to whisking. **(a)** Shift in whisking period (T1 -T0) relative to the reset by an inspiration (at times treset). As in Figure S4, there is a bias for the intervening whisks to be shortened by the onset of breathing during basal respiration. The inhalation locked whisks during sniffing are not in steady state and not so constrained. **(b)** Shift in respiratory period (T1 -T0) relative to the reset by a vibrissa protraction (at times treset). There is a no apparent bias for the period of breathing to be shifted by the presence of a whisk during either sniffing or basal respiration.

## Facial muscles involved in whisking and breathing

Whisking and breathing-associated nose movements share facial muscle groups (Dorfl, 1982; Haidarliu et al., 2012; Sherrey and Megirian, 1977). Thus the difference in the pattern of whisking versus basal respiration (bottom, **Fig. 3.1b**) raises the issue of which muscle groups follow the sequence of motor commands associated with whisking (Hill et al., 2008) as opposed to those associated with breathing (Smith et al., 2009). In particular, protraction of the vibrissae is primarily driven by intrinsic papillary muscles that wrap around the individual vibrissa follicles (**Fig. 3.7a**), while retraction involves viscoelastic forces as well as translation of the mystacial pad (Berg and Kleinfeld, 2003) that is driven by the "extrinsic" *nasolabialis* and *maxillolabialis* muscles (Hill et al., 2008) (**Fig. 3.7a**). This determination of motor control is essential to understand the premotor brainstem circuits that drive different aspects of whisking.

We observe that the activity of the intrinsic muscles, measured via their differential electromyogram (∇EMG), leads protraction for both sniffing (**Fig. 3.7b**) and basal respiration (**Fig. 3.7c**). The *nasolabialis* muscle, also measured via its ∇EMG, is active for every whisk during sniffing (**Fig. 3.7b**) yet is only active for inspiratory-locked whisks during basal breathing (**Fig. 3.7c**). The timing and extent of this process was quantified in terms of

the population averaged cross-correlations between the different features of whisking and the |∇EMG| of the different muscle groups (3600 inspiratory-locked and 500 intervening whisks in two rats). This analysis indicates consistent modulation of the intrinsic |∇EMG| during both inspiratory and intervening whisks but modulation of the extrinsic |∇EMG| activity only for inspiratory whisks (**Fig. 3.8**), thus extending past results on the role of extrinsic muscles (Berg and Kleinfeld, 2003; Hill et al., 2008). These data imply that protraction is driven by the hypothesized whisking oscillator, while retraction of the mystacial pad is controlled, at least in part, by respiratory patterning circuitry.

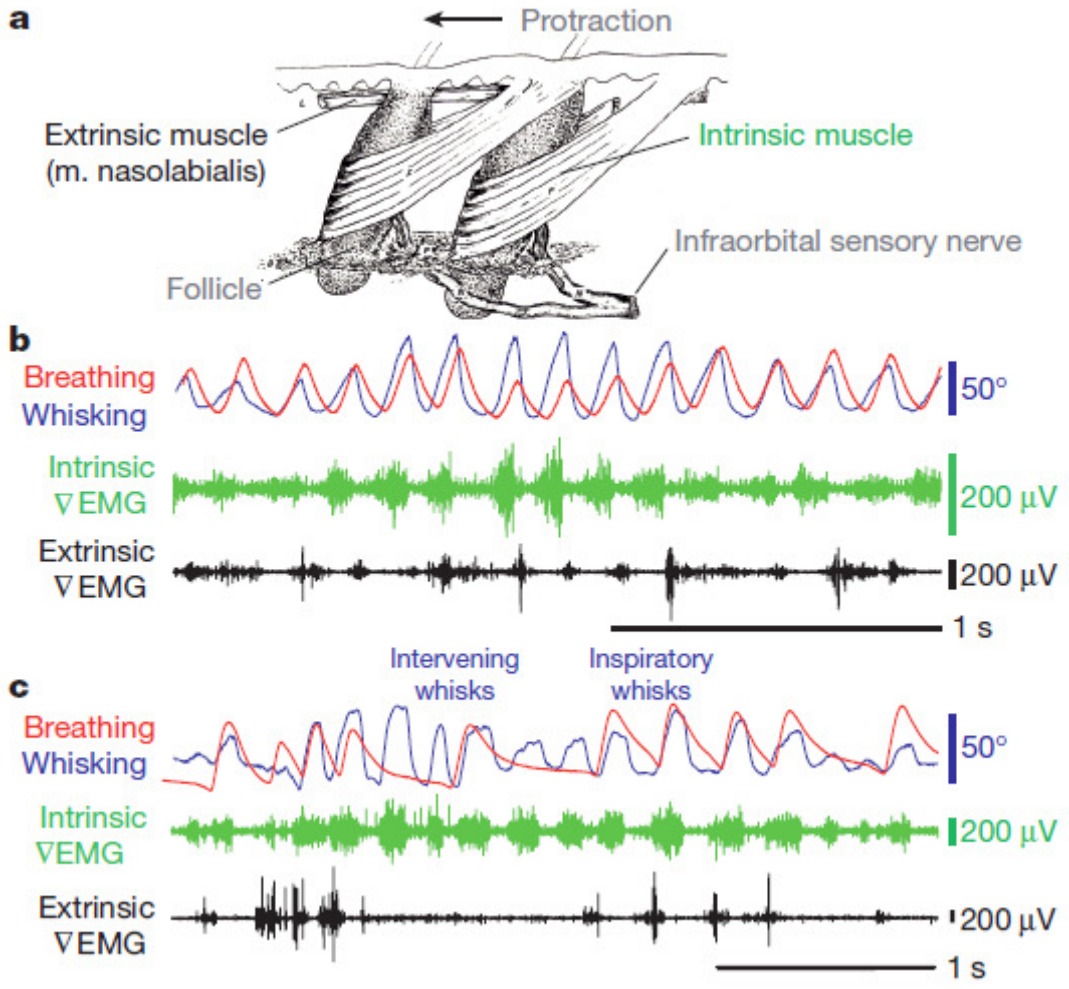


**Figure 3.7. Facial muscle activity during whisking and breathing**.

**(a)** The musculature responsible for vibrissa and mystacial pad motion; adapted from Dorfl (Dorfl, 1982). **(b)** Vibrissa motion (blue), breathing (red), and intrinsic (green) and extrinsic (black) ∇EMG activity during whisking and sniffing. **(c)** The same activity during whisking and mixed basal respiration and sniffing.

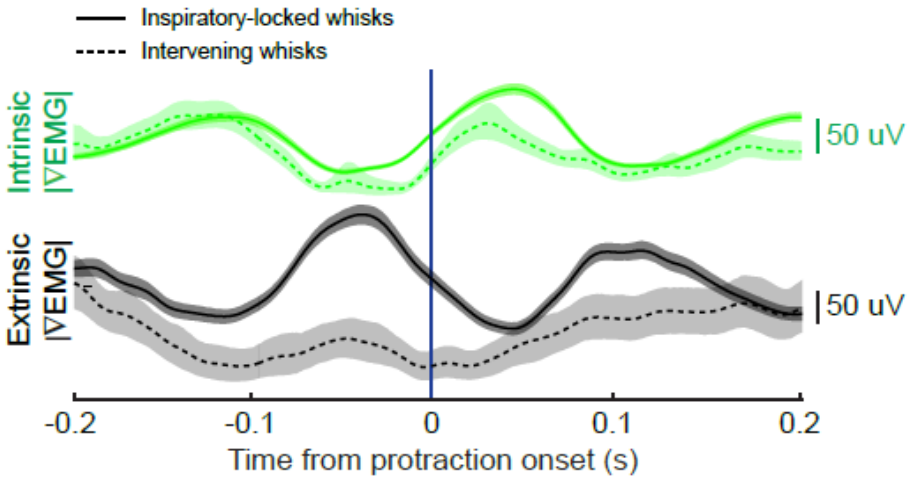


**Figure 3.8. Cross-correlation between EMG activity and vibrissa movement.**

Cross-correlation of the smoothed |∇EMG| for intrinsic (green) and extrinsic (black) muscles with the protraction onset times for inspiratory and intervening whisks. Solid traces represent correlation with inspiratory whisks and dashed traces represent correlation with intervening whisks. Bands represent 95 % confidence intervals.

## Identification of a region that signals whisking

The coordination of whisking with breathing and the resetting of whisking by inspiration suggests that a vibrissa pattern generator is driven by respiratory nuclei, which are known to lie in the ventral medulla (Smith et al., 2009). Further, the difference in the basal respiration and whisking patterns provides a signature to discriminate between breathing and potential whisking neuronal centers (**bottom, Fig. 3.1b**). We recorded multiunit spiking activity in the area of the preBötzinger, Bötzinger and adjoining ventral and parafacial respiratory regions (**Fig. 3.9a-c**) identified each recording site by subsequent reconstruction (**Fig. 3.9d,e)**. The functional attributes of each multi-unit signal were assigned as inspiratory/protraction (32 units), expiratory/retraction (29 units), or whisking (5 units) based on their patterns of activity during whisking and sniffing (**Fig. 3.9f**). We find that units that have a similar phase preference also lie in close spatial proximity (**Fig. 3.9d-f**). Specifically, multiunit activity in the region of the preBötzinger complex and the ventral respiratory group occurred in phase with inspiration and protraction of inspiratory-locked whisks (**Fig. 3.9a,** red dots in **Fig. 3.9d,e**). Multiunit activity in the region of the Bötzinger complex and the parafacial respiratory group occurred in approximate phase with expiration and retraction of inspiratory-locked whisks (**Fig. 3.9b,** yellow dots in **Fig. 3.9d,e**). In neither case did the activity track the intervening whisks. In contrast, we located a subset of units

in the intermediate band of the reticular formation (IRt) whose spiking was tightly phase-locked to the protraction of both inspiratory-locked and intervening whisks (**Figs. 3.9c** & **3.10**). These units are potential pre-motor drivers of the intrinsic muscles that serve rhythmic whisking (**Fig. 3.7a**) and are henceforth referred to as "whisking units". They are located in the ventral part of the IRt, medial to the *ambiguus* nucleus *pars semicompacta* and near the preBötzinger complex (blue dots in **Fig. 3.9d,e**). We denote this new region the vibrissa zone of the IRt (vIRt).

The phase of the neuronal activity of the above three classes of rhythmically spiking units with respect to behavior was compared with that of the intrinsic (green bars in **Fig. 3.9f**) and *nasolabialis* |∇EMG| (black bars in **Fig. 3.9f**). First, there is a slight phase lead between the majority of whisking units and the intrinsic muscles. Second, the activity of inspiratory/protraction units tends to lead that of the whisking units, which is particularly robust during near synchronous whisking and sniffing (**Fig. 3.9f**). These data are consistent with inspiratory/protraction units in or near the preBötzinger complex resetting a group of rhythmic whisking units in the vIRt to initiate protraction. In addition, expiratory/retraction units exhibit a phase shift between sniffing and basal respiration that is paralleled by a concurrent shift in activation of the *nasolabialis* muscle (**Fig. 3.9f**).

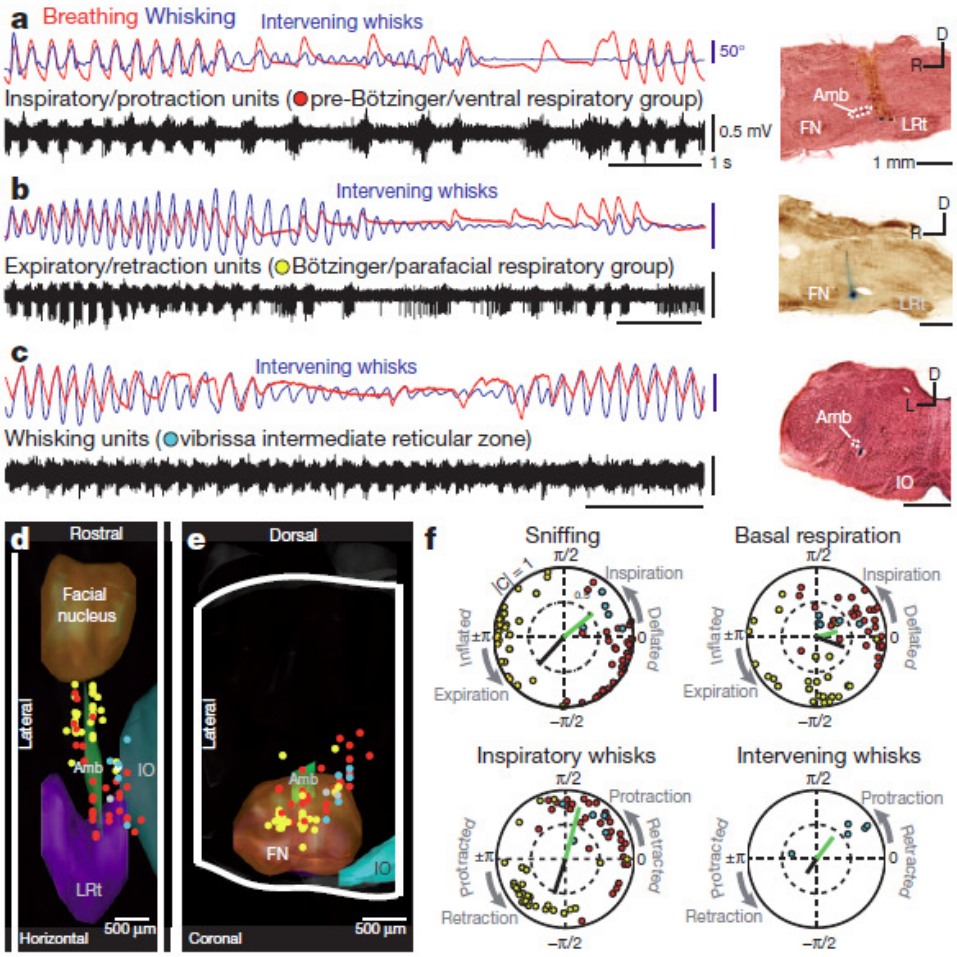


**Figure 3.9. Activity in medullary respiratory centers during breathing and whisking**.

**(a)** Concurrent recordings of breathing (red), whisking (blue), and multiunit activity (black) in the preBötzinger complex. The location of the recording site is labeled with Chicago sky blue and is shown in a sagittal section counterstained with neutral red. LRt denotes the lateral reticular nucleus, FN the facial nucleus, Amb the *ambiguus* nucleus, and IO the inferior olive. **(b)** Multiunit spike activity in the Bötzinger complex. The section is counterstained for cytochrome oxidase. **(c)** Multiunit spike activity in the vibrissa zone of the intermediate reticular formation. The section is counterstained with neutral red. **(d,e)** The recording sites for all data imposed on a three dimensional reconstruction of the medulla. Whisking units are located dorsomedially to the preBötzinger complex in the IRt. Two units whose spiking had no relation to breathing or whisking are shown in white. **(f)** Polar plots of the magnitude (0 to 1 radial coordinate) and phase (angular coordinate) of the coherence between multiunit spiking activity and measured behaviors at the peak frequency for each behavior, *i.e.*, 2 Hz for basal respiration, 6 Hz for sniffing and inspiratory whisks, and 8 Hz for intervening whisks (**Fig. 1c**). Only units with significant coherence ($p < 0.01$) are shown and correspond to the point in panels d to f. The coherence between the measured behavior and the ∇EMG of the intrinsic muscles (green bar) and *Nasolabialis* muscle ∇EMG (black bar) are shown.

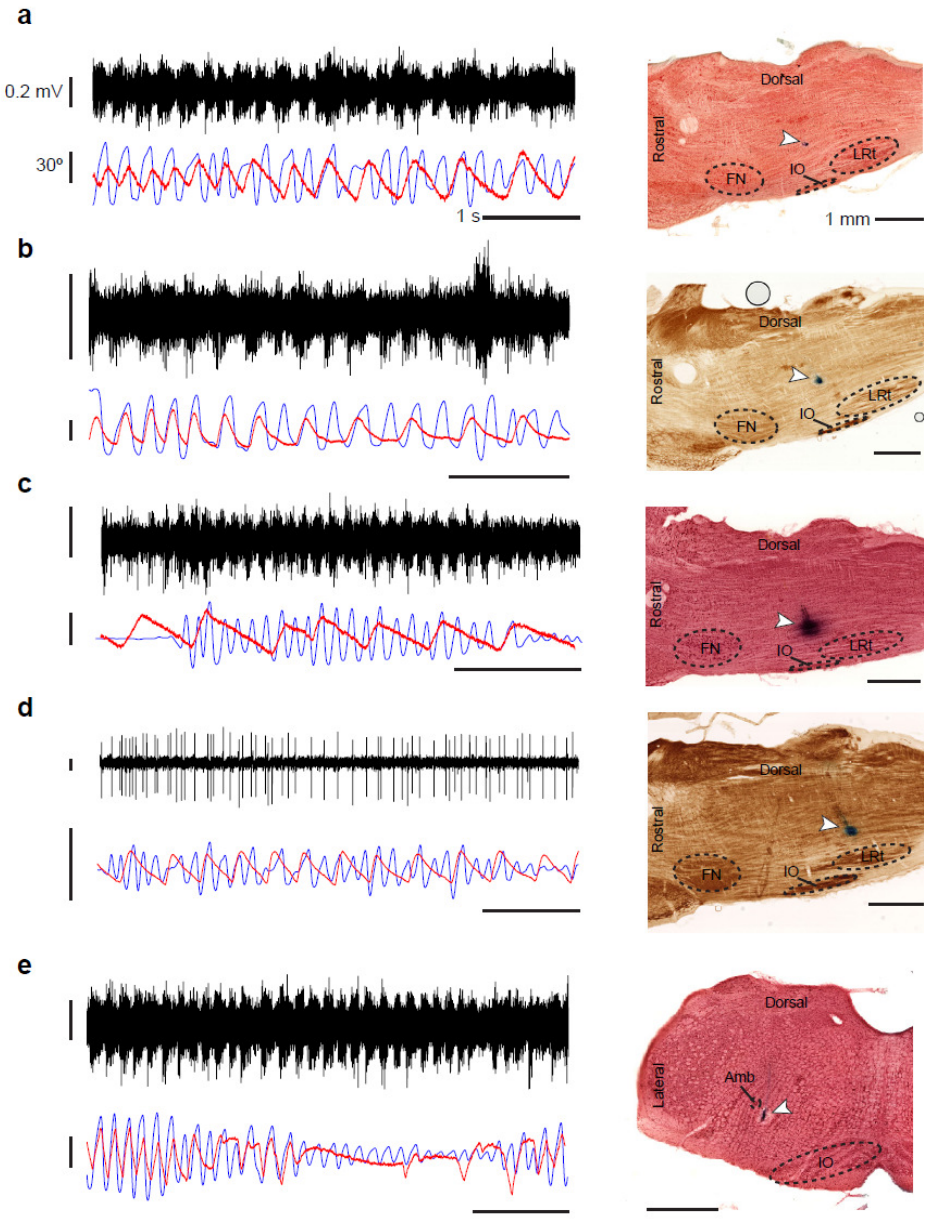


**Figure 3.10. Compendium of spiking records from all vlRt whisking units during breathing and whisking in alert rats.**

**(a-e)** Concurrent recordings of breathing (red), whisking (blue), and multiunit spike activity (black) in the lRt for all whisking units. The location of the recording site labeled with Chicago sky blue is shown on the right a sagittal section (panels a to d) or coronal section (panel e) counterstained with neutral red (panels a, c, and e) or cytochrome oxidase (panels b and d). Landmarks, including the facial nucleus (FN), inferior olive (IO), lateral reticular nucleus (LRt), and ambiguus nucleus (Amb), are outlined in black. Arrowheads mark the labeled recording site. Scale bars are as defined in panel a.

## Activation of cells in the vIRt induces whisking

The hypothesis that whisking in the vIRt constitute the oscillator for whisking predicts that activation of this region will lead to prolonged autonomous activity. Indeed, microinjection of the glutamate receptor agonist kainic acid in the vicinity of the vIRt is a salutary means to induce prolonged rhythmic muscular activation (**Figs. 3.11a & 3.12**) and coordinated vibrissa protraction (**Fig. 3.13**), near 10 Hz, in the lightly anesthetized head-fixed rat (**Fig. 3.11b)**. The frequency of whisking decreases over time, and the amplitude increases, as the effect of anesthesia declines, while the frequency of breathing remains constant (**Fig. 3.11b**). This implies that the chemical activation is sufficiently strong to decouple rhythmic protraction from breathing (**Fig. 3.14**). Quantitatively, the modulation depth of protraction with breathing was less than 0.01 and insignificant for all but one case (11 epochs across three rats), compared with 0.08 for basal respiration and 0.26 for sniffing in awake animals. Lastly, consistent with the conclusions from the EMG studies (**Fig. 3.7c**), the mystacial pad moves in synchrony with breathing (**Fig. 3.11a**).

Chemical activation of rhythmic whisking, with a frequency incommensurate with that of breathing, provides an opportunity to stably record from units whose firing times were coherent with rhythmic protraction

(inserts, **Fig. 3.11c**). We identified units that spiked in synchrony with protraction, as in the case of units identified during intervening whisks in the behaving animal (**Fig. 3.9c-f & 3.10**), as well as units that spiked in anti-phase (32 units across four rats) (**Fig. 3.11c**). Microinjection of Neurobiotin™ at the recording site (**Fig. 3.11d**) resulted in anterograde labeling of axon terminals in the ventrolateral part of the facial nucleus, where motoneurons that innervate the intrinsic muscles are clustered (**Fig. 3.11e**). The recording sites were located medial to the *ambiguus* nucleus (**Fig. 3.11f**), similar to the region localized by recording in behaving animals (**Fig. 3.9d, e**).

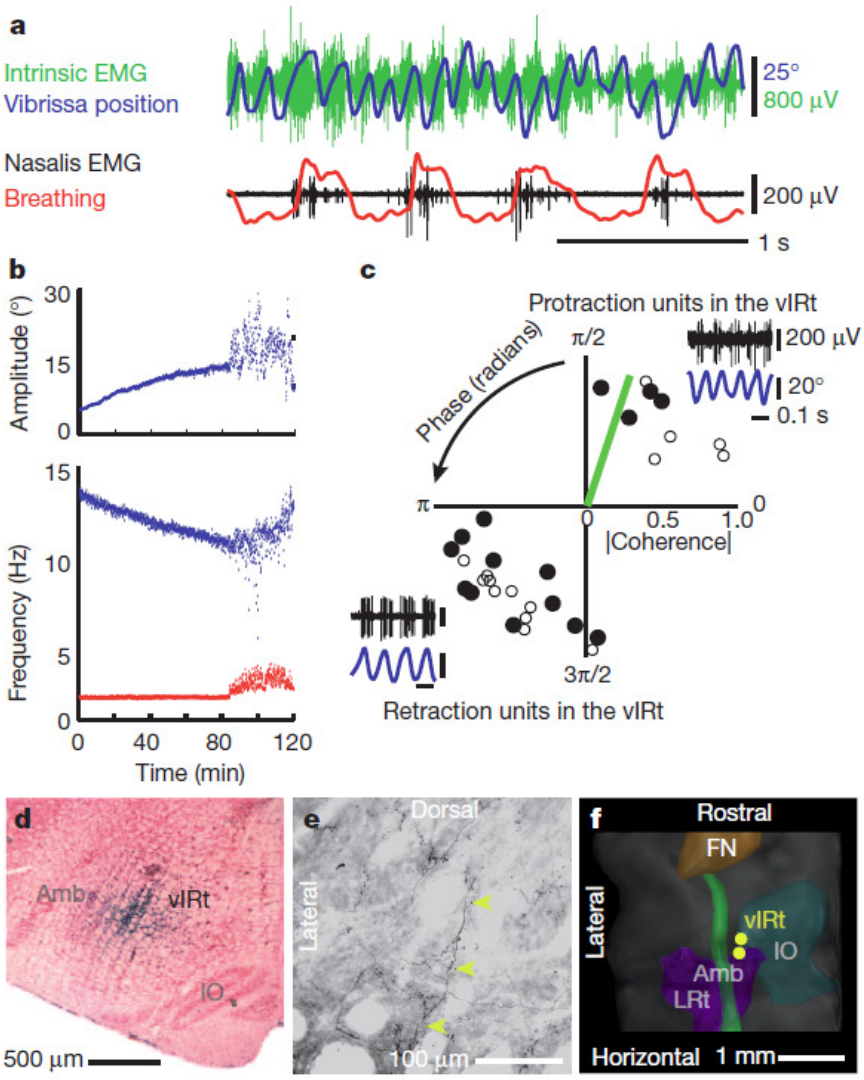


**Figure 3.11. Injection of kainic acid in the medullary reticular formation induces whisking.**

**(a)** Vibrissa motion (blue), breathing (red), intrinsic (green) and extrinsic (black) ∇EMG. **(b)** Time-course of kainic-acid induced whisking. Instantaneous peak-to-peak amplitude (top) and frequency (bottom) of vibrissa motion (blue) and frequency of breathing (red). The animal starts to wake by 100 minutes. **(c)** Polar plots of the coherence between spiking activity and vibrissa motion at the peak frequency of whisking (8.8 Hz median); only units with statistically significant coherence (32 of 33 units, $p < 0.01$) are shown. Open circles represent multiunit activity and closed circles represent single units. The green bar represents the coherence of the ∇EMG for the intrinsic muscle (panel b) with vibrissa motion. (Inserts) Spiking activity of neuronal units in the vIRt (black) in relation to vibrissa motion (blue). **($d_1$)** One of the locations that corresponded to a units in panel c, labeled via ionophoretic injection of Neurobiotin™ through the recording electrode. **($d_2$)** Axons (yellow arrows) and terminals in the ventral lateral division of the facial nucleus labeled after Neurobiotin™ injection at the recording site in panel $d_1$. **(e)** Three dimensional reconstruction of the labeled recording locations for the units in panel d.

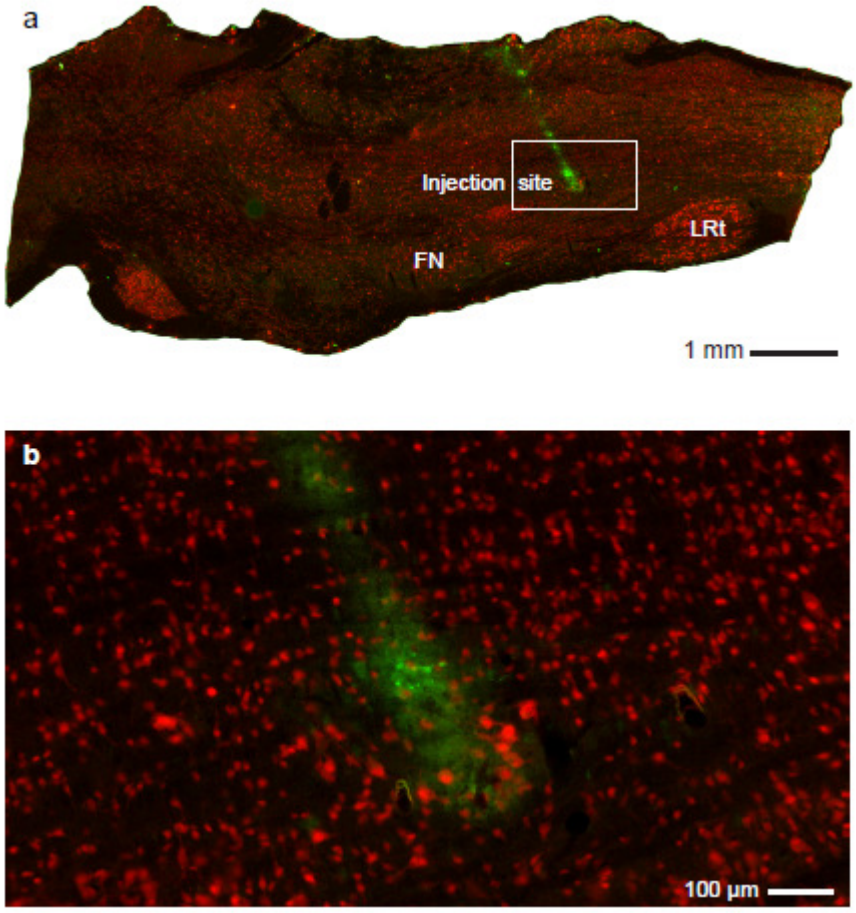


**Figure 3.12. Kainic acid injection site and surrounding brainstem tissue.**

Injection at this site resulted in sustained, coordinated ipsilateral whisking. Whisking appeared normal the day following the injection and thereafter (data not shown). **(a)** The injection site is labeled with biotinylated dextran amine, and the tissue is counterstained with an antibody against neuronal nuclear protein after three days of recovery. **(b)** Magnified view of the white box in panel a. Cells around the injection site remain intact.

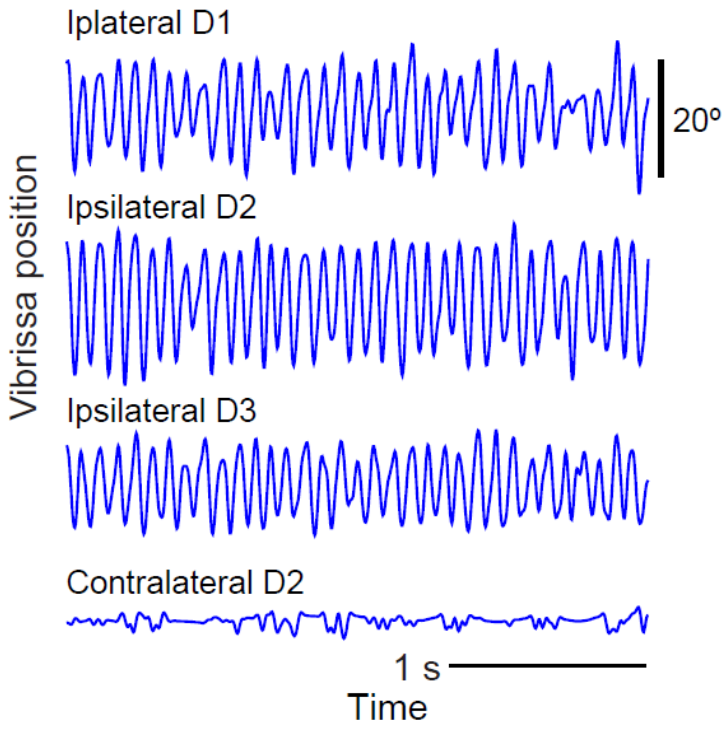


**Figure 3.13. Coordinated movement of ipsilateral vibrissae following kainic acid injection in the vicinity of the vIRT**

Simultaneously recorded motion of three neighboring vibrissae, i.e., D1, D2 and D3, on the ipsilateral side, and the D2 vibrissa on the contralateral side, after activation of whisking by kainic acid injection.

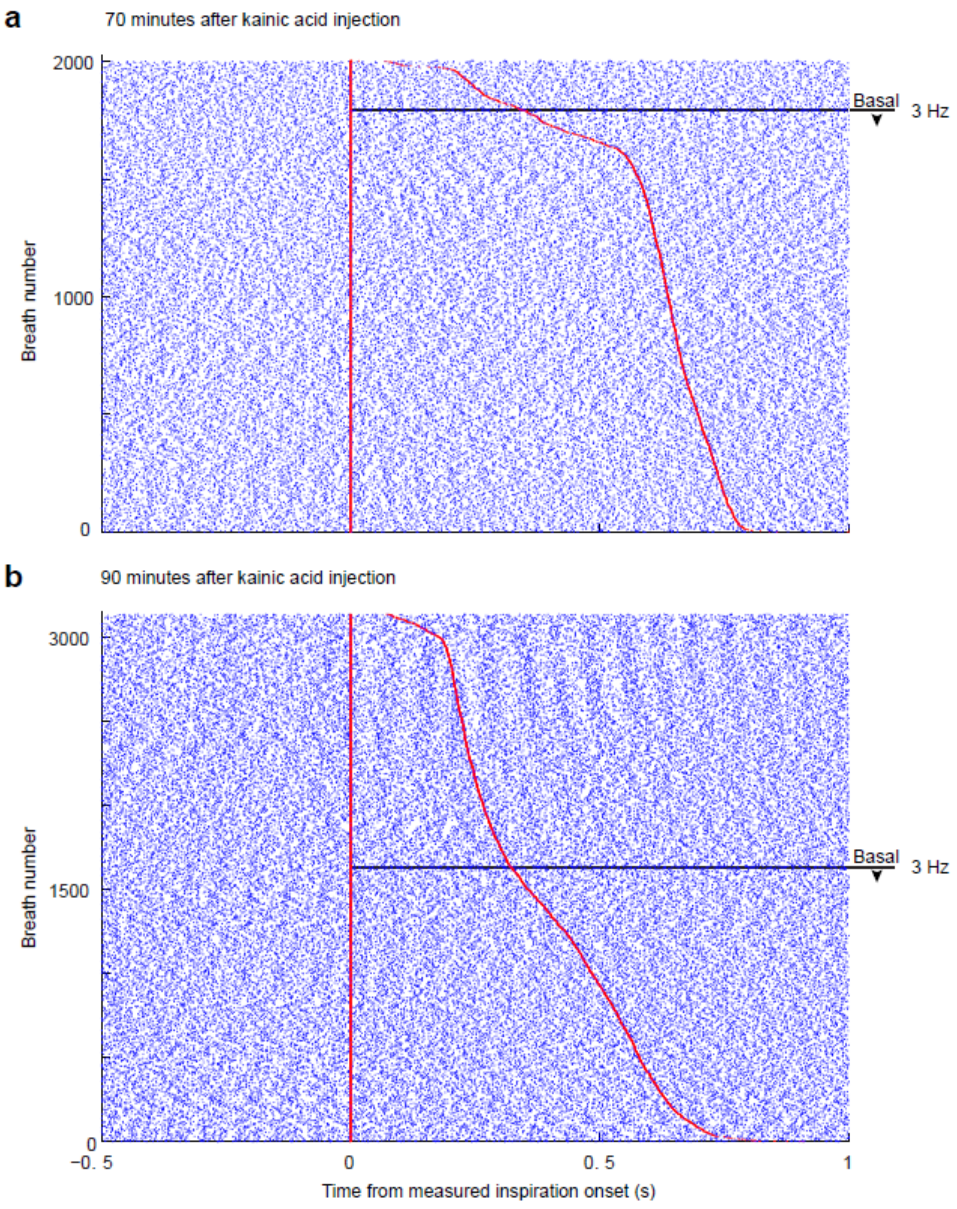


**Figure 3.14. Lack of coordination of kainic acid-induced whisking and breathing.**

Temporal relationship between whisking and breathing events for kainic acid induced whisking in the lightly anesthetized rat. Raster plots of inspiration (red dots) and protraction (blue dots) onset times relative to each breath are sorted by the duration of the breath. **(a)** At basal respiratory frequencies, correlation with event times was low and significant in only one of eleven different twenty minute epochs ($p < 0.01$) across three animals; shown here is this single case. **(b)** The correlation of the remaining ten out of the eleven epochs was found to be statistically insignificant ($p > 0.05$); one of the ten cases is shown here.

## Lesion of the vIRt abolishes ipsilateral whisking

The above results provide evidence for the sufficiency of neurons in the vIRt to drive rhythmic protraction. We now consider the necessity of the vIRt for rhythmic motion and test if a lesion to this zone suppresses whisking. First, small electrolytic lesions of the IRt medial to the *ambiguus* nucleus abolish whisking on the side of the lesion, while whisking persists on the contralateral side (**Fig. 3.15a**). Neither basal respiration nor sniffing is affected by the lesion. Further, the suppression of whisking appeared permanent as no recovery was observed up to 10 days after the lesion. Qualitatively similar results were found with ibotenic acid or Sindbis viral lesions (**Fig. 3.16**), which indicates that the abolition of whisking is not attributable to severed axons of passage.

The spatial specificity of the ablations was assessed by lesioning various regions in the pons and medulla in an ensemble of animals (head-fixed: three electrolytic; free-ranging: 16 electrolytic, one ibotenic acid, and five Sindbis). Lesions made in the dorsal part of IRt, in the parvocellular reticular formation, in the paragigantocellular reticular formation, or in the caudal part of the medullary reticular formation excluding the preBötzinger complex, only minimally affected whisking (**Fig. 3.15d-f**). Critically, lesions within the vIRt that were as small as 200 µm in diameter were sufficient to

severely impair whisking on the ipsilateral side (**Figs. 3.15a,e,f**). We conclude that units in the vIRt play an obligatory role in the generation of whisking.

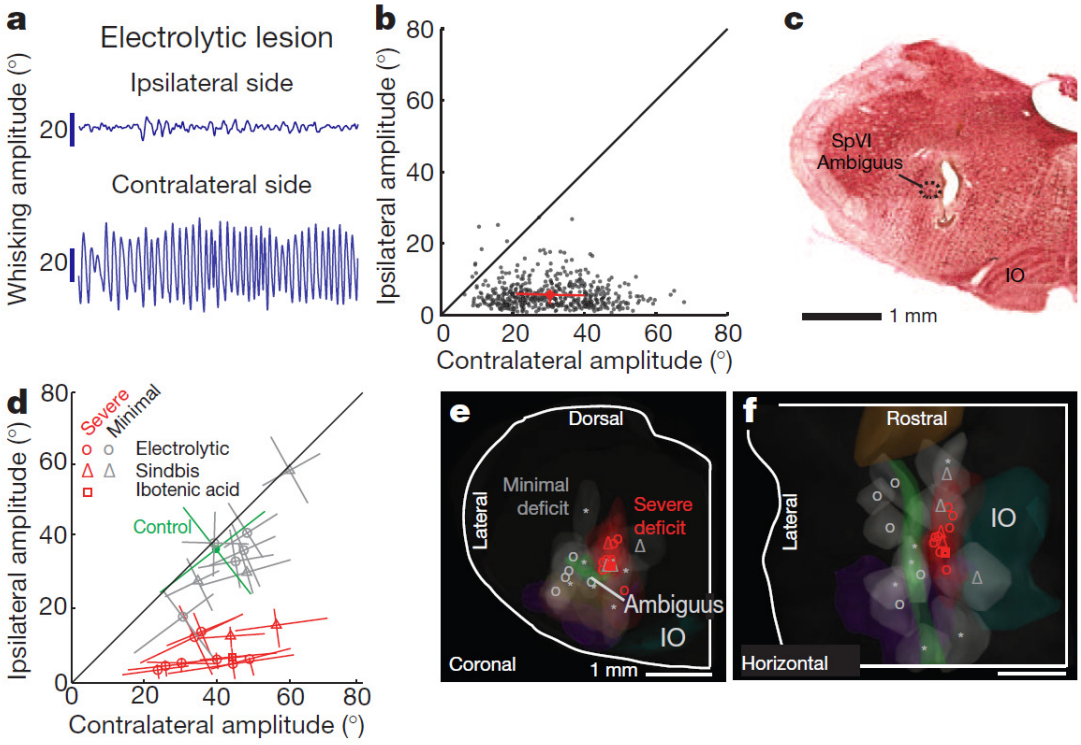


**Figure 3.15. Lesion of the vlRt impairs ipsilateral whisking.**

**(a)** Example of whisking bout following an electrolytic lesion. **(b)** Scatter plot of ipsilateral versus contralateral whisk amplitudes reveals the functional completeness of the lesion; each dot represents one whisk, circle represents the mean, and lines represent the inter-quartile range. **(c)** Histological analysis confirms that the lesion is in the vlRt; coronal section stained with neutral red. **(d)** Composite results for a subset of lesions (19 rats) where vibrissa position was tracked; lines are central quartiles. Symbols correspond to the method of lesion. Results were scored by the severity of the ipsilateral whisking deficit: severe (red), for > 50 % reduction as in panels a and b, or minimal (gray), < 50 % reduction. Whisking of a non-lesioned control rat is shown in green. **(e-f)** Lesion sites were mapped onto a three dimensional reconstruction of the medulla and selected anatomical substructures, as in **Figure 3.11f**. The lesion centroids are denoted with the symbols in panel d and have a median volume of 0.2 µL. Sites marked with an asterisk (six rats) represent additional lesions not shown in panel d where animals were observed to have minimal whisking deficits by visual inspection.

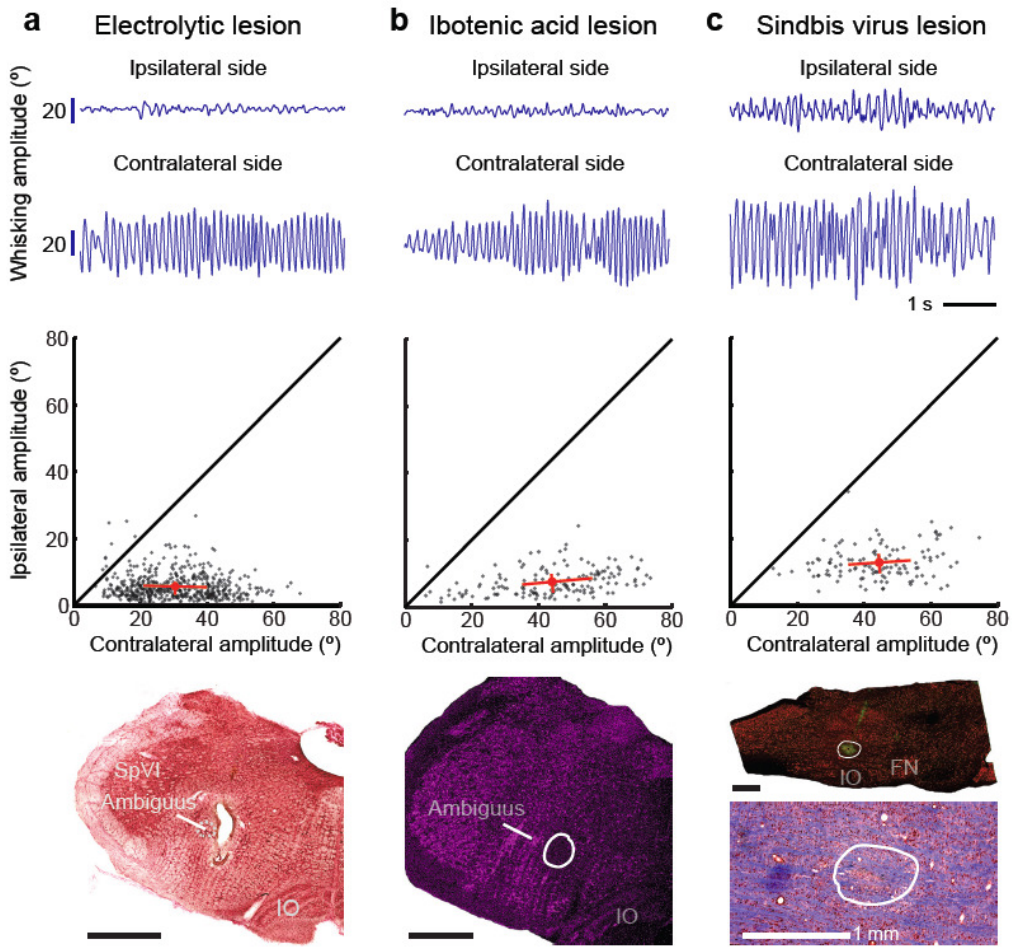


**Figure 3.16. Three different methods of lesion in the vIRt that result in ipsilateral whisking impairment**

**(a)** Example of whisking bout following an electrolytic lesion in the vIRt (top). As in Figure 5, a full analysis of ipsilateral versus contralateral whisk amplitudes reveals the functional completeness of the lesion (middle; each dot represents one whisk, circle represents the mean, and lines represent the inter-quartile range). Histological analysis confirms that the lesion is in the vIRt; coronal section stained with neutral red (bottom). This panel is a replication of Figure 5a, included here for comparison to other lesion methods. **(b)** Example of a whisking bout after an excitotoxic lesion in the vIRt made by pressure injection of ibotenic acid (top). The analysis of whisking amplitudes (middle) is as in panel a. The histological section (bottom) shows the extent of neuronal degeneration after staining with α-NeuN. **(c)** Example of a whisking bout after a lesion in the vIRt made by microinjection of a Sindbis viral vector that codes for the expression of green-fluorescent protein (top). The analysis of whisking amplitudes (middle) is as in panels a and b, and the histology (bottom) is as in panel b. We further show an adjacent 30 µm section stained with Luxol fast blue to label myelin and neutral red to label Nissl bodies; the outlined region corresponds to the location where there was a loss of cells as revealed by the α-NeuN staining.

## Anatomy of the circuit for rhythmic whisking

The behavioral (**Figs. 3.1, 3.7**) and physiological data (**Figs. 3.9, 3.11, 3.15**) suggest that cells in inspiratory nuclei reset an oscillatory network of whisking units in the vIRt that can drive protraction of the vibrissa concurrent with each inspiration. We used tract tracing methods to assess this hypothesized connection. Injections of biotinylated dextran amine (BDA) into the preBötzinger complex, identified by the phase relation of units relative to breathing (two rats) (**Fig. 3.17a, top**), led to dense anterograde labeling in the IRt medial to the *ambiguus* nucleus (**Fig. 3.17a, middle**), including a number of axon terminals (**Fig. 3.17a, bottom**). This corresponds to the same region in which we observed whisking units (**Figs. 3.9d,e** & **3.11d-f**) and where lesions extinguished ipsilateral whisking (**Fig. 3.15e-f**). These results support a direct connection from the preBötzinger complex to the vIRt.

We next delineated the projections from neurons in the vIRt to facial motoneurons (**Fig. 3.11e**). Neurobiotin™ (three rats) or Fluoro-Gold™ (two rats) was injected in the lateral aspect of the facial nucleus (**Figs. 3.17b**, **top** & **3.18**). We observed a cluster of retrogradely labeled cells in the IRt that lie medial to the *ambiguus* nucleus (**Fig. 3.17b**, **bottom**). A detailed map of the location of cells that were retrogradely labeled from an injection in the lateral aspect of the facial nucleus (1300 cells in one rat) reveals a rostrocaudal

band of cells in the IRt; we identify this region as vIRt (**Figs. 3.17c** & **3.18**). *In toto*, these and previous (Isokawa-Akesson and Komisaruk, 1987; Takatoh et al., 2013) patterns of neuronal labeling in the IRt support a direct connection from the vIRt to the facial nucleus and substantiate the role of the vIRt as a premotor nucleus.

The neurotransmitter content of neurons in the vIRt that project to the facial motoneurons was assessed by the combination of retrograde labeling and *in situ* hybridization (Furuta et al., 2008) (**Figs. 3.19 & 3.20**). We find a fractional contribution of 0.12 ± 0.02 (mean ± SE; 259 cells in 3 rats) glutamatergic, 0.85 ± 0.02 (303 cells) glycinergic, and 0.53 ± 0.03 (237 cells) Gaba-ergic neurons. These data support either monosynaptic excitatory transmission via glutamate receptors and via glycine NR1/NR3b receptors (Chatterton et al., 2002) or monosynaptic inhibitory transmission via glycine and Gaba receptors in the presence of a tonic excitatory drive.

The involvement of the *nasolabialis* muscle during inspiratory-locked whisks, but not intervening whisks, suggests that retraction of the mystacial pad is controlled by units in the Bötzinger/parafacial complex (**Figs. 3.7c**, **3.9b** & **3.11a**). These units are phase-locked with expiration (**Figs. 3.9f**). The Bötzinger/parafacial region is in close proximity to the facial nucleus(Smith et al., 2009) and is reported to modulate the activity of facial motoneurons

(Onimaru et al., 2006; Pagliardini et al., 2011) that drive the *nasolabialis* muscle (Klein and Rhoades, 1985). In support of a direct connection from the Bötzinger complex to facial motoneurons, we observed that the map of retrogradely labeled projections to the facial nucleus shows strong labeling (**Fig. 3.17c**). In addition, small injections of Neurobiotin™ that were made in the parafacial region (three rats) (**Fig. 3.17d, top**) labeled of axon terminals specifically in the dorsolateral part of the facial nucleus, where motoneurons that innervate the extrinsic muscles are clustered (**Fig. 3.17d, bottom**). This result supports the conclusion that retraction of the vibrissae is at least partially mediated by neurons in Bötzinger/parafacial region.

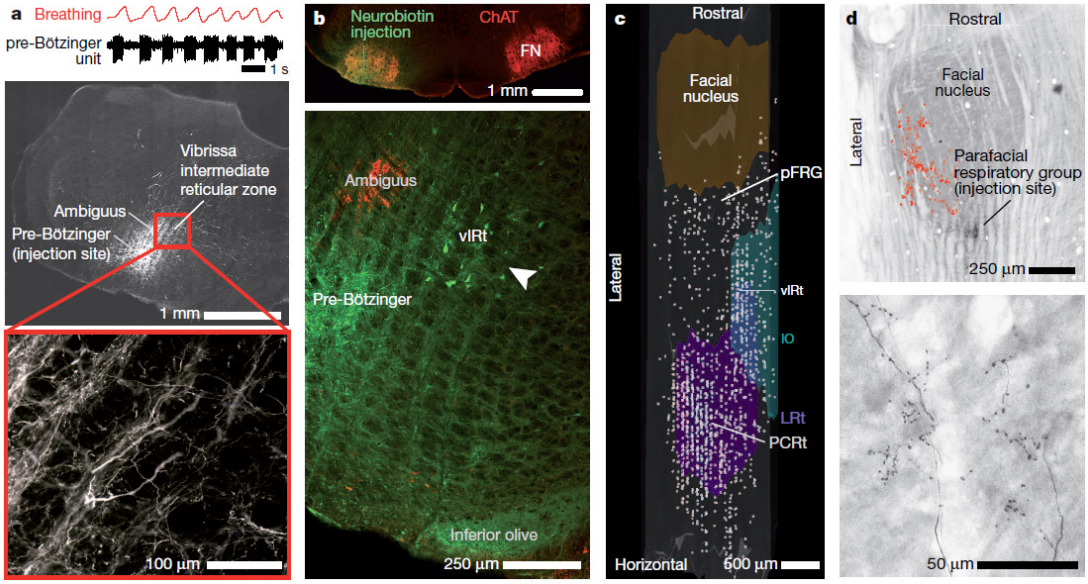


**Figure 3.17. Anatomical evidence for connections between respiratory and whisking zones.**

**($a_1$-$a_3$)** Recording of a single inspiratory unit in the preBötzinger complex, together with breathing (panel a1). Injection of biotinylated dextran amine through the same pipette (panel a2) leads to anterograde labeling of axons and terminals in the vIRt (panel $a_3$); panels $a_2$ and a3 are coronal sections. **($b_1$,$b_2$)** Injection of Neurobiotin™ (green) into the facial nucleus (FN) (panel $b_1$) retrogradely labels neurons in the vIRt (panel $b_2$; white arrow). Labeling with □-choline acetyl-transferase highlights motoneurons in the facial and *ambiguus* nuclei (red). **(c)** Compendium of the locations of cells that were retrogradely labeled from the facial nucleus with Neurobiotin™, superimposed on a three dimensional reconstruction of the medulla. Note labeled cells in the vIRt, located between coronal planes -12.5 and -13.0 mm relative to bregma, that span ~ 200 µm along the lateral-medial axis. pFRG denotes the parafacial respiratory group and PCRt the parvocellular reticular nucleus. **($d_1$,$d_2$)** Injection of Neurobiotin™ into the parafacial region labels terminals in the dorsolateral aspect of the facial nucleus (panel e1). Individual axons and terminals are seen in panel e2, while a compendium across three consecutive sections is summarized in panel e1 (red dots). Horizontal sections stained for cytochrome oxidase.

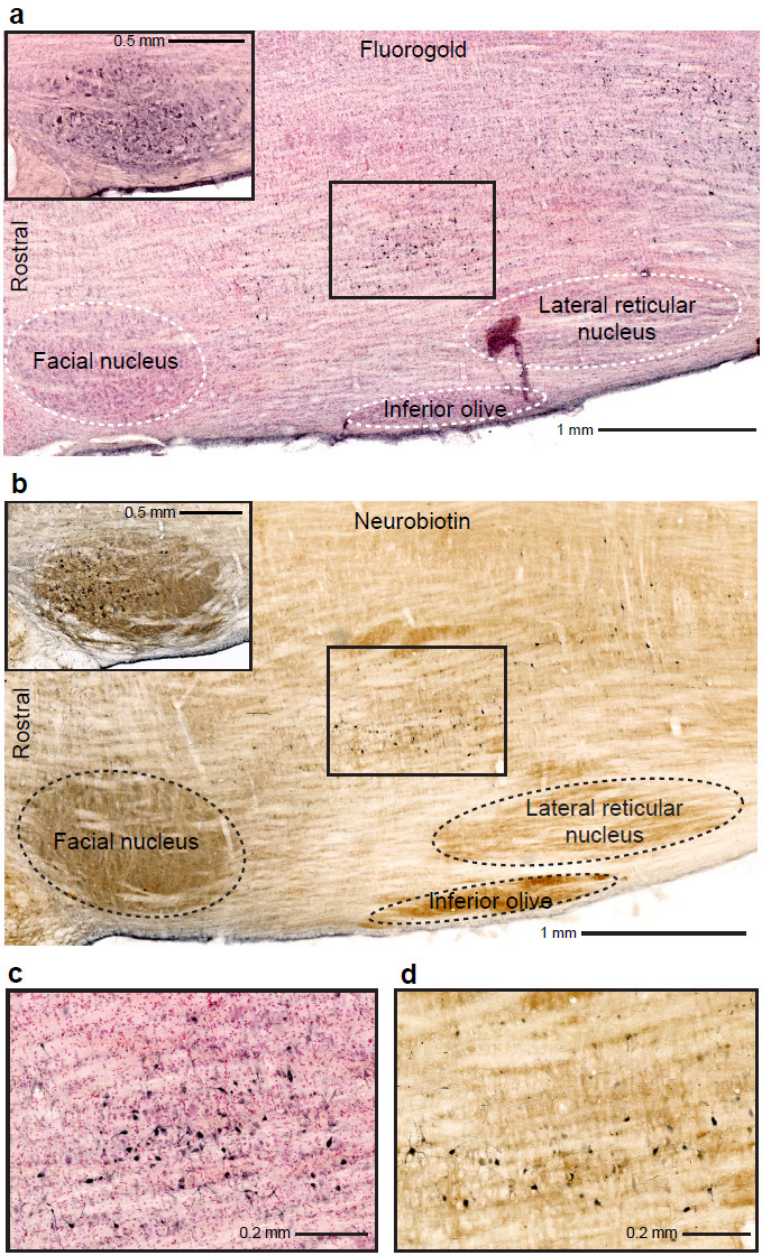


**Figure 3.18. Fluoro-Gold™ and Neurobiotin™ retrogradely label vlRt cells that project to the facial motor nucleus.**

**(a)** Cells are retrogradely labeled in vlRt and PCRt following an injection of Fluoro-Gold™ in the lateral aspect of the facial nucleus (inset). Sagittal section. **(b)** A similar pattern of labeling is observed after injection of Neurobiotin™ into the lateral facial nucleus (inset). **(c-d)** Magnification of the vlRt regions outlined in panels a and b, respectively.

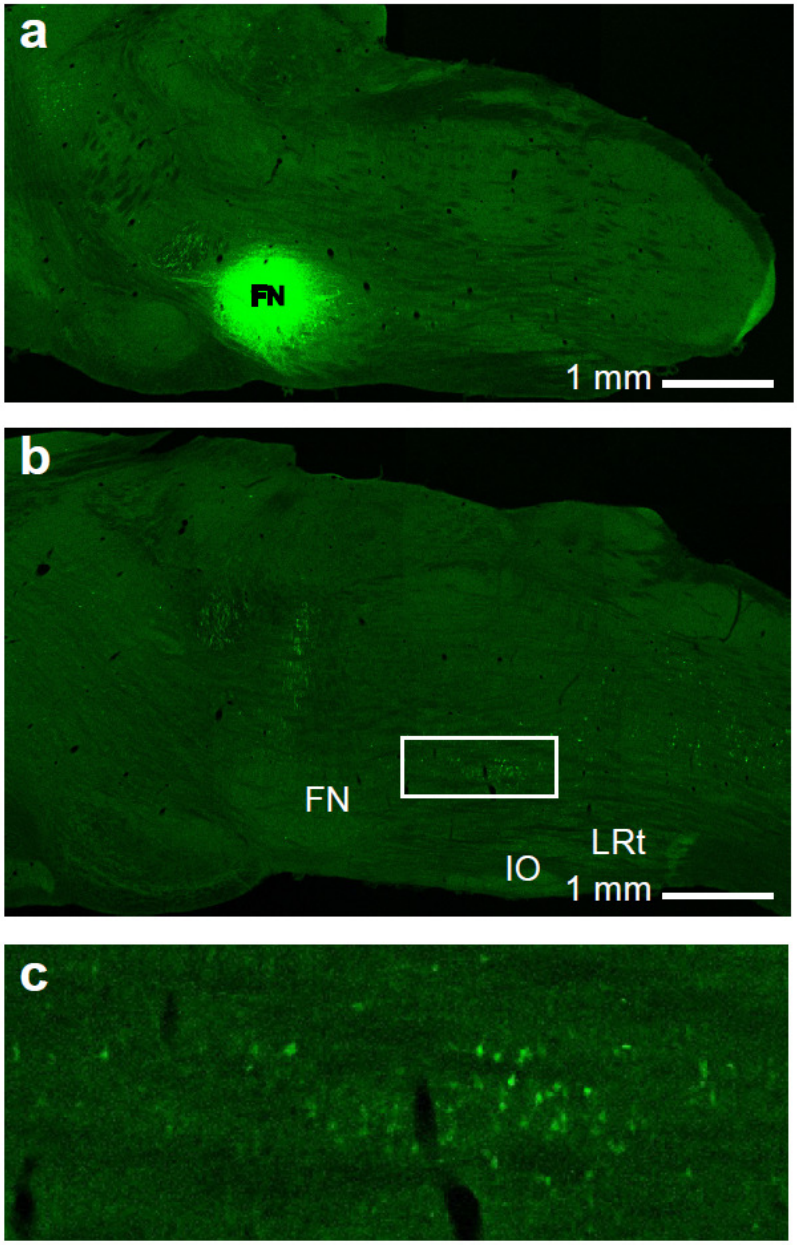


**Figure 3.19. Fluoro-Gold™ retrograde labeling for characterization of the neurotransmitter phenotypes of facial pre-motoneurons.**

**(a)** Example of a Fluoro-Gold™ injection site in the lateral facial nucleus. **(b)** Region in which counts of cells double-labeled with Fluoro-Gold™ and in situ hybridization for vGluT2, GlyT2, or GAD67 were performed. **(c)** Magnified view of the cell counting region in panel b.

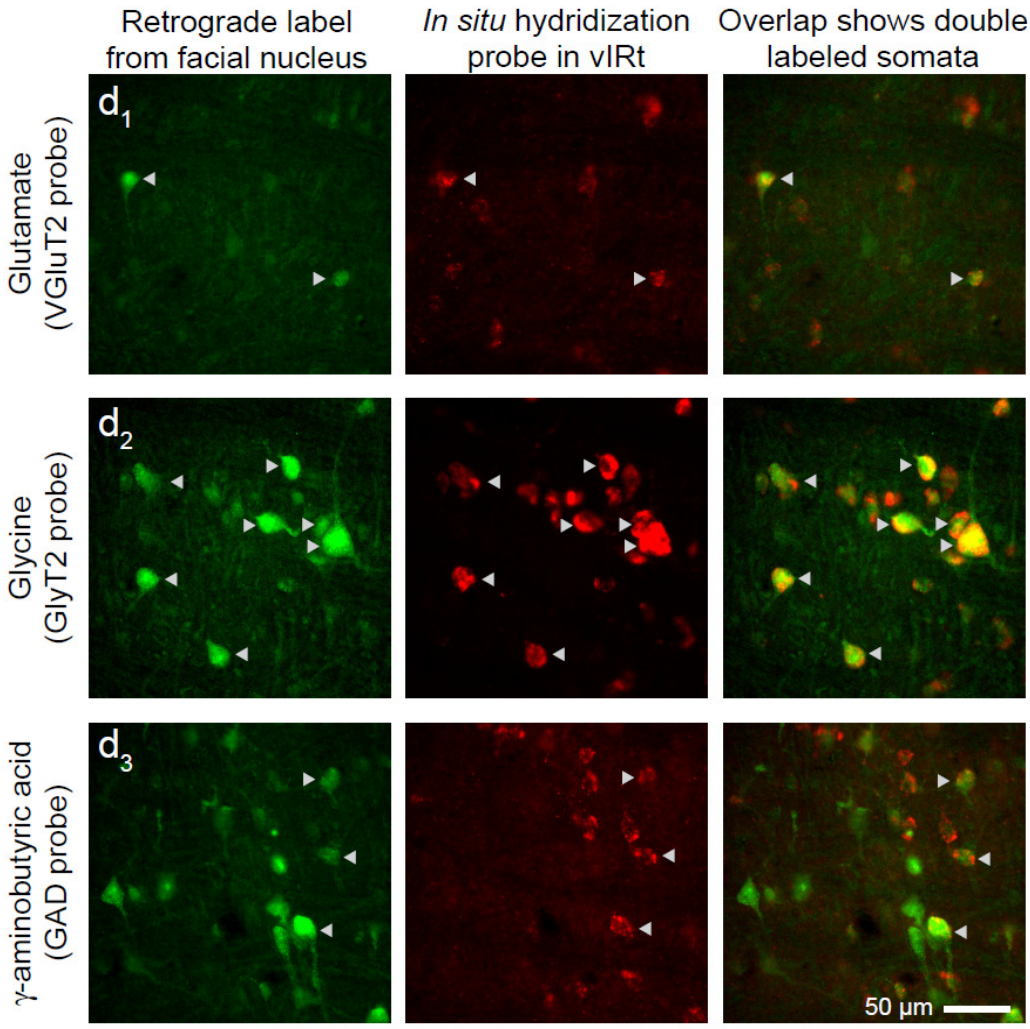


**Figure 3.20. Determination of the neurotransmitter phenotype of neurons that project from the vlRt to the facial motoneurons that drive protraction of the vibrissae.**

Neurons were labeled via retrograde transport of Fluor-Gold™ from the lateral aspect of the facial nucleus (left column) and the tissue was processed for in situ hybridization (middle column) with probes for glutamate (top row), glycine (middle) and g-aminobutyric acid (bottom). The merged images (right column) reveal double-labeled cells, denoted with arrows.

## *3.4 Discussion*

We have identified units in a newly defined zone of the intermediate band of the reticular formation in the medulla, denoted vIRt, that oscillate in phase with motion of the vibrissae (**Fig. 3.21a**). This zone functions as the premotor pattern generator for rhythmic whisking and is part of a larger circuit whereby cells in nuclei that are obligatory for inspiration (Bouvier et al., 2010; Gray et al., 2010; Tan et al., 2008) reset the phase of vIRt units with each breath (**Fig. 3.21b**). Thus, whisking during sniffing is effectively driven on a cycle-by-cycle basis by the inspiratory rhythm generator, while intervening whisks between successive inspirations result from oscillations of the whisking units in vIRt. Retraction of the vibrissae by extrinsic muscles in the mystacial pad is likely controlled by nuclei that lie immediately caudal to the facial nucleus and are active during expiration.

Our results bear on the generation of other rhythmic orofacial behaviors, for which licking is particularly well described. First, tongue protrusions are coordinated with the respiratory cycle (Welzl and Bures, 1977). Second, the hypoglossal premotoneurons are concentrated in the IRt dorsomedially to the preBötzinger complex (Koizumi et al., 2008; Travers et al., 1997), and are driven by bursts of spikes that are locked to inspiration (Ono et al., 1998). Third, the output of units in the hypoglossal IRt zone locks to rhythmic licking

(Travers et al., 2000). Lastly, infusion of an inhibitory agonist into the IRt blocks licking (Chen et al., 2001). These past results are consistent with a model in which preBötzinger units reset the phase of bursting in a network of hypoglossal premotor neurons in the IRt zone, in parallel with our circuit for whisking (**Fig. 3.21b**). Serotonergic and other modulatory inputs may serve to gate and accelerate all of these rhythms (Depuy et al., 2011; Doi and Ramirez, 2008; Harish and Golomb, 2010; Hattox et al., 2003; Van der Maelen and Aghajanian, 1980).

The common architecture of the control circuits for whisking (**Fig. 3.21b**) and licking (Travers et al., 1997) supports the primary role of breathing in the coordination of orofacial behaviors. In the absence of interruptions, such as from swallowing (Saito et al., 2003) or aversive stimuli (Lawson et al., 1991), we propose that the inspiratory pattern generator broadcasts a master clock signal to the various patterning circuits throughout the IRt and nearby zones (**Fig. 3.21c**). Coordination by this breathing clock can ensure that these rhythmic behaviors, which share muscle groups, do not confound each other. It is a further possibility that the breathing clock serves to perceptually bind olfactory and tactile sensory inputs.

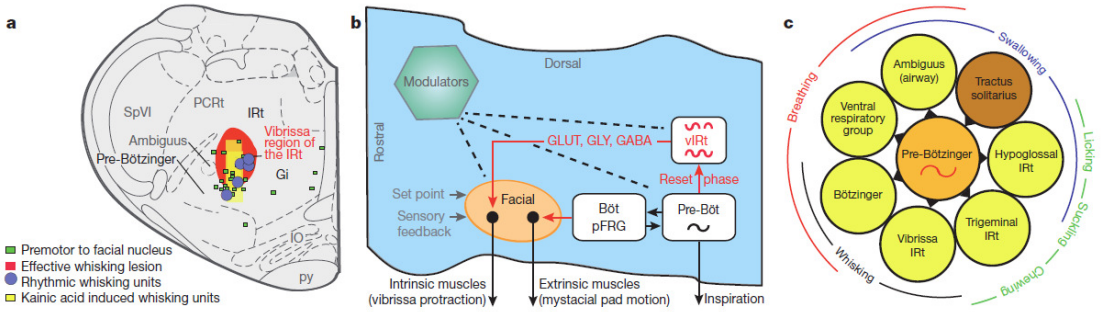


**Figure 3.21. The whisking rhythm generator circuit in the broader context of orofacial behaviors.**

**(a)** Summary of evidence for a rhythm generator in the vibrissa zone of the intermediate band of the reticular formation (IRt; gray). This region contains units that fire in phase with all whisking events in freely behaving animals as well as when whisking is induced by microinjection of kainic acid. This region also contains cells that project to the facial nucleus, and lesions of this area severely disable whisking on the ipsilateral side. **(b)** Model of the medullary circuitry that generates whisking in coordination with breathing. **(c)** Summary of all premotor nuclei (yellow) that are known to receive rhythmic drive from the preBötzinger complex (orange), or conjectured to receive input based on anatomical projections, along with a potential resetting circuit (brown). The nuclei subserve shared oral facial behaviors, as demonstrated here for whisking (black) and breathing (red).

## *3.5 Acknowledgements*

We thank A. Kepecs and F. Wang for sharing unpublished work, and these colleagues along with M. S. Fee, J. L. Feldman, H. J. Karten, P. M. Knutsen, D. W. Matthews and K. Svoboda for discussions. We further thank K. Svoboda for sponsorship of the mouse experiments, M. Agrochao and B. el Jundi for assistance with these experiments, T. Ito and D. L. Oliver for use of their GlyT2 probe, K. K. Baldwin for the gift of the Sindbis viral vector, and K. Yang for assistance with behavioral training. We are grateful to the Canadian Institutes of Health Research (grant MT-5877), the Howard Hughes Medical Institute, the Japan Society for the Promotion of Science (KAKENHI grants 23135519 and 24500409), the National Institutes of Health (grants NS058668, NS066664 and NS047101), and the US-Israeli Binational Science Foundation (grant 2003222).

This chapter follows from work that is currently published in:

Moore JD*, Deschênes M*, Furuta T, Huber D, Smear MC, Demers M, Kleinfeld D.Hierarchy of orofaical rhythms revealed through whisking and breathing. Nature. 497(7448): 205-210 (2013)

This material is included with the generous consent of all authors and permission of the journal. The dissertation author is a primary researcher on this work.

# Chapter 4 – Self-generated vibrissa movement and touch are concurrently represented throughout trigeminal and thalamic nuclei in the behaving rat

Active sensation requires keeping track of external as well as internally-generated sensory events. Here we consider the representation of self-generated whisking in the brainstem trigeminal nuclei and their respective target thalamic nuclei. These thalamic nuclei project to primary somatosensory (S1) cortex where re-afferent whisking and ex-afferent touch signals are known to interact. However, the mechanism by which a re-afferent whisking signal is encoded at the periphery is unknown, and the corresponding anatomical pathway to cortex remains under debate. Therefore, to understand the sensory encoding of self-generated vibrissa movement, we recorded single- and multi-unit activity in freely whisking, head restrained rats from the subcortical trigeminal regions known to provide input to S1 cortex. Units in nuclei comprising the lemniscal pathway, specifically the principal trigeminal nucleus of the brainstem (PrV) and the ventral posterior medial (VPM) thalamus are substantially modulated by whisking on a cycle-by-cycle basis. Units with tactile receptive fields representing the vibrissae as well as units representing the skin or fur around the nose and mouth are also modulated by whisking. In contrast, modulation of units along the paralemniscal pathway, specifically in the rostral division of the spinal

trigeminal nucleus pars interpolaris (SpVIr), the posterior medial (PO) thalamus, and the ventral division of zona incerta (ZIv), is comparatively weak. Our results support the simultaneous representation of self-motion and touch within the lemniscal as opposed to the paralemniscal pathway. Further, lemniscal units corresponding to the skin or fur regions surrounding the vibrissae may signal self-motion of the mystacial pad during whisking independently of vibrissa contact.

## *4.1 Introduction*

Biological sensors report the properties of external stimuli in an animal's environment, as well as stimuli produced by the animal's own movements. Von Host defined these two different types of sensory stimuli as "ex-afference" and "re-afference", respectively (von Holst, 1954). In order to make sense of the world though the use of moving sensors, then, animals must be able to distinguish these two types of sensory stimuli (Cullen, 2004). This can be done either by independently sensing the movement itself, as has been shown in skate (Hjelmstad et al., 1996), or by tracking an "efference copy" of a motor command, as has been demonstrated in mormyrid fish (Bell, 1981) and monkeys (Roy and Cullen, 2001). Rodents too use active movements to sense the external world, through the use of their mystacial vibrissae (Vincent, 1912). By rhythmically sweeping the vibrissae back and

forth in a behavior known as “whisking”, the vibrissae contact objects near the face. The whisking behavior, combined with the ability to locomote and make head movements, allows the animal to form perceptions about its immediate surroundings. When a muscle contraction causes the vibrissae to be thrust against an object, ex-afferent spiking signals of contact, as well as re-afferent signals of the vibrissa motion itself are generated in the trigeminal ganglion. These signals appear both during electrically induced muscle contractions (Szwed et al., 2003; Zucker and Welker, 1969) and active whisking (Khatri et al., 2009; Leiser and Moxon, 2007).

Recent behavioral work demonstrates that rodents can indeed keep track of self-generated vibrissa movements (Mehta et al., 2007; O'Connor et al., 2010a). These studies demonstrated that rats and mice can report the anterior-posterior position of a stationary object placed in the vibrissal field using a single vibrissa (Mehta et al., 2007). Successful completion of this and other object position based tasks requires S1 cortex (Hutson and Masterton, 1986; O'Connor et al., 2010a). Rats employed a motor strategy that produced similar vibrissa velocities upon contact regardless of object position, suggesting that they possess knowledge of vibrissa position within a whisk cycle. Other studies in rats and mice show that units in primary somatosensory (S1) cortex are tuned to specific preferred phases of the whisk cycle. Because vibrissa-related motor and sensory signals are carried

along separate cranial nerves, these studies were able to demonstrate that this tuning is the result of peripheral re-afference (Fee et al., 1997; Poulet and Petersen, 2008). A subset of these units drastically increase their firing rates when the vibrissa contacts an object during the preferred phase of the whisk cycle (Curtis and Kleinfeld, 2009). Therefore, it seems plausible that the re-afferent signal underlies the animal's ability to localize objects in space through its interaction with ex-afferent signals (Kleinfeld and Deschênes, 2011), though alternative strategies have been proposed. These other strategies assume the animal restricts the range of whisking to an attended location and keeps track of the intended range (Bagdasarian et al., 2013; O'Connor et al., 2010a; O'Connor et al., 2013).

The nature of the observed ex-afferent and re-afferent interaction in vibrissa S1 cortex remains unknown. However, in the somatosensory representation of the limbs, ex-afferent and re-afferent signals are generated by separate physical sensors, and rise along parallel ascending pathways to S1 cortex. Cutaneous signals from the skin and proprioceptive signals from muscle spindles are represented in separate compartments of VPL thalamus in monkeys (Friedman and Jones, 1981) and rats (Francis et al., 2008), which in turn project to S1 cortex. In the vibrissa system, the existence of parallel ascending pathways could explain the non-linear interaction between touch and whisking phase that is observed in S1 cortex, as has been previously

proposed (Curtis and Kleinfeld, 2009; Yu et al., 2006). While most facial muscles controlled by the 7$^{th}$ cranial nerve, including vibrissa muscles, are thought not to contain muscle spindles (Bowden and Mahran, 1956; Hines, 1927; Semba and Egger, 1986; Stål et al., 1990; Welt and Abbs, 1990) (but see (Mameli et al., 2010; Mameli et al., 2008)), there is a vast array of different trigeminal mechanoreceptor types and spatial arrangements in the vibrissa follicle (Rice et al., 1997) and intervibrissal fur (Fundin et al., 1997) innervating the expansive trigeminal column in the brainstem. In anesthetized rats, different trigeminal ganglion neurons respond differentially to internally- versus externally-generated vibrissa deflections, including approximately 20% that respond only to internally-generated events (Szwed et al., 2003). Together, these observations raise the possibility that there exist segregated pathways for vibrissa re-afference and ex-afference, like those observed in the somatosensory representation of the limbs.

Specifically, primary sensory axons from the trigeminal ganglion branch and innervate each of the trigeminal subnuclei (Henderson and Jacquin, 1995), including: (1) the principal trigeminal nucleus (PrV), (2) the spinal trigeminal nucleus pars oralis (SpO), (3) the spinal trigeminal nucleus pars interpolaris (SpVI), which is further subdivided into distinct rostral and caudal divisions (SpVIr and SpVIc, respectively), (4) the spinal trigeminal nucleus pars caudalis (SpVC), and (5) the newly re-classified spinal

trigeminal nucleus pars muralis (SpVM) (Matthews, 2012; Olszewski, 1950). Distinct cytoarchitectonic regions that correspond to the individual vibrissae, termed “barrelettes”, exist in PrV, SpVIc, and SpC(Ma and Woolsey, 1984). A similar cytoarchitectonic map of the mystacial pad is observed in ventral posterior medial (VPM) thalamus, where each vibrissa is represented by a corresponding “barreloid”(Haidarliu et al., 2008; Land and Simons, 1985; Sugitani et al., 1990). Yet another map of the vibrissae exists in layer 4 of S1 cortex, where each vibrissa is represented by a corresponding “barrel” (Woolsey and Van Der Loos, 1970). There are at least three main sensory pathways from the trigeminal complex in the brainstem to S1 cortex, summarized in **Fig 4.1** and described as follows:

(1) The well-described “lemniscal” pathway originates with neurons in the PrV barrelettes. Approximately 70% of these neurons have single-vibrissa receptive fields in deeply anesthetized animals and they project the center, or “core”, of the VPM barreloids (Veinante and Deschênes, 1999). The VPM core, in turn, contains neurons that project to the barrels in layer 4 of S1 cortex. A newly discovered a sub-division of this pathway originates with multi-vibrissae receptive field neurons in the PrV barrelettes. These neurons project to the dorsomedial edge, or “head”, of the barreloids (Urbain and Deschênes, 2007b). The barreloid head neurons in turn project heavily to the inter-barrel “septa” in layer 4 of S1

cortex (Furuta et al., 2009), and are modulated by descending projections from motor cortex (Urbain and Deschênes, 2007b).

(2) The well-described “paralemniscal” pathway originates in the rostral division of SpVI (SpVIr). These neurons have multi-vibrissae receptive fields and project to neurons in PO thalamus (Veinante et al., 2000), which also have multi-vibrissae receptive fields. Neuronal units in PO have longer-latency, variable responses to deflections of several whiskers (Diamond et al., 1992b). They project to layers 1 and 5a of S1 cortex, and also to motor cortex(Deschênes et al., 1998). The lack of a short latency response to vibrissa deflections in PO is hypothesized to be the result of feedforward inhibition from the subthalamic region, zona incerta (ZI). This hypothesis is derived from work done in rats under light ketamine anesthesia, in which selective lesioning of the ventral division of ZI (ZIv) produced robust PO responses to external vibrissa deflections (Urbain and Deschênes, 2007a). ZIv is known to receive inputs from the same trigeminal brainstem neurons that drive PO (SpVIr), and also provides strong feedforward inhibition to PO (Lavallee et al., 2005).

(3) The third pathway, the “extralemnsical” pathway, originates with neurons in the caudal division of SpVI (SpVIc). These neurons have multi-vibrissae receptive fields and project to the ventrolateral portion, or “tail” of the VPM

barreloids (VPMvl)(Veinante et al., 2000). Extralemsnical neurons in VPMvl project mainly to S2 cortex but also terminate in S1 cortex (Pierret et al., 2000).

While it is generally agreed upon that an ex-afferent touch signal that reports contact with external objects is conveyed through the lemniscal pathway (Nakamura et al., 2009), the functional pathway by which the whisking re-afferent signal reaches cortex remains unclear. Although it has been demonstrated that trigeminal ganglion neurons encode whisking motion on a cycle by cycle basis (Khatri et al., 2009), the corresponding representation of self-generated whisking has not been studied in any of the different brainstem trigeminal nuclei. The nature of this representation is particularly intriguing given the recently discovered inhibitory interactions between these nuclei (Bellavance et al., 2010; Furuta et al., 2008). At the level of the thalamus, there are conflicting reports in the literature regarding the location of a re-afferent whisking signal. Two studies study utilizing rhythmic stimulation of the facial motor nerve to elicit fictive whisking in urethane anesthetized rats (Brown and Waite, 1974; Yu et al., 2006) suggest that VPM represents whisking and touch in the same neurons, and one of these studies demonstrates that PO represents *only* whisking (Yu et al., 2006). However, a separate study in awake rats instead suggests that re-afference is not represented in PO (Masri et al., 2008b). Another study in

awake rats indicates that VPM units are responsive to kinematic parameters of active whisking such as amplitude, speed, and direction (Khatri et al., 2010). However, neither of the studies in alert rats quantified the strength of phase relationships between thalamic spiking activity and whisking or reported the locations of the recording sites, which has led to recent debate regarding the ability of different thalamic and cortical neurons to encode whisking (Ahissar et al., 2008; de Kock and Sakmann, 2009; Masri et al., 2008a). No study to date has directly compared the encoding of self-generated whisking in the different ascending anatomical pathways in alert rodents. Thus, the purpose of the present study is to provide a quantitative description of the subcortical origin of the re-afferent whisking signal that is observed in S1 (Curtis and Kleinfeld, 2009; Fee et al., 1997; Poulet and Petersen, 2008). We examine whether different anatomical pathways contain re-afferent versus ex-afferent information by monitoring neuronal activity in the lemniscal and paralemniscal pathways, the two major ascending pathways from trigeminus to S1 cortex in alert, whisking rats. We find evidence for a concurrent representation of whisking and touch within the lemniscal pathway, but only a minimal representation the paralemniscal pathway. Units in the lemniscal pathway exhibit a broad range of sensitivities to different phases of the whisk cycle. We discuss the implications of this representation for active touch in the vibrissa system.

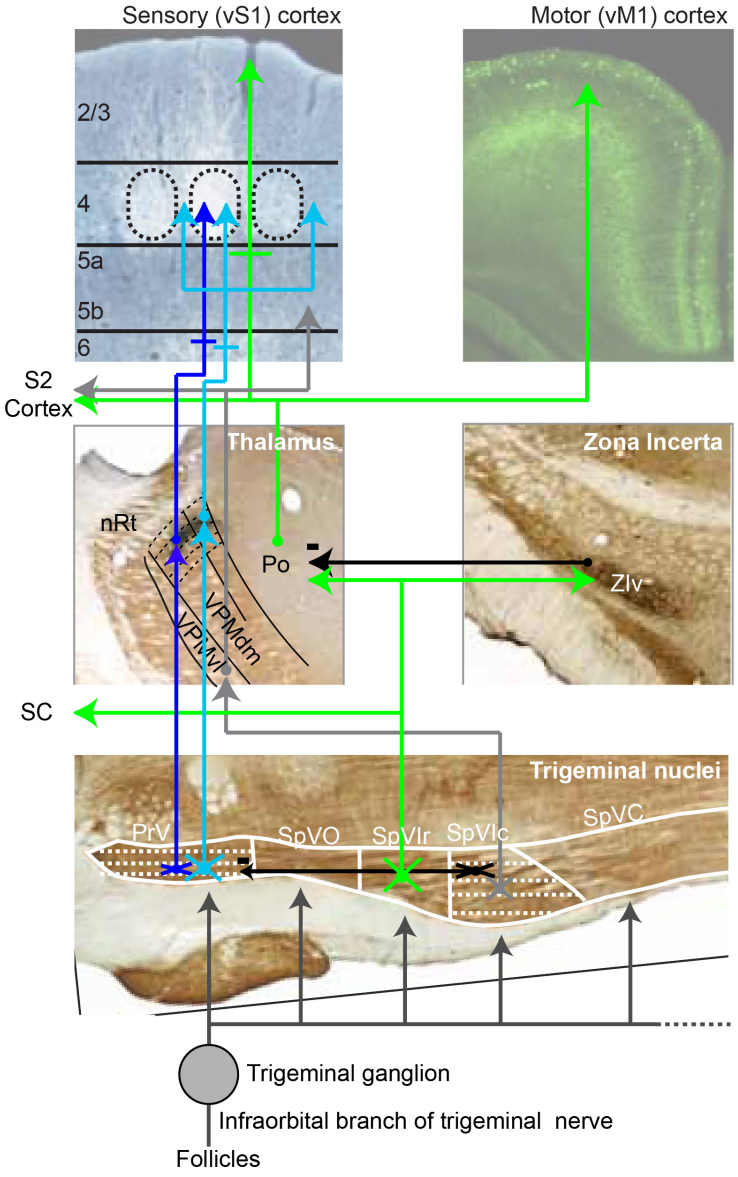


**Figure 4.1. Map of vibrissa ascending pathways from the periphery to cortex**

Dashed arrows represent individual barrelettes, barreloids, and barrels. The classical lemniscal pathway is shown in blue, and the more recently discovered subclass of the lemniscal pathway is shown in light blue. The paralemniscal pathway is shown in green, and the extralemniscal pathway in grey. Inhibitory interactions are shown in black. Adapted from (Deschenes and Urbain, 2009) and (Kleinfeld and Deschênes, 2011).

## *4.2 Methods*

### Animals

42 female Long Evans rats (250 to 350 g, Charles River) were used for combined behavioral and electrophysiological experiments. Experimental protocols were carried out in accordance with federally prescribed animal care and use guidelines and were approved by the Institutional Animal Care and Use Committee at the University of California San Diego.

### Neuronal recording

To examine neuronal signaling in the trigeminal complex of the brainstem, we first identified the PrV and SpVi regions based on stereotaxic coordinates and multiunit spiking responses to manual or air-puff deflections of the macro-vibrissae, micro-vibrissae, and peri-mystacial fur (20-50 ms, 0.1-0.2 Hz). We then used the neuronal recording procedures described previously (**Section 3.2, Recording and Analysis**) to monitor single- and multi-unit spiking activity in the alert rat. After a subset of the recordings, we briefly anesthetized the rat using isoflurane, with the electrode still in the same location as the previously recorded unit. To determine the approximate multi-unit receptive field of the region from which the previous recording was made, we manually deflected small patches (approximately 1-5 mm) of peri-

mystacial fur as well as individual macro- and micro-vibrissae with a hand-held probe and listened for spiking activity on an audio monitor. We mapped approximate receptive fields qualitatively based on the location of the face that produced the maximal multiunit spiking response. We marked the location of a subset of the recorded units by iontophoretic injections of Chicago sky blue dye as described (**Section 3.2, Recording and Analysis**). We used previously described post-hoc spike sorting algorithms and software (Fee et al., 1996; Hill et al., 2011b).

To examine neuronal signaling in alert rats within VPM thalamus, PO thalamus, and ZIv, we used neuronal recording procedures similar to those reported for brainstem recordings, except that recordings were made in the juxtacellular configuration. Briefly, a craniotomy was made based on stereotaxic coordinates, centered 3 mm posterior and 3 mm lateral to bregma. For juxtacellular monitoring we used quartz pipettes with 1-3 μm tips. We first identified the VPM thalamic region and the somatosensory region of ZIv based on stereotaxic coordinates and air-puff deflections of the macro-vibrissae, micro-vibrissae, and peri-mystacial fur (5-20 ms, 2-3 Hz). The somatosensory region of ZIv is located ventrally to the portion of VPM that corresponds to the A and B vibrissa rows. We identified units in PO thalamus based on their proximity to the previously identified VPM region, within approximately 400 μm of the VPM/PO border. Once a unit was located we

continued to move the pipette in 1 µm increments until the spike waveform displayed an initial positive voltage deflection, which was usually accompanied by a 1.5x or greater increase in electrode resistance. Spike sorting was not required for identifying single units in this configuration. Recordings sites were labeled with Chicago sky blue dye and the anatomical location was determined in post-hoc histology, as described. After a subset of the VPM thalamic recordings, we anesthetized the rat with isoflurane to determine the approximate receptive field of the previously recorded unit, as described above for the brainstem recordings.

## Behavior

We monitored vibrissa position simultaneously with neuronal spiking activity under two behavioral conditions: (1) as the rats were coaxed to whisk in air by presenting food or bedding from their home cage (Ganguly and Kleinfeld, 2004), and (2) as vibrissae were deflected externally by brief puffs of air applied to the face (Kleinfeld et al., 2002). We monitored whisking in head-restrained rats using methods similar to those described previously (**Section 3.2, Recording and Analysis**), and summarized below:

We monitored vibrissa position with a Basler A602f camera at a spatial resolution of 120 µm/pixel. For measurements in conjunction with juxtacellular

recordings in thalamus and zona incerta, 360x250 pixel planar images were acquired at 250 Hz with a white light emitting diode backlight for trials of 10 s each. Vibrissae were clipped to approximately 2/3 of their original length, and pixel intensity in the image was thresholded. The mean position of the full set of vibrissae was tracked by computing the center of mass of the thresholded pixels in each image. The mean angle of the set of the vibrissae was defined by a line that extends between this center of mass point and the center of mass of the projections of each individual vibrissa onto a line through the mystacial pad (**Fig 4.2**) For measurements in conjunction with extracellular recording from brainstem, we used the Basler A602f camera in line-scan mode with a 1 kHz scan rate and imaged motion along a line that was 5 to 10 mm from the edge of the mystacial pad. Pixel intensity along the line was thresholded and the centroid of the detected vibrissa was converted to a voltage proportional to pixel position in real time.

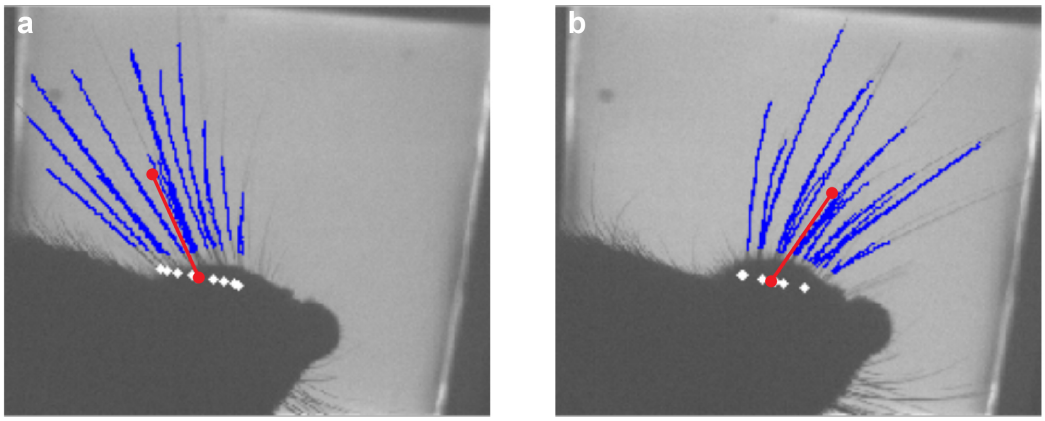


**Figure 4.2. Estimation of vibrissa angle from video images**

Detected vibrissae are shown in blue, and their estimated insertion points on the mystacial pad are shown in white. The centroid of the detected vibrissae and insertion points are shown in red. The line between these two points defines the estimated angle. Sample images are shown for protracted **(a)** and retracted **(b)** vibrissa positions.

## Analysis

To determine the modulation of neuronal units by whisking on a cycle-by-cycle basis we first computed the instantaneous phase of vibrissa motion within the whisk cycle using methods similar to those described previously(Hill et al., 2011a; Moore et al., 2013). Briefly, the vibrissa position signal was separated into single whisks by band-pass filtering between 3 and 25 Hz and computing the Hilbert transform of the resulting signal. The Hilbert transform is computed by first calculating the Fourier transform of the entire signal, setting the power at the resulting negative frequency components to zero, and then applying the inverse Fourier transform to generate the complex-valued “analytic signal”. At each sample time the instantaneous phase is defined as the angle of the analytic signal in polar coordinates(Boashash, 1992). The instantaneous phase signal is then phase shifted by π yielding a signal, $\Phi(t)$, such that by convention, phase $\Phi(t) = 0$ corresponds to the onset of protraction, and $\Phi(t) = \pi$ corresponds to the onset of retraction. Individual candidate whisks were identified by phase resets of $\Phi(t)$, i.e. $\Phi(t) \geq N \cdot 2\pi$ (for integer values of N). Candidate were accepted as “detected whisks” only if the minimum-to-maximum amplitude exceeded a minimum threshold and the whisk lasted less than 250 ms. The

threshold value was chosen based on the linear vibrissa position signal (in mm) at a level that corresponds to an angle of approximately 5º.

For neuronal unit recordings in the trigeminal brainstem, thalamus, and zona incerta, each spike that occurred during a detected whisk, at time Ts, was assigned an instantaneous phase Φ(Ts). Similarly each video frame, at time Tv, that comprised a detected whisk was assigned an instantaneous phase Φ(Tv). The range of possible phases during a single whisk (0 to 2π) was divided into 32 bins, each spanning π/16 radians. We define Ns as the number of spikes in a bin for all detected whisks. We similarly define Np as the number of frames in a bin. The mean spike rate, R, for each phase bin, Φi, is then defined as:

$$R(\Phi_i) = F_V \cdot N_s(\Phi_i)/N_p(\Phi_i)$$

where Fv represents the video frame or scan rate.

We characterized the modulation of each unit with whisking phase by fitting a sine wave with a period 2π to the mean rate function, R(Φi), using standard linear least-squares regression techniques. The sinusoidal fit is completely described by three parameters, its amplitude, mean, and phase, which characterize the modulation of each unit. We determine whether or not

each unit is significantly modulated by statistically comparing the distributions of all spike phases, Φ(Ts) and all whisk phases, Φ(Tv), using a Kuiper test(Batschelet et al., 1981), a modification of the standard Kolmogorov-Smirnov test that accounts for circular variables.

For neuronal recordings in VPM, PO, and ZIv we characterized the modulation of each unit in response to air-puff deflections based on the peri-stimulus time histogram of spiking activity aligned to the air-puff onset. The histograms were computed by counting the number of spikes in 10 s bins every 2 ms. We then computed the maximum and the minimum binned spike rates in the first 100 ms post stimulus onset, and the background rate as the mean rate between 150 – 250 ms post stimulus. We determined whether the response to air-puffs was statistically significant for each neuron by comparing the distribution of spike times in the first 100 ms post-stimulus to a uniform distribution (Kolmogorov-Smirnov test).

## Anatomy

For localizing recording sites, brains were sectioned at 60 μm in either the coronal or horizontal plane, stained for cytochrome oxidase reactivity, and scanned at a resolution of 0.5 μm/pixel on a Nanozoomer™ slide scanner (Hamamatsu). For recording sites in the thalamus and zona incerta, brains

were cut in the coronal plane and mapped onto a reference atlas. The reference atlas consisted of a single brain prepared in the same way. Sections containing dye labels were manually assigned to the nearest plane in the reference atlas. Standard anatomical features were traced on the sections containing the dye labels using Illustrator™ software (Adobe). The sections were then manually rotated and scaled to approximately match the corresponding anatomical borders on the reference atlas. On each section, a subset of the following structures were used for alignment: ventrobasal thalamus, VPM thalamus, VPL thalamus, thalamic reticular nucleus, habenula, dorsal lateral geniculate nucleus, ventral lateral geniculate nucleus, dorsal zona incerta, ventral zona incerta, subthalamic nucleus, external medullary lamina, mammilothalamic tract, fornix bundle, and the third ventricle. The scaled and rotated dye label was then transferred to the reference atlas. The mapped locations of the recording sites on the reference atlas, along with nearby anatomical borders, were then traced and reconstructed in three dimensions using Neurolucida™ software (Microbrightfield).

## *4.3 Results*

### Spiking activity in trigeminal brainstem nuclei during whisking

Since trigeminal mechanosensory afferents are a likely source of the re-afferent signal of whisking phase, we monitored neuronal activity in their target nuclei in the brainstem. We recorded single and multi-unit activity in PrV (25 putative single unit and 31 multi-unit spiking signals), and SpVIr, (16 putative single unit and 10 multi-unit spiking signals). Units in PrV are substantially modulated on a cycle-by-cycle basis during whisking. An example is depicted in **Fig 4.3a**, which shows spiking activity at one recording site (**Fig 4.3b**), monitored simultaneously with motion of the C2 vibrissa as the rat was coaxed to whisk freely in air. It has previously been demonstrated that the vibrissae tend to move in phase with one another during free-air whisking (Hill et al., 2011a); thus, the position of the C2 vibrissa was used to represent the kinematic parameters of the full whisking behavior. Specifically, we identified individual whisk events, as well as the instantaneous phase of vibrissa motion at all times during each whisk, using the Hilbert transform (**Section 4.2, Methods**). The normalized vibrissa position for each whisk is shown as a function of the instantaneous phase in the whisk cycle (**Fig 4.3c**), along with a raster of the phases at which spikes occurred (**Fig 4.3d**). The probability density functions of the observed phases and of the observed

phases conditioned on a spike are also shown (**Fig 4.3e**). From these probability density distributions, we estimated the spike rate (R) as a function of phase in the whisk cycle (φ) (**Fig 4.3f**). To describe the modulation in spike rate we fit a sinusoid with a period of 2π to the estimated rate function:

$$R(\varphi) = A \cdot \cos(2\pi\varphi + \Phi) + M$$

where the parameters A, Φ, and M describe the amplitude, phase offset, and mean spike rate. For the unit in **Figure 4.3**, the majority of spikes occurred during the retraction phase of the whisk cycle, when the vibrissae were moving in the caudal direction. For a subset of the recorded units, including the one shown in **Fig 4.3,** we characterized the approximate receptive field of multi-unit activity at the same recording site after briefly anesthetizing the rat with isoflurane. This unit was located among units that responded to vibrissa E3. The firing rates of additional example units vs. phase in the whisk cycle, along with these local receptive fields, are shown in **Fig 4.4.** We note that units in the sub-region of PrV that corresponds to the macrovibrissae (**Fig 4.4a**), as well as units in sub-regions corresponding to the skin or fur around the mouth and nose (**Fig 4.4b**) were significantly modulated. SpVIr also contained some units that were significantly modulated (**Fig 4.4c).**

We used the sinusoidal fits of spike rates (**Fig 4.3f**) to estimate the fidelity with which these units can report whisking phase. We define the modulation depth (D) for each unit as the ratio of the difference between the maximum and minimum spike rates to the mean. That is:

$$D = 2A/M$$

**Figure 4.5a** shows the estimated modulation depth (D) vs. the mean spike rate (M). The units are labeled with the approximate receptive fields at the recording site, if known. All recording sites were from regions in which multi-unit spiking activity was elicited by air-puff deflections of the vibrissae and surrounding fur. We note that for a point process with Poisson distributed arrival times, the signal to noise ratio of the rate (SNR) is can be approximated as:

$$SNR = \frac{2A}{\sqrt{M}} = D \cdot \sqrt{M}$$ (Hill, 2009)

The dotted lines in **Figure 4.5a** show combinations of amplitudes and mean rates that yield equivalent SNRs (iso-SNR contours). Across the population of PrV and SpVIr units, different units spiked preferentially at different phases of the whisk cycle. The population of spiking responses to whisking is summarized with a polar plot (**Fig 4.6a**), in which each unit is characterized in

terms of the SNR (radial axis) and preferred phase (tangential axis) of the sinusoid that describes its modulation of spiking activity through the whisk cycle. 46/56 PrV units (82%) in 3 rats and 11/26 (42%) SpVIr units in 3 rats were significantly modulated (Kuiper test, $p<0.01$). As a population, PrV units had significantly greater modulation SNRs than SpVIr units (Wilcoxon ranked sum test, $p=1.5 \times 10^{-4}$). PrV units tended to fire more spikes when the animal was whisking as opposed to not whisking (Wilcoxon signed rank test, $p=6 \times 10^{-6}$), whereas spikes rates were not significantly different between these conditions in SpVIr (Wilcoxon signed rank test, $p=0.17$; **Fig 4.6b**)

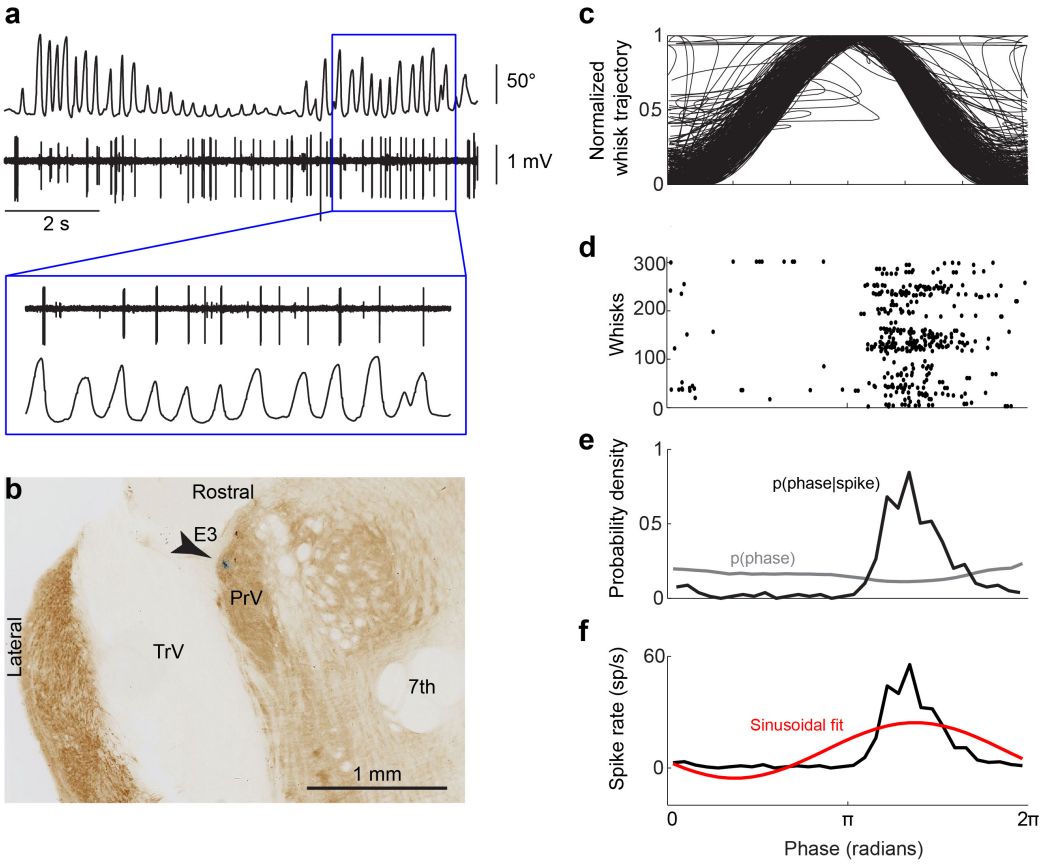


**Figure 4.3. Spiking activity of a histologically identified PrV unit in response to free-air whisking**

**(a)** Simultaneously recorded vibrissa motion and spiking activity during free-air whisking. **(b)** Location of the recorded unit in a horizontal brainstem section. Multiunit activity at this recording site was detected in response to manual deflections of vibrissa E3. **(c)** Normalized vibrissa position as a function of phase in the whisk cycle. All whisks during the record are superimposed. **(d)** Raster of phases in the whisk cycle at which spikes occurred. Each line on the y-axis represents on whisk. **(e)** Probability density function of all observed instantaneous phases (gray) and phases conditioned on a spike (black). **(f)** Spike rate as a function of phase in the whisk cycle (black) and a sinusoidal fit of this function (red).

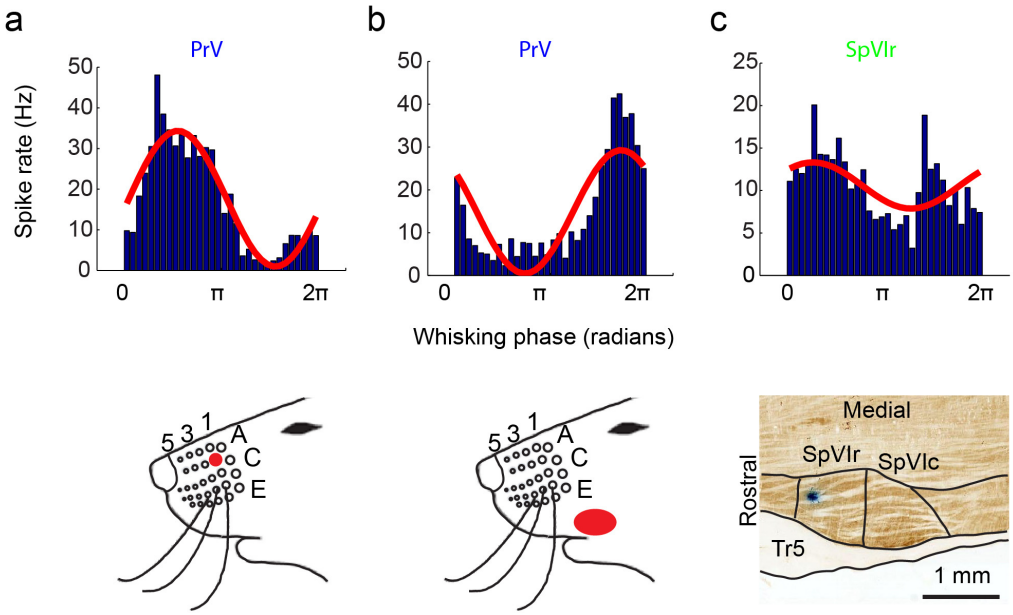


**Figure 4.4. Spiking responses of additional PrV and SpVIr units to free-air whisking**

**(a)** Spike rate versus phase in the whisk cycle (blue histogram, top) and sinusoidal fit (red, top). Multiunit activity at the same recording site was elicited in response to deflections vibrissa B1 (bottom). **(b)** Same as **panel a**, but for a unit located among units that responded to brushing the fur on the upper lip. **(c)** Spike rate versus phase in the whisk cycle (blue histogram, top) and sinusoidal fit (red, top) for a unit located in SpVIr (bottom).

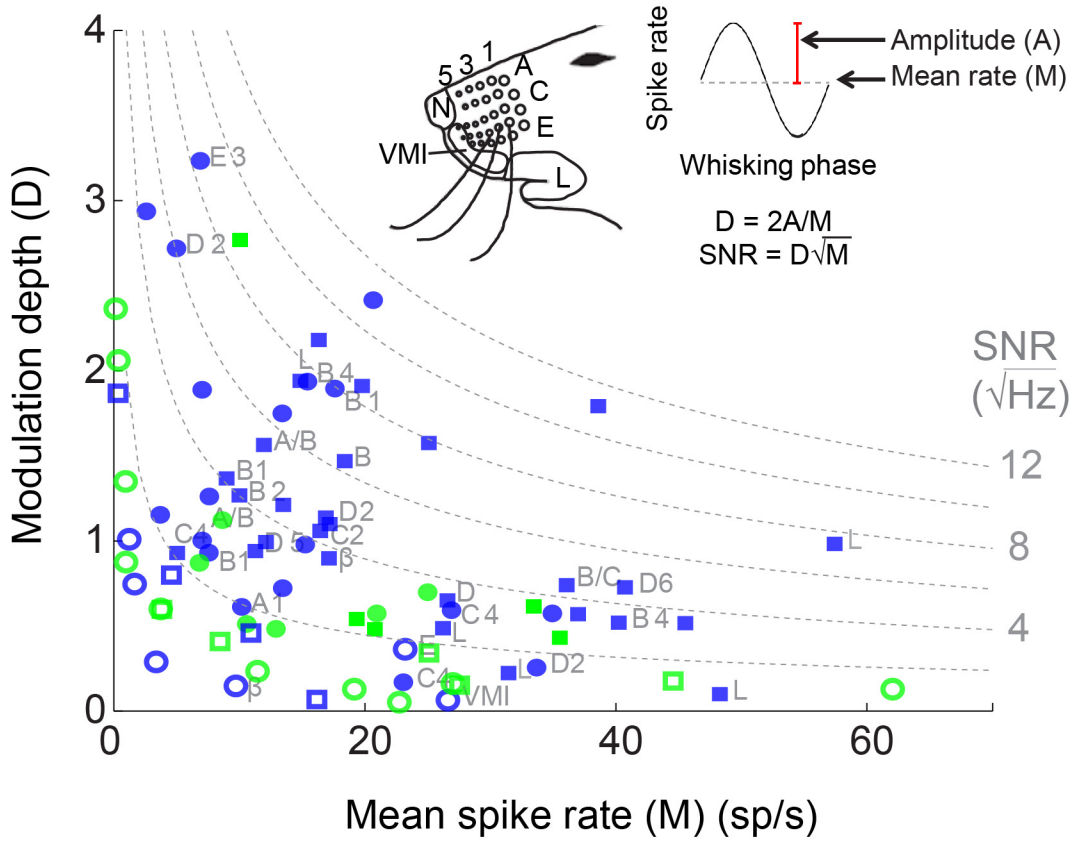


**Figure 4.5. Modulation of spiking activity with free-air whisking in the trigeminal nuclei**

Whisking phase modulation depth versus mean spike rate for putative single-unit (circles) and multi-unit (squares) in PrV (blue) and SpVIr (green). Significantly modulated units (solid symbols) and non-significantly modulated units (open symbols) are shown. Points with the equal whisking phase SNRs are shown as dashed lines, and approximate receptive fields at the recording sites are labeled. Definitions of modulation depth, SNR, and receptive field locations are shown in the inset.

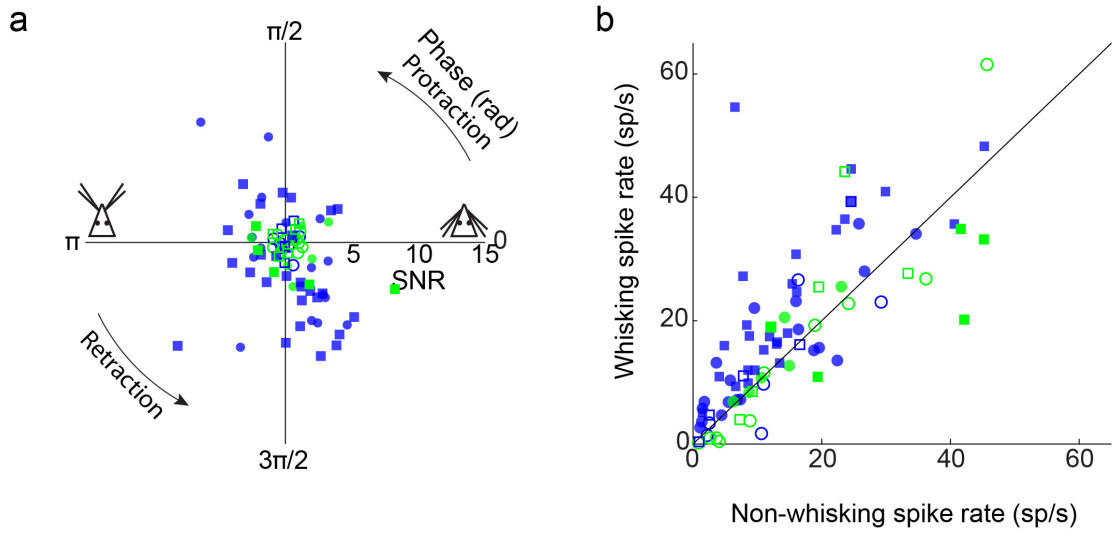


**Figure 4.6 Preferred whisking phases and spike rates of units in the trigeminal nuclei**

**(a)** Polar plot of the SNR (radial axis) versus preferred phase (tangential axis) for the units in **Figure 4.5.** Phase zero corresponds to the vibrissa fully retracted, and π represents fully protracted, as in **Figures 4.3-4.4**. **(b)** Mean spike rates during whisking and non-whisking epochs for the same units. Symbols are defined as in **Figure 4.5.**

## Spiking activity in somatosensory thalamic nuclei during whisking

We recorded spiking activity of single neurons using the juxtacellular configuration in VPM and PO thalamus, areas which receive inputs primarily from PrV and SpVIr respectively. Occasionally, extracellular recordings of additional units were obtained on the same electrode (3 of 56 records). These units had negative initial deflections, as opposed to the initial positive spike deflections of the juxtacellularly recorded neurons. Units in VPM thalamus are substantially modulated on a cycle-by-cycle basis during whisking. An example is depicted in **Fig 4.7a**, which shows spiking activity of one neuron **Fig 4.7b**, monitored simultaneously with motion of the vibrissae during free whisking in air. We identified individual whisk events based on the motion of the aggregate set of vibrissae as described (**Section 4.2 Methods**). The normalized mean vibrissa position for each whisk is shown as a function of the instantaneous whisk cycle phase (**Fig 4.7c**), along with all other metrics previously shown in **Fig 4.3** for brainstem neurons: raster of spike phases, probability density of all whisking phases and whisking phases conditioned on a spike, and spike rate as a function of phase (**Fig 4.7d-f**). For the unit in **Figure 4.7,** the majority of spikes occurred during the protraction phase of the whisk cycle, when the vibrissae were moving in the rostral direction. This unit was located among units that responded to vibrissa C4.

Additional example units from VPM thalamus and the adjacent sub region in PO thalamus, along with their anatomical locations as labeled with Chicago sky blue at the recording site, are shown in **Fig 4.8.** We note that units in the sub-region of VPM that corresponds to the macrovibrissae (**Fig 4.8a**), as well as units in sub-regions corresponding to the skin or fur around the mouth and nose (**Fig 4.8b**) were significantly modulated. PO also contained a minority of units that were significantly modulated (**Fig 4.8c).**

Similarly to PrV and SpVIr units, **Figure 4.9a** shows the estimated modulation depths (D) vs. the mean spike rate (M) for units in VPM and PO, the associated iso-SNR contours, and receptive fields. The majority of VPM neurons were significantly modulated (33/39 or 85%, Kuiper test $p<0.01$; closed circles), whereas only a minority of PO neurons were significantly modulated (4/17 or 23%, Kuiper test $p<0.01$; closed circles). **Figure 4.9b** shows the SNR of modulation as a function of the perpendicular distance to the VPM/PO border. Of the significantly modulated units, different units spiked preferentially at different phases of the whisk cycle (**Fig 4.9c**). As with PrV units and consistent with past results(Poulet et al., 2012), VPM neurons tended to fire more spikes when the animal was whisking as opposed to not whisking (Wilcoxon signed rank test, p=1.0 x 10^-6), and as with SpVIr, spikes rates were not significantly different between these conditions in PO

(Wilcoxon signed rank test, p=0.08; **Fig 4.9d**). Overall, PO neurons tended to have lower spike rates than in VPM during whisking epochs (Wilcoxon ranked sum text, p=0.001).

There does not appear to be a well-defined relationship between the distance to the VPM/PO border and modulation SNR. We note that there are neurons with particularly high SNR's in VPM both close to the border as well as deeper in the nucleus (**Fig 4.9b**). To further clarify whether there is a segregation of function within VPM we reconstructed the locations of the recording sites in three dimensions (**Fig 4.10; see Methods**). Again, there is no clear spatial relationship between location within VPM and modulation SNR, suggesting that self-generated motion and touch are signaled within the same anatomical pathway.

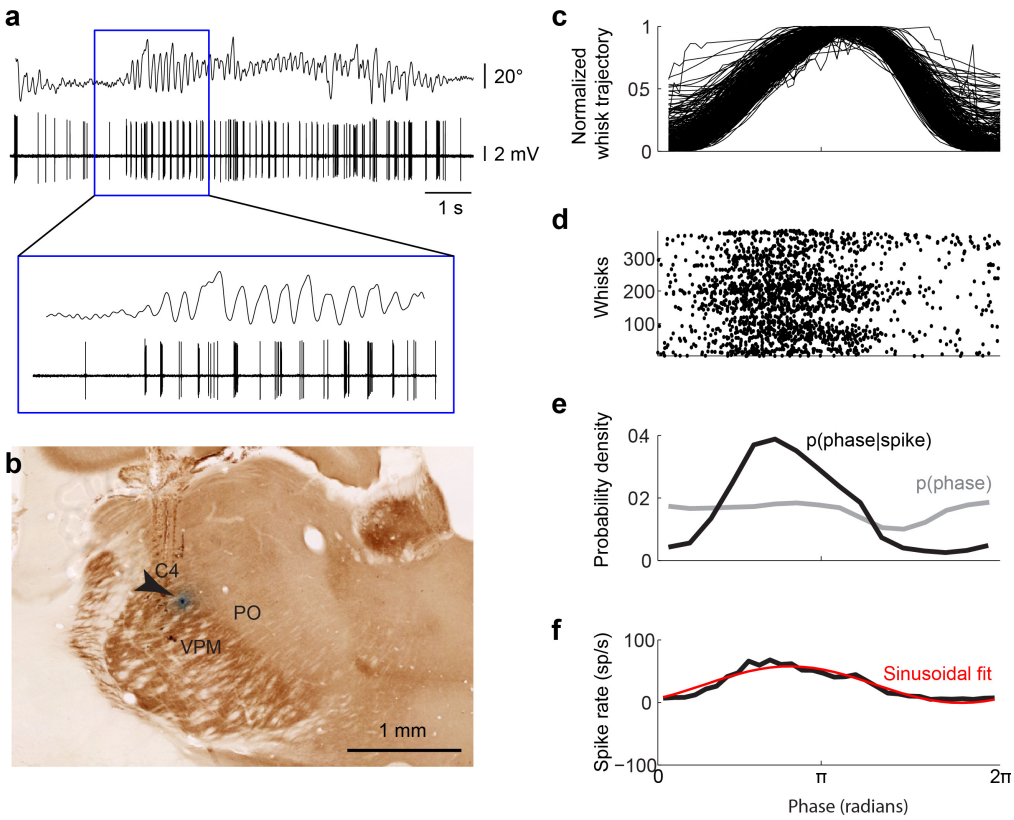


**Figure 4.7. Spiking activity of a histologically identified VPM unit in response to free-air whisking**

**(a)** Simultaneously recorded vibrissa motion and spiking activity during free-air whisking. **(b)** Location of the recorded unit in a coronal section. Multiunit activity at this recording site was detected in response to manual deflections of vibrissa C4. **(c)** Normalized vibrissa position as a function of phase in the whisk cycle. All whisks during the record are superimposed. **(d)** Raster of phases in the whisk cycle at which spikes occurred. Each line on the y-axis represents on whisk. **(e)** Probability density function of all observed instantaneous phases (gray) and phases conditioned on a spike (black). **(f)** Spike rate as a function of phase in the whisk cycle (black) and a sinusoidal fit of this function (red).

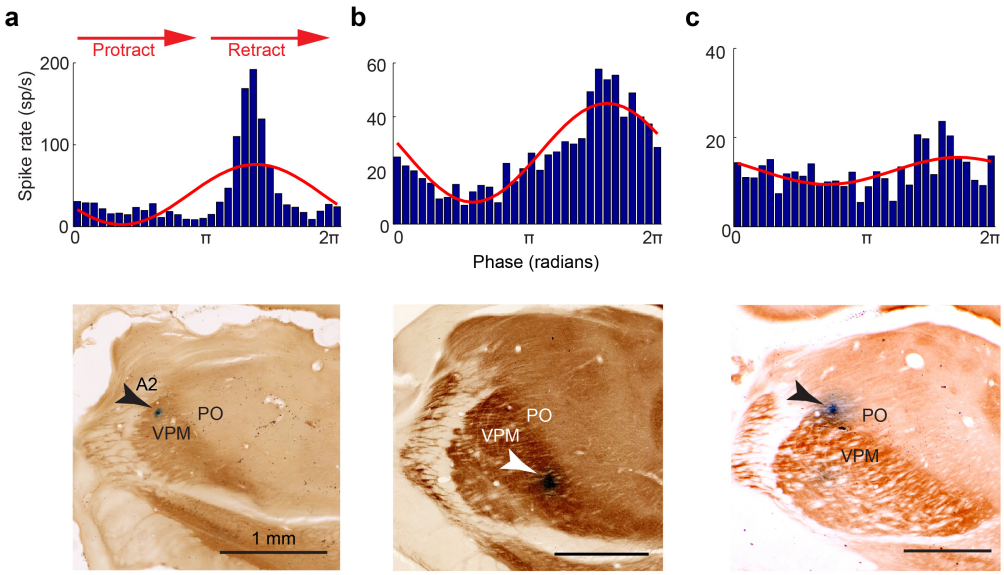


**Figure 4.8. Spiking responses of additional VPM and PO units to free-air whisking**

**(a)** Spike rate versus phase in the whisk cycle (blue histogram, top) and sinusoidal fit (red, top). Multiunit activity at the same recording site was elicited in response to deflections vibrissa A2. The recording site was identified in VPM in post-hoc histology (bottom) **(b)** Same as **panel a**. The receptive field at this recording site is unknown, but it is located in a region of VPM medial to the barreloids (bottom). The receptive field **(c)** Spike rate versus phase in the whisk cycle (blue histogram, top) and sinusoidal fit (red, top) for a unit located in PO (bottom).

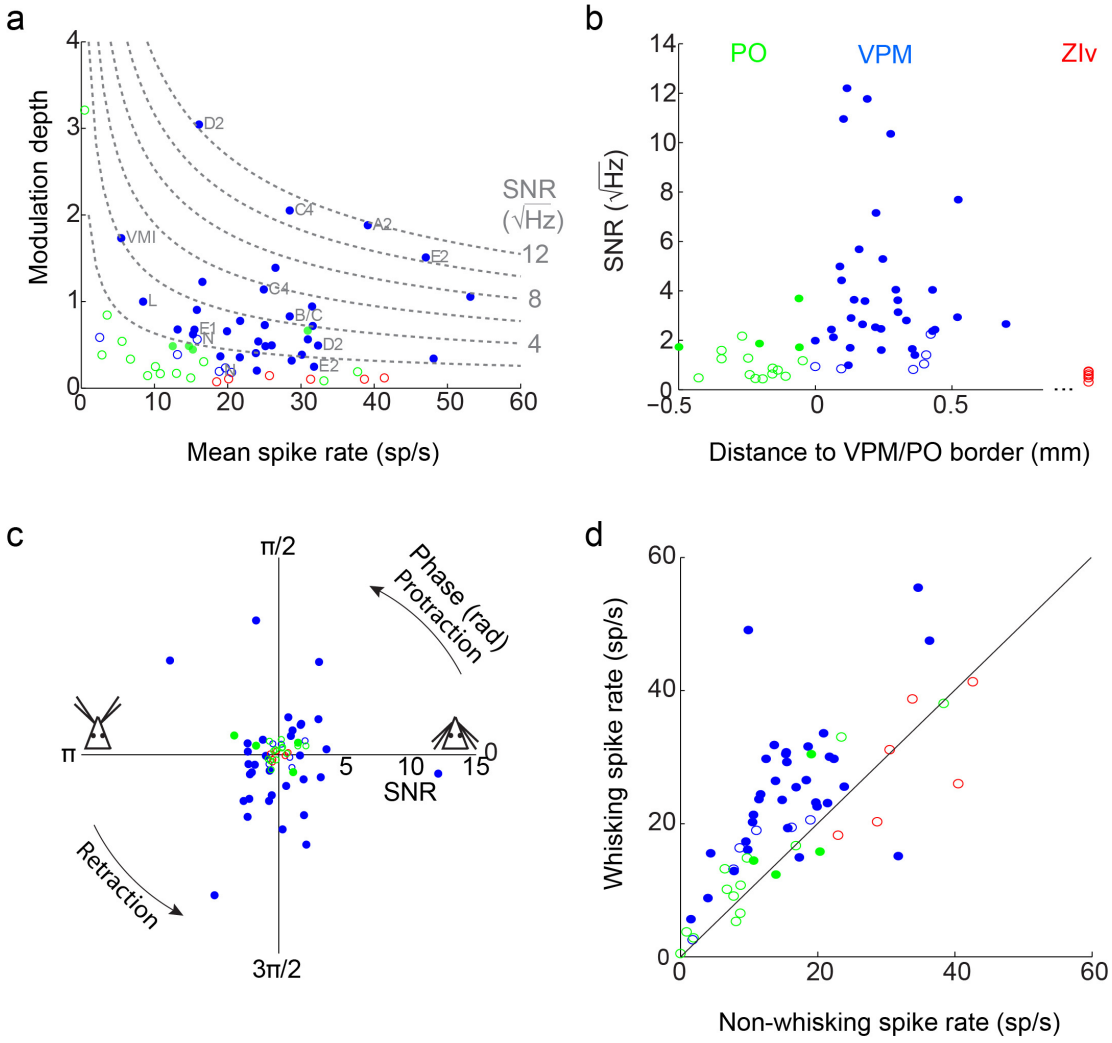


**Figure 4.9. Modulation of spiking activity with free-air whisking in the somatosensory thalamus and zona incerta**

**(a)** Whisking phase modulation depth versus mean spike rate for single neurons in VPM (blue), PO (green), and ZIv (red). Significantly modulated units (solid symbols) and non-significantly modulated units (open symbols) are shown. Points with the equal whisking phase SNRs are shown as dashed lines, and approximate receptive fields at the recording sites are labeled. Definitions of modulation depth, SNR, and receptive field locations are as shown in the inset of **Figure 4.5**. **(b)** SNR versus perpendicular distance to the VPM/PO border for the units VPM and PO units in **panel a**. SNRs for ZIv units are shown to the right (red). **(c)** Polar plot of the SNR (radial axis) versus preferred phase (tangential axis) for the units in **panel a.** Phase zero corresponds to the vibrissa fully retracted, and π represents fully protracted. **(d)** Mean spike rates during whisking and non-whisking epochs for the same units.

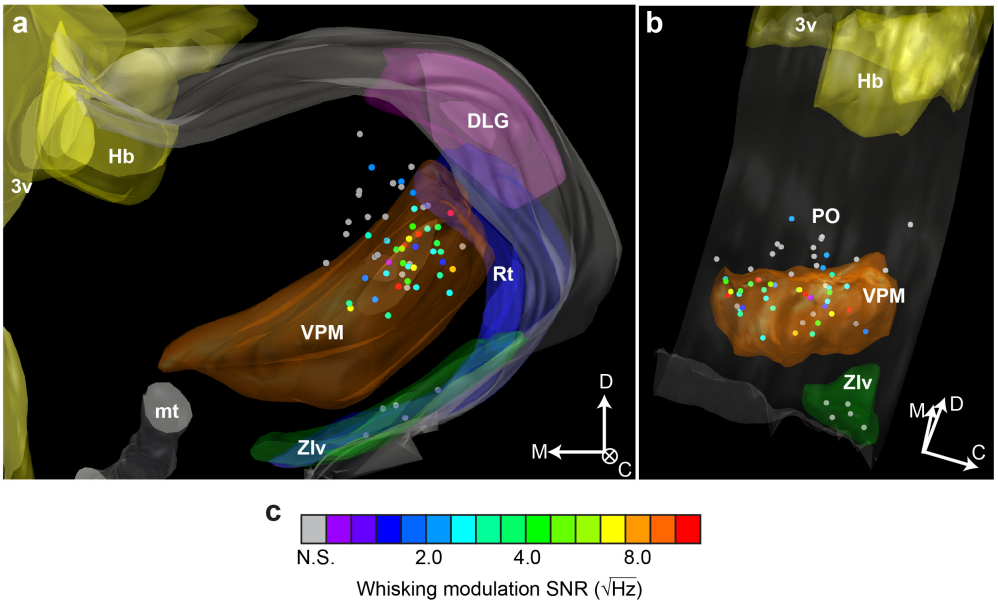


**Figure 4.10. Three-dimensional reconstruction of recording sites in the somatosensory thalamus and zona incerta**

**(a)** Rostral view of the reconstructed locations of recording sites (circles) and select anatomical borders. The colors of the circles represent the whisking phase SNR for each recorded neuron, and are defined in **panel c**. Labeled structures correspond to the third ventricle (3v, yellow), habenula (Hb, yellow), mammothalamic tract (mt, gray), dorsal lateral geniculate (DLG, purple), thalamic reticular nucleus (Rt, blue), and ventral division of zona incerta (Zlv, green). The anatomical axes are shown in the lower right hand corner: dorsal (D), medial (M), and caudal (C). **(b)** An oblique view of the reconstruction in **(a). (c)** Color map for the recording sites in **panels a,b**. Gray corresponds to neurons that were not significantly modulated (N.S.) by whisking phase.

## Spiking activity in somatosensory thalamic nuclei in response to external vibrissa deflections

To determine whether the same neurons that respond to self-generated vibrissa motion also respond to externally-induced activation of trigeminal mechanoreceptors, we quantified the responses of the these same neurons in somatosensory thalamus to vibrissa deflections with air-puffs. Consistent with the notion of a single anatomical pathway for re-afferent whisking and ex-afferent touch, the same VPM units that were modulated by self-generated whisking tended to also be modulated by air-puff deflections (**Fig 4.11a**), while PO neurons responded tended to respond less robustly to air puff deflections (**Fig 4.11b**). Across the population, 33/36 VPM neurons (92%) and 9/17 PO neurons (53%) were significantly modulated by air-puffs (**Fig 4.11c-d; closed circles**). Of the 36 VPM neurons, 29 were significantly modulated by both air-puffs and whisking, four by air-puffs only, two by whisking only, and one by neither type of vibrissa motion (**Fig 4.11e**).

We define modulation depth ($D_{air-puff}$) of the thalamic units similarly to that for whisking (**Fig 4.11c-d**), as the ratio of the difference between the maximum and minimum airpuff-induced spike rates to the baseline spike rate (**see Section 4.2, Methods**). That is:

$$D_{air-puff} = \frac{Maximum\ spike\ rate - Minimum\ spike\ rate}{Baseline\ spike\ rate}$$

$$SNR_{air-puff} = D_{air-puff} \cdot \sqrt{Baseline\ spike\ rate}$$

While the vast majority of VPM units respond to both whisking and air-puff deflections, there does not appear to be a relationship between the relative strengths of modulation by these two types of vibrissa motion (**Fig 4.11e**). There are VPM units that are relatively strongly modulated by whisking and weakly modulated by air-puff deflections, and vice versa. Thus, although the air-puff deflections do not produce the diversity of mechanical forces that are likely to impinge on trigeminal mechanoreceptors during active touch, it is possible that internally and externally generated movements are distinguished based on the relative strength of modulation among different VPM neurons.

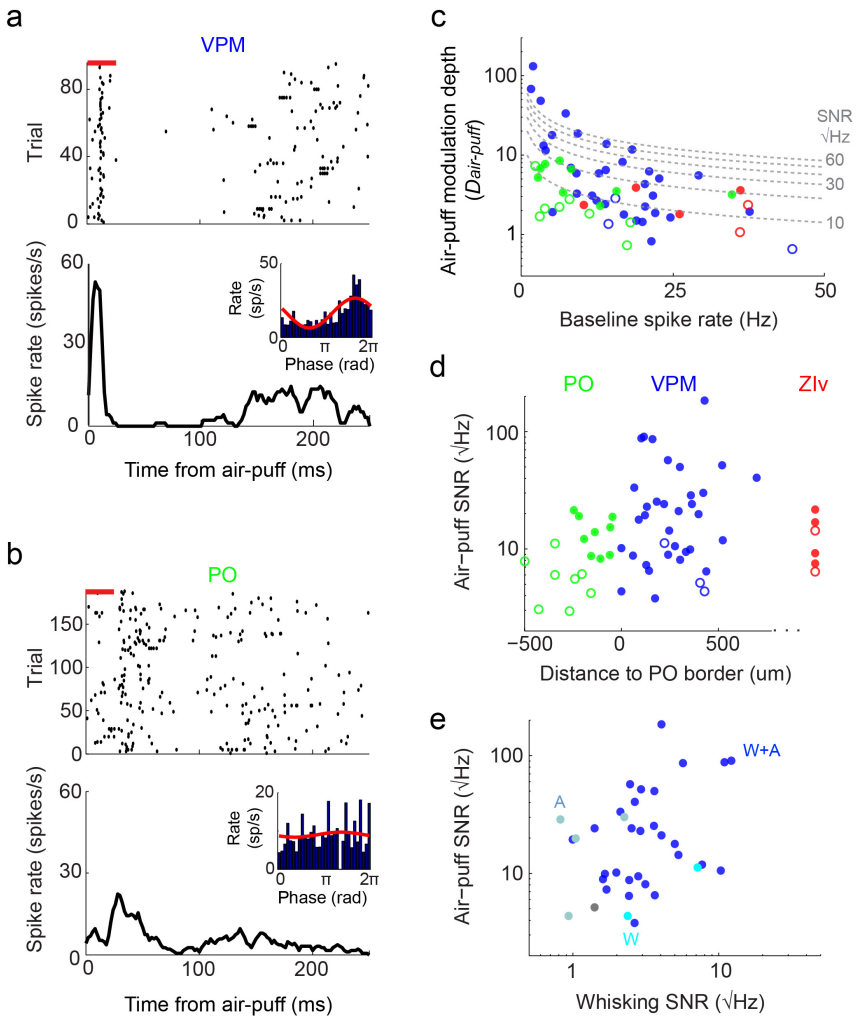


**Figure 4.11 Modulation of spiking activity in response to air-puff deflections in the somatosensory thalamus and zona incerta**

**(a)** Raster of spike times relative to air-puff onset for a VPM neuron (black ticks) and the duration of the airpuff (red bar). A corresponding peristimulus time histogram is shown below, and the response of the same neuron to free-air whisking is shown in the inset. **(b)** Raster of spike times relative to air-puff onset for a PO neuron. Conventions are as in **panel a**. **(c)** Modulation depth of the response to air-puff deflections for VPM (blue), PO (green) and ZIv (red) neurons versus the baseline spike rate. Points that correspond to equal air-puff SNRs are shown as dashed lines (gray). Air-puff modulation depth and SNR are as defined in the text ($D_{air-puff}$ and $SNR_{airpuff}$, respectively). Units with significant modulation (solid circles) and non-significant modulation (open circles) are shown. **(d)** Air-puff SNR versus perpendicular distance to the PO/VPM border. Conventions are as in **panel c**. **(e)** Air-puff SNR versus whisking phase SNR for VPM neurons. Neurons significantly modulated by both whisking and air-puffs (W+A, blue), air-puffs only (A, teal), whisking only (W, cyan), or neither (gray) are shown.

## Spiking activity in zona incerta during whisking

The somatosensory region of ZIv is known to receive projections from axon collaterals of the same SpVir neurons that project to PO, as well as providing feedforward inhibition to PO (**Fig 4.1**). As such, the responses of these neurons during whisking are of considerable interest. We therefore identified the somatosensory region of ZIv by applying air puffs to the face and recorded single unit activity in this region (N = 6 units). Units in ZIv responded with single short latency, precisely timed spikes (**Fig 4.12a,b**). During whisking, these units spiked at relatively high tonic rates (20-40 Hz) and were unaffected by the phase of vibrissa motion (**Figs 4.9-4.11; 4.12c-f**). These results suggest that ZIv exerts a tonic inhibitory influence on PO during whisking independently of the phase of movement.

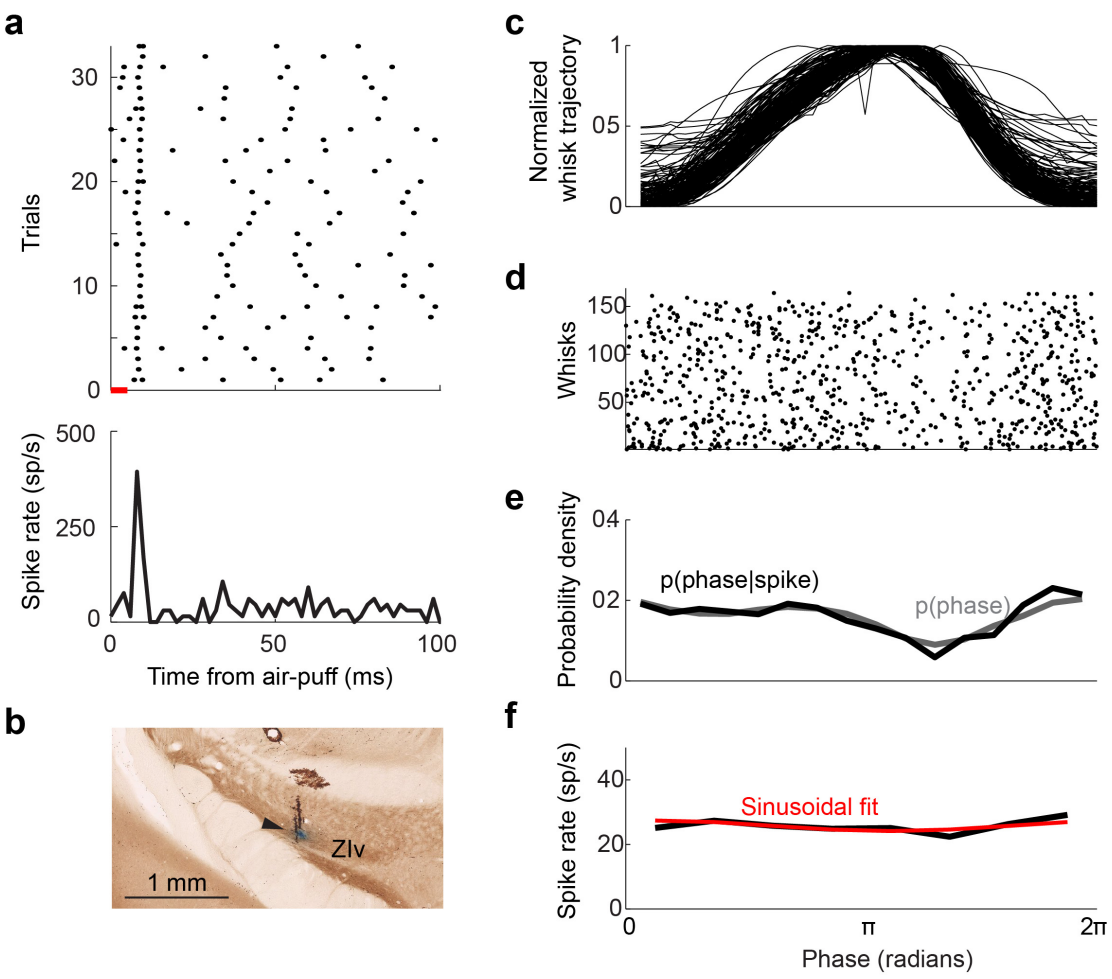


**Figure 4.12 Spiking activity of a histologically identified ZIv unit in response to free-air whisking and air-puffs**

**(a)** Raster of spike times relative to air-puff onset (black ticks) and the duration of the airpuff (red bar). A corresponding peristimulus time histogram is shown below. **(b)** Location of the recorded unit in a coronal section. **(c)** Normalized vibrissa position as a function of phase in the whisk cycle. All whisks during the record are superimposed. **(d)** Raster of phases in the whisk cycle at which spikes occurred. Each line on the y-axis represents on whisk. **(e)** Probability density function of all observed instantaneous phases (gray) and phases conditioned on a spike (black). **(f)** Spike rate as a function of phase in the whisk cycle (black) and a sinusoidal fit of this function (red).

## *4.4 Discussion*

### Summary

We find a mixed representation of re-afferent and ex-afferent signals in the vibrissa system of alert, whisking rats. Specifically, substantial re-afferent signals of whisking phase are represented throughout the lemniscal pathway, in PrV (**Figs 4.3-4.6**) and VPM (**Figs 4.7-4.9**) thalamus, the same sensory regions that have the highest acuity for vibrissal ex-afferent touch. The whisking responses in VPM are consistent with, and extend the results of past studies in done in alert and anesthetized rats (Brown and Waite, 1974; Khatri et al., 2010; Yu et al., 2006). Within VPM, we observe substantial re-afferent signals in both the multi-vibrissa "head" region and the single vibrissa "core" region (**Fig 4.10**), contrary to recent hypotheses (Urbain and Deschênes, 2007b); however we are unable to assess whether there is structure on a finer scale at the level of individual barreloids (Timofeeva et al., 2003). We also observe modulation in some units corresponding to the trigeminal skin or fur (**Figs 4.4b, 4.5**); their location within PrV is dorsal to the barrelletes (Jacquin et al., 1983), and more medial to the VPM barreloids (Haidarliu et al., 2008) (**Fig 4.8b**). Most VPM barreloid neurons, regardless of location, were responsive to both internally generated whisking (re-afference) and externally generated vibrissa deflections (ex-afference). However, there was an approximately 10-fold range in the sensitivity to the ex-afferent and

re-afferent stimuli, and sensitivity to one did not predict sensitivity to the other (**Fig 4.11**). There is some modulation with whisking in SpVIr, but much of this modulation is lost in PO. Spike rates are comparatively low in PO, possibly due to feedforward inhibition from zona incerta (Urbain and Deschênes, 2007a) which appears to exert its influence regardless of whether the animal is whisking (**Fig 4.9, 4.12**).

## How are whisking and touch differentiated?

The observation that re-afferent and ex-afferent signals are conveyed through the same thalamocortical pathway raises several questions as to how animals are able to determine the position of objects that they contact with their vibrissae (Mehta et al., 2007; O'Connor et al., 2010a). First, there are several alternative proposals that do not require the use of a re-afferent signal: (1) that the physical forces impinging the follicle are different at different object locations, or (2) that rodents use an adaptive motor strategy to whisk in a region that maximizes the number of contacts, while keeping track of an efference copy of the motor commands to set the whisking range (O'Connor et al., 2010a; O'Connor et al., 2013). This could be done through primary motor cortex, which contains information about the whisking range (Hill et al., 2011a), and sends task specific signals to S1 cortex (Petreanu et al., 2012). Nonetheless, the existence of re-afferent phase-dependent contact

neurons already in layer 4 of S1, and the fact the weak phase preference during whisking in air matches the strong phase preference during touch (Curtis and Kleinfeld, 2009), suggests that object position could be read out by comparing the relative spike counts in neurons with different preferred phases.

The present observations on the subcortical origin of the re-afferent whisking signal constrain the possible mechanisms for the combination of re-afferent and ex-afferent signals. Several potential mechanisms are discussed in light of these constraints:

(1) The lemniscal pathway may represent functionally separate but intermingled whisking and touch channels. Units within the lemniscal pathway are heterogeneous in their sensitivity to whisking and external deflections, and these sensitivities seem to be independent. While air-puffs to the entire vibrissal field provide only a crude metric of sensitivity to external deflections, these data are consistent with previous reports of the diverse set of kinematic features that activate VPM neurons (Ito, 1988; Petersen et al., 2008; Waite, 1973). Thus, it is possible that units which are strongly activated by re-afference and weakly modulated by air-puffs have different anatomical and/or functional roles in the thalamocortical circuit, and thus act as a functionally separate channel of information.

Similarly,re-afferent signals from outside the follicle may represent a separate pathway of re-affererent information. Whisking responses in these units are unlikely to be affected by vibrissal contact, and thus could represent a separate “whisking only” channel of information.

(2) Re-afferent and ex-afferent signals may be multiplexed in a single channel. Whisking and object contact have different kinematic features and therefore elicit changes in spike rates at different temporal frequencies. These two stimuli also represent different spatial frequencies, as the whiskers tend to move in synchrony during whisking (Hill et al., 2011a), but contact occurs separately on each whisker (Grant et al., 2009). Temporal and spatial filters at the mechanoreceptors themselves or at early sensory processing stages may amplify these differences. For example, SpVIc receives the same primary sensory afferents as PrV and sends inhibitory projections back to PrV with at least a one synapse delay. This mechanism could implement a temporal derivative that amplifies particular frequencies already at the level of the first central synapse in PrV (Furuta et al., 2008). Furthermore, monovibrissa PrV cells are inhibited by stimulation of surround vibrissa, so this mechanism could also serve as a spatial derivative filter. Corticofugal feedback from S1 cortex to SpVIc (Furuta et al., 2010) could tune these filters to differentiate between whisking and touch signals in a context specific manner. Such a

mechanism has been proposed in the retina to differentially process self-motion versus object motion (Ölveczky et al., 2003). Future experiments comparing the re-afferent representation of whisking in PrV before and after inactivation of SpVIc could elucidate the function of this inhibition. Differential filtering of input types may also be achieved by convergence of units tuned to different preferred phases. The PrV to VPM synapse is one cell to one cell in adult animals (Arsenault and Zhang, 2006), and correspondingly there is a similar representation of whisking in both regions. However, in the absence of contact, the re-afferent whisking phase signal appears to be dampened in S1 cortex relative to VPM (Curtis and Kleinfeld, 2009; Hill, 2009). There is substantial convergence at the VPM to S1 projection (Bruno and Sakmann, 2006), and convergence of VPM units tuned to different phases could explain such dampening. When contact occurs during active touch, though, the relatively strong response observed in S1 (Curtis and Kleinfeld, 2009) could result from synchrony of VPM afferents (Bruno and Sakmann, 2006).

Still, the mechanisms by which re-afferent position and ex-afferent touch signals are parsed within the lemniscal pathway remains to be tested explicitly.

## What is the role of the paralemniscal pathway in active touch?

The potential role of the paralemniscal pathway in sensing active touch has been a mystery since its discovery (Ahissar et al., 2000; Deschenes and Urbain, 2009; Diamond et al., 1992a; Diamond et al., 1992b; Masri et al., 2008b; Urbain and Deschênes, 2007a). The majority of SpVIr neurons are similarly tuned to upward vibrissa deflections of many vibrissae in anesthetized rats (Furuta et al., 2006), but are only weakly tuned to phase during whisking (**Fig 4.5-4.6**). Their recipient neurons in PO respond only weakly to external deflections due to feedforward inhibition from ZIv. Disinhibition of PO is under the control of motor cortex (Lavallee et al., 2005), but only when the proper precise temporal relationship exists between the two areas. The fact that whisking signals in motor cortex primarily reflect whisking parameters that vary over slow time scales during exploratory whisking (Friedman et al., 2012; Gerdjikov T.V. et al., 2013; Hill et al., 2011a) is consistent with previous predictions that ZIv and PO should remain gated off during this mode of whisking (Urbain and Deschênes, 2007a). Indeed, the present observation that ZIv and PO have similar sustained firing rates whether or not the animal is generating exploratory whisks (**Fig 4.9d**) supports this prediction, and demonstrates that exploratory whisking alone is insufficient to engage the paralemniscal pathway. If PO is in fact disinhibited during some behavioral context, such a context remains to be elucidated. The numerous projection targets of SPVIr cells (Deschenes and Urbain, 2009)

could suggest many possibilities, and thus the discovery of a behavioral context which disinhibits PO will likely require exploratory experiments in freely moving animals.

## *4.5 Acknowledgements*

We thank H. J. Karten for discussions, and K. Yang for assistance with behavioral training. We are grateful to the Canadian Institutes of Health Research (grant MT-5877), the National Institutes of Health (grants NS058668, NS066664 and NS047101), and the US-Israeli Binational Science Foundation (grant 2003222).

The content of this chapter is a manuscript that is currently in preparation for submission and will include Profs. Martin Deschênes and David Kleinfeld as authors. This material is included with the generous consent of all authors. The dissertation author is a primary researcher on this work.

# Chapter 5 - Conclusion

We have examined the generation, coordination, and re-afferent signaling of rhythmic exploratory whisking at the level of the brainstem and its outputs. We have identified the premotor circuitry that is likely responsible for generation of this rapid oscillatory behavior, and we show that the coordination of the different muscle groups involved relies on intimate interactions between the breathing and whisking patterning circuitry. We further demonstrate that the lemniscal trigeminal sensory pathway contains re-afferent signals of whisk-cycle phase that are the most likely source of re-afferent signals observed in S1 cortex. These findings raise several interesting issues which we discuss below:

First, the nature of the synaptic interactions among different excitatory and inhibitory cell types both the vIRt, as well as between the various breathing centers and the vIRt, remains uncharacterized. Remarkably, the vIRt, preBotzinger complex, and the hypoglossal nucleus are, as best we can tell, largely coplanar and thus likely amenable to further study in brain slice preparations (Maler, 2013).

A second issue relates to various time scales upon which rodents can control and sense the movement of their vibrissae. Behavioral evidence suggests that rats modulate the range of whisking on much slower time scales than the oscillatory rhythm, analogous to AM radio (Hill et al., 2011a). Certain neuropharmacological agents affect the range of whisking without affecting the frequency (Pietr et al., 2010), and spiking activity primary motor cortex preferentially reports this slowly varying component (Friedman et al., 2012; Gerdjikov T.V. et al., 2013; Hill et al., 2011a), as noted in Chapter 4. Together the results suggest that control of the vibrissae may involve the combination of a fast rhythmic drive signal controlled by the vIRt, and slower amplitude and set-point modulation controlled by one or more independent mechanisms. Likewise on the sensory end, while the phase of vibrissa motion during whisking seems to be conveyed to S1 cortex via peripheral re-afference through the lemniscal pathway, the whisking range signals remain even after inactivating peripheral mechanisms (Fee et al., 1997). This result suggests the presence of an efference copy of this slowly varying signal in S1 cortex, likely arising from motor cortex (Petreanu et al., 2012). Thus, just like the generation of whisking, its sensory representation seems to be similarly split among independent signals for the fast versus slow timescales. The studies in Chapters 3 and 4 clarify the nature of the motor and sensory signals specifically related to the rapidly varying component of whisking; however, nature of the slowly varying whisking components, how they interact

with the vIRt and/or facial motoneurons, as well as the role of motor cortex, remain to be determined.

As a final point of speculation, we can return to our review of the phase encoding of olfactory stimuli in Chapter 2 in light of our subsequent experimental findings on whisking in Chapter 3. As with the phase-dependent object contact signals observed in S1 cortex (Curtis and Kleinfeld, 2009), mitral cell responses to odors occur at precise and diverse phases of the sniff cycle (Shusterman et al., 2011). When rodents are actively exploring, the precise one-to-one phase locking between whisking and sniffing ensures that spikes induced by ex-afferent tactile and olfactory stimuli occur with a fixed temporal relationship to one another. In given pairs of olfactory and somatosensory neurons, then, the delay between these ex-afferent spikes should correspond to both a particular location and a particular smell. Such a representation could in principle enable the assignment of smells to specific object locations via computations in downstream neurons.

# References


Ahissar, E., Golomb, D., Haidarliu, S., Sosnik, R., and Yu, C. (2008). Latency coding in POm: Importance of parametric regimes. Journal of neurophysiology *100*, 1152-1154.

Ahissar, E., Sosnik, R., and Haidarliu, S. (2000). Transformation from temporal to rate coding in a somatosensory thalamocortical pathway. Nature *406*, 302-306.

Alheid, G.F., and McCrimmon, D.R. (2008). The chemical neuroanatomy of breathing. Respiratory Physiology & Neurobiology *164*, 3-11.

Arsenault, D., and Zhang, Z.w. (2006). Developmental remodelling of the lemniscal synapse in the ventral basal thalamus of the mouse. The Journal of physiology *573*, 121-132.

Bagdasarian, K., Szwed, M., Knutsen, P.M., Deutsch, D., Derdikman, D., Pietr, M., Simony, E., and Ahissar, E. (2013). Pre-neuronal morphological processing of object location by individual whiskers. Nature neuroscience.

Baker, S.N., Olivier, E., and Lemon, R.N. (1997). Coherent oscillations in monkey motor cortex and hand muscle EMG show task-dependent modulation. Journal of Physiology *501*, 225-241.

Batschelet, E., Batschelet, E., Batschelet, E., and Batschelet, E. (1981). Circular statistics in biology, Vol 371 (Academic Press London).

Bell, C.C. (1981). An efference copy which is modified by reafferent input. Science *214*, 450-453.

Bellavance, M.A., Demers, M., and Deschênes, M. (2010). Feedforward inhibition determines the angular tuning of vibrissal responses in the principal trigeminal nucleus. Journal of Neuroscience *30*, 1057-1063.

Benjamini, Y., Fonio, E., Galili, T., Havkin, G.Z., and Golani, I. (2011). Quantifying the buildup in extent and complexity of free exploration in mice. Proceedings of the National Academy of Sciences *108*, 15580-15587.

Berg, R.W., and Kleinfeld, D. (2003). Rhythmic whisking by rat: Retraction as well as protraction of the vibrissae is under active muscular control. Journal of Neurophysiology *89*, 104-117.

Bieger, D., and Hopkins, D.A. (1987). Viscerotopic representation of the upper alimentary tract in the medulla oblongata in the rat: the nucleus ambiguus. Journal of Comparative Neurology *262*, 546-562.

Bindra, D., and Campbell, J. (1967). Motivational effects of rewarding intracranial stimulation. Nature *215*, 375-376.

Boashash, B. (1992). Estimating and interpreting the instantaneous frequency of a signal. I. Fundamentals. Proceedings of the IEEE *80*, 520-538.

Bosman, L.W.J., Houweling, A.R., Owens, C.B., Tanke, N., Shevchouk, O.T., Rahmati, N., Teunissen, W.H.T., Ju, C., Gong, W., Koekkoek, S.K.E.*, et al.* (2011). Anatomical pathways involved in generating and sensing rhythmic whisker movements. Frontiers in Integrative Neuroscience *5*, 1.

Bouvier, J., Thoby-Brisson, M., N., R., Dubreuil, V., Ericson, J., Champagnat, J., Pierani, A., A., C., and Fortin, G. (2010). Hindbrain interneurons and axon guidance signaling critical for breathing. Nature Neuroscience *13*, 1066-1074.

Bowden, R.E.M., and Mahran, Z.Y. (1956). The functional significance of the pattern of innervation of the muscle quadratus labii superioris of the rabbit, cat, and rat. Journal of Anatomy *90*, 221-227.

Brecht, M., and Freiwald, W.A. (2012). The many facets of facial interactions in mammals. Current opinion in neurobiology *22*, 259-266.

Brecht, M., Preilowski, B., and Merzenich, M.M. (1997). Functional architecture of the mystacial vibrissae. Behavioral Brain Research *84*, 81-97.

Brown, A.W.S., and Waite, P.M.E. (1974). Responses in the rat thalamus to whisker movements produced by motor nerve stimulation. Journal of Physiology *238*, 387-401.

Bruno, R.M., and Sakmann, B. (2006). Cortex is driven by weak but synchronously active thalamocortical synapses. Science *312*, 622-1627.

Cao, Y., Roy, S., Sachdev, R.N., and Heck, D.H. (2012). Dynamic correlation between whisking and breathing rhythms in mice. Journal of Neuroscience *32*, 1653-1659.

Carvell, G.E., and Simons, D.J. (1990). Biometric analyses of vibrissal tactile discrimination in the rat. Journal of Neuroscience *10*, 2638-2648.

Chatterton, J.E., Awobuluyi, M., S., P.L., Takahashi, H., Talantova, M., Shin, Y., Cui, J., Tu, S., Sevarinok, K.A., Nakanishi, N.*, et al.* (2002). Excitatory

glycine receptors containing the NR3 family of NMDA receptor subunits. Nature *415*, 793-798.

Chen, Z., Travers, S.P., and Travers, J.B. (2001). Muscimol infusions in the brain stem reticular formation reversibly block ingestion in the awake rat. American Journal of Physiology: Regulatory, Intergrative, and Comparative Physiology *280*, R1085-1094.

Clarke, S., and Trowill, J.A. (1971). Sniffing and motivated behavior in the rat. Physiology & Behavior *6*, 49-52.

Crochet, S., and Petersen, C.C.H. (2006). Correlating membrane potential with behaviour using whole-cell recordings from barrel cortex of awake mice. Nature Neuroscience *9*, 608-609.

Cullen, K.E. (2004). Sensory signals during active versus passive movement. Current opinion in neurobiology *14*, 698-706.

Curtis, J.C., and Kleinfeld, D. (2009). Phase-to-rate transformations encode touch in cortical neurons of a scanning sensorimotor system. Nature Neuroscience *12*, 492-501.

Cury, K.M., and Uchida, N. (2010). Robust odor coding via inhalation-coupled transient activity in the mammalian olfactory bulb. Neuron *68*, 570-585.

de Kock, C.P., and Sakmann, B. (2009). Spiking in primary somatosensory cortex during natural whisking in awake head-restrained rats is cell-type specific. Proceedings of the National Academy of Sciences USA *106*, 16446-16450.

Depuy, S.D., Kanbar, R., Coates, M.B., Stornetta, R.L., and Guyenet, P.G. (2011). Control of breathing by raphe obscurus serotonergic neurons in mice. Journal of Neuroscience *31*, 1981-1990.

Descartes, R. (1637). Discourse on Methods, Optics, Geometry, and Meteorology (translated by P. J. Olscamp) (Indianapolis: Hackett Publsihing Compant).

Deschênes, M., Moore, J.D., and Kleinfeld, D. (2012). Sniffing and whisking in rodents. Current opinion in neurobiology *22*, 243-250.

Deschênes, M., Timofeeva, E., and Lavallee, P. (2003). The relay of high frequency sensory signals in the whisker-to-barreloid pathway. Journal of Neuroscience *23*, 6778-6787.

Deschenes, M., and Urbain, N. (2009). Vibrissal afferents from trigeminus to cortices. Scholarpedia *4*, 7454.

Deschênes, M., Veinante, P., and Zhang, Z.-W. (1998). The organization of cortico-thalamic pathways: Reciprocity versus parity. Brain Research Review *28*, 286-308.

Diamond, M.E., Armstrong-James, M., Budway, M.J., and Ebner, F.F. (1992a). Somatic sensory responses in the rostral sector of the posterior group (POm) and in the ventral posterior medial nucleus (VPM) of the rat thalamus: Dependence on the barrel field cortex. Journal of Comparative Neurology *319*, 66-84.

Diamond, M.E., Armstrong-James, M., and Ebner, F.F. (1992b). Somatic sensory responses in the rostral sector of the posterior group (POm) and in the ventral posterior medial nucleus (VPM) of the rat thalamus. Journal of Comparative Neurology *318*, 462-476.

Dobbins, E.G., and Feldman, J.L. (1994). Brainstem network controlling descending drive to phrenic motoneurons in rat. Journal of Comparative Neurology *347*, 64-86.

Doi, A., and Ramirez, J.M. (2008). Neuromodulation and the orchestration of the respiratory rhythm. Respiratory Physiology & Neurobiology *164*, 96-104.

Dorfl, J. (1982). The musculature of the mystacial vibrissae of the white mouse. Journal of Anatomy *135*, 147-154.

Ermentrout, G.B., and Kleinfeld, D. (2001). Traveling electrical waves in cortex: Insights from phase dynamics and speculation on a computational role. Neuron *29*, 1-12.

Fanselow, E.E., and Nicolelis, M.A.L. (1999). Behavioral modulation of tactile responses in the rat somatosensory system. Journal of Neuroscience *19*, 7603-7616.

Fee, M.S., Mitra, P.P., and Kleinfeld, D. (1996). Automatic sorting of multiple unit neuronal signals in the presence of anisotropic and non-Gaussian variability. Journal of Neuroscience Methods *69*, 175-188.

Fee, M.S., Mitra, P.P., and Kleinfeld, D. (1997). Central versus peripheral determinates of patterned spike activity in rat vibrissa cortex during whisking. Journal of Neurophysiology *78*, 1144-1149.

Feldman, J.L., and Del Negro, C.A. (2006). Looking for inspiration: new perspectives on respiratory rhythm. Nature Reviews Neuroscience *7*, 232-241.

Feldman, J.L., Del Negro, C.A., and Gray, P.A. (2013). Understanding the rhythm of breathing: So near, yet so far. Annual Review of Physiology *75*, 423-452.

Ferezou, I., Bolea, S., and Petersen, C.C.H. (2006). Visualizing the cortical representation of whisker touch: Voltage-sensitive dye imaging in freely moving mice. Neuron *50*, 617-629.

Fox, C.W., Mitchinson, B., Pearson, M.J., Pipe, A.G., and Prescott, T.J. (2009). Contact type dependency of texture classification in a whiskered mobile robot. Autonomous Robots *26*, 223-239.

Francis, J.T., Xu, S., and Chapin, J.K. (2008). Proprioceptive and cutaneous representations in the rat ventral posterolateral thalamus. Journal of Neurophysiology *99*, 2291-2304.

Friedman, D., and Jones, E. (1981). Thalamic input to areas 3a and 2 in monkeys. Journal of neurophysiology *45*, 59-85.

Friedman, W.A., Zeigler, H.P., and Keller, A. (2012). Vibrissae motor cortex unit activity during whisking. Journal of Neurophysiology *107*, 551-563.

Fukuda, Y., and Honda, Y. (1982). Differences in respiratory neural activities between vagal (superior laryngeal), hypoglossal, and phrenic nerves in the anesthetized rat. Japanese Journal of Physiology, *32*, 387-398.

Fundin, B.T., Arvidsson, J., Aldskogius, H., Johansson, O., Rice, S.N., and Rice, F.L. (1997). Comprehensive immunofluorescence and lectin binding analysis of intervibrissal fur innervation in the mystacial pad of the rat. Journal of Comparative Neurology *385*, 185-206.

Furuta, T., Kaneko, T., and Deschênes, M. (2009). Septal neurons in barrel cortex derive their receptive field input from the lemniscal pathway. The Journal of Neuroscience *29*, 4089-4095.

Furuta, T., Nakamura, K., and Deschenes, M. (2006). Angular tuning bias of vibrissa-responsive cells in the paralemniscal pathway. The Journal of neuroscience *26*, 10548-10557.

Furuta, T., Timofeeva, E., Nakamura, K., Okamoto-Furuta, K., Togo, M., Kaneko, T., and Deschênes, M. (2008). Inhibitory gating of vibrissal inputs in the brainstem. Journal of Neuroscience *28*, 1789-1797.

Furuta, T., Urbain, N., Kaneko, T., and Deschênes, M. (2010). Corticofugal control of vibrissa-sensitive neurons in the interpolaris nucleus of the trigeminal complex. Journal of Neuroscience *30*, 1832-1838.

Ganguly, K., and Kleinfeld, D. (2004). Goal-directed whisking behavior increases phase-locking between vibrissa movement and electrical activity in primary sensory cortex in rat. Proceedings of the National Academy of Sciences USA *101*, 12348-12353.

Gao, P., Bermejo, R., and Zeigler, H.P. (2001). Vibrissa deaffentation and rodent whisking patterns: Behavioral evidence for a central pattern generator. Journal of Neuroscience *21*, 5374-5380.

Garcia, A.J., Zanella, S., Koch, H., Doi, A., and Ramirez, J.M. (2011). Networks within networks: The neuronal control of breathing. Progress in Brain Research *188*, 31-50.

Gerdjikov T.V., Haiss F., Rodriguez-Sierra O.E., and Schwarz, C. (2013). Rhythmic Whisking Area (RW) in Rat Primary Motor Cortex: An Internal Monitor of Movement-Related Signals? Journal of Neuroscience *33*, 14193-14204.

Ghosh, S., Larson, S.D., Hefzi, H., Marnoy, Z., Cutforth, T., Dokka, K., and Baldwin, K.K. (2011). Sensory maps in the olfactory cortex defined by long-range viral tracing of single neurons. Nature *472*, 217-220.

Grannan, E.R., Kleinfeld, D., and Sompolinsky, H. (1993). Stimulus dependent synchronization of neuronal assemblies. Neural Computation *5*, 550-569.

Grant, R.A., Mitchinson, B., Fox, C.W., and Prescott, T.J. (2009). Active touch sensing in the rat: anticipatory and regulatory control of whisker movements during surface exploration. Journal of neurophysiology *101*, 862-874.

Gray, P.A., ., Hayes, J.A., Ling, G.Y., Llona, I., Tupal, S., Picardo, M.C., Ross, S.E., Hirata, T., Corbin, J.G., Eugenín, J.*, et al.* (2010). Developmental origin of preBötzinger complex respiratory neurons. Journal of Neuroscience *30*, 14883-148895.

Haidarliu, S., Golomb, D., Kleinfeld, D., and Ahissar, E. (2012). Dorsorostral snout muscles in the rat subserve coordinated movement for whisking and sniffing. Anatomical record *295*, 1181-1191.

Haidarliu, S., Simony, E., Golomb, D., and Ahissar, E. (2010). Muscle architecture in the mystacial pad of the rat. The Anatomical Record *293*, 1192–1206.

Haidarliu, S., Yu, C., Rubin, N., and hissar, E. (2008). Lemniscal and extralemniscal compartments in the VPM of the rat. Frontiers of Neuroanatomy *2*, 4.

Harish, O., and Golomb, D. (2010). Control of the firing patterns of vibrissa motoneurons by modulatory and phasic synaptic inputs: A modeling study. Journal of Neurophysiology *103*, 2684-2699.

Hattox, A.M., Li, Y., and Keller, A. (2003). Serotonin regulates rhythmic whisking. Neuron *39*, 343-352.

Henderson, T.A., and Jacquin, M.F. (1995). What makes subcortical barrels? Requisite trigeminal circuitry and developmental mechanisms. In Cerebral Cortex: The Barrel Cortex of Rodents, E.G. Jones, and I.T. Diamond, eds. (Berlin: Springer Press), pp. 123-188.

Hentschke, H., Haiss, F., and Schwarz, C. (2006). Central signals rapidly switch tactile processing in rat barrel cortex during whisker movements. Cerebral Cortex *16*, 1142-1156.

Hill, D.N. (2009). Biomechanics and Cortical Representation of Whisking in the Rat Vibrissa System (University of California, San Diego).

Hill, D.N., Bermejo, R., Zeigler, H.P., and Kleinfeld, D. (2008). Biomechanics of the vibrissa motor plant in rat: Rhythmic whisking consists of triphasic neuromuscular activity. Journal of Neuroscience *28*, 3438-3455.

Hill, D.N., Curtis, J.C., Moore, J.D., and Kleinfeld, D. (2011a). Primary motor cortex reports efferent control of vibrissa position on multiple time scales. Neuron *72*, 344–356.

Hill, D.N., Mehta, S.B., and Kleinfeld, D. (2011b). Quality metrics to accompany spike sorting of extracellular signals. Journal of Neuroscience *31*, 8699–8705.

Hines, M. (1927). Nerve and muscle. The Quarterly Review of Biology *2*, 149-180.

Hjelmstad, G., Parks, G., and Bodznick, D. (1996). Motor corollary discharge activity and sensory responses related to ventilation in the skate vestibulolateral cerebellum: implications for electrosensory processing. Journal of experimental biology *199*, 673-681.

Huangfu, D., Koshiya, N., and Guyenet, P.G. (1993). Central respiratory modulation of facial motoneurons in rats. Neuroscience Letters *151*, 224-228.

Hutson, K.A., and Masterton, R.B. (1986). The sensory contribution of a single vibrissa's cortical barrel. Journal of Neurophysiology *56*, 1196-1223.

Hwang, J.C., and St John, W.M. (1988). Respiratory-modulated activities of motor units of the facial nerve. Respiratory Physiology *73*, 189-200.

Ikemoto, S., and Panksepp, J. (1994). The relationship between self-stimulation and sniffing in rats: does a common brain system mediate these behaviors? Behavioural brain research *61*, 143-162.

Isokawa-Akesson, M., and Komisaruk, B.R. (1987). Difference in projections to the lateral and medial facial nucleus: Anatomically separate pathways for rhythmical vibrissa movement in rats. Experimental Brain Research *65*, 385-398.

Ito, M. (1988). Response properties and topography of vibrissa-sensitive VPM neurons in the rat. Journal of neurophysiology *60*, 1181-1197.

Ito, T., and Oliver, D.L. (2010). Origins of glutamatergic terminals in the inferior colliculus identified by retrograde transport and expression of VGLUT1 and VGLUT2 genes. Frontiers of Neuroanatomy *4*, 135.

Jacquin, M.F., Semba, K., Egger, M.D., and Rhoades, R.W. (1983). Organization of HRP-labeled trigeminal mandibular, primary afferent neurons in the rat. Journal of Comparative Neurology *215*, 397-420.

Jin, T.E., Witzemann, V., and Brecht, M. (2004). Fiber types of the intrinsic whisker muscle and whisking behavior. Journal of Neuroscience *24*, 3386-3393.

Kepecs, A., Uchida, N., and Mainen, Z.F. (2005). The sniff as a unit of olfactory processing. Chemical Senses *31*, 167-179.

Kepecs, A., Uchida, N., and Mainen, Z.F. (2007). Rapid and precise control of sniffing during olfactory discrimination in rats. Journal of neurophysiology *98*, 205-213.

Khatri, V., Bermejo, R., Brumberg, J.C., Keller, A., and Zeigler, H.P. (2009). Whisking in air: Encoding of kinetmatics by trigeminal ganglion neurons in awake rats. Journal of Neurophysiology *101*, 836-886.

Khatri, V., Bermejo, R., Brumberg, J.C., and Zeigler, H.P. (2010). Whisking in air: Encoding of kinematics by VPM neurons in awake rats. Somatosensory and Motor Research *27*, 11-20.

Klein, B., and Rhoades, R. (1985). The representation of whisker follicle intrinsic musculature in the facial motor nucleus of the rat. Journal of Comparative Neurology *232*, 55-69.

Kleinfeld, D., and Deschênes, M. (2011). Neuronal basis for object location in the vibrissa scanning sensorimotor system. Neuron *72*, 455-468.

Kleinfeld, D., Sachdev, R.N.S., Merchant, L.M., Jarvis, M.R., and Ebner, F.F. (2002). Adaptive filtering of vibrissa input in motor cortex of rat. Neuron *34*, 1021-1034.

Knutsen, P.M., Derdikman, D., and Ahissar, E. (2005). Tracking whisker and head movements in unrestrained behaving rodents. Journal of Neurophysiology *93*, 2294-2301.

Koizumi, H., Wilson, C.G., Wong, S., Yamanishi, T., Koshiya, N., and Smith, J.C. (2008). Functional imaging, spatial reconstruction, and biophysical analysis of a respiratory motor circuit isolated *in vitro*. Journal of Neuroscience *28*, :2353–2365.

Krupa, D.J., Matell, M.S., Brisben, A.J., Oliveira, L.M., and Nicolelis, M.A.L. (2001). Behavioral properties of the trigeminal somatosensory system in rats performing whisker-dependent tactile discriminations. Journal of Neuroscience *21*, 5752-5763.

Land, P.W., and Simons, D.J. (1985). Metabolic and structural correlates of the vibrissae representation in the thalamus of the adult rat. Neuroscience letters *60*, 319-324.

Lavallee, P., Urbain, N., Dufresne, C., Bokor, H., Acsady, L., and Deschênes, M. (2005). Feedforward inhibitory control of sensory information in higher-order thalamic nuclei. Journal of Neuroscience *25*, 7489-7498.

Lawson, E.E., Richter, D.W., Czyzyk-Krzeska, M.F., Bischoff, A., and Rudesill, R.C. (1991). Respiratory neuronal activity during apnea and other breathing patterns induced by laryngeal stimulation. Journal of Applied Ohysiology *70*, 2742-2749.

Lee, S., Carvell, G.E., and Simons, D.J. (2008). Motor modulation of afferent somatosensory circuits. Nature neuroscience *11*, 1430-1438.

Lefort, S., Tomm, C., Sarria, J.-C.F., and Petersen, C.C.H. (2009). The excitatory neuronal network of the C2 barrel column in mouse primary somatosensory cortex. Neuron *61*, 301-316.

Leiser, S.C., and Moxon, K.A. (2007). Responses of trigeminal ganglion neurons during natural whisking behaviors in the awake rat. Neuron *53*, 117-133.

Lewis Jr., T.L., Mao, T., and Svoboda, K. (2009). Myosin-dependent targeting of transmembrane proteins to neuronal dendrites. Nature Neuroscience *12*, 568–576.

Lu, L., Cao, Y., Tokita, K., Heck, D.H., and Boughter Jr, J.D. (2013). Medial cerebellar nuclear projections and activity patterns link cerebellar output to orofacial and respiratory behavior. Frontiers in neural circuits *7*.

Ma, P.M., and Woolsey, R.A. (1984). Cytoarchitectural correlates of vibrissae in the medullary trigeminal complex of the mouse. Brain Research *306*, 374-379.

Maler, L. (2013). F1000Prime Recommendation of [Moore JD et al., Nature 2013, 497(7448):205-10]. In F1000Prime.

Mameli, O., Stanzani, S., Mulliri, G., Pellitteri, R., Caria, M., Russo, A., and De Riu, P. (2010). Role of the trigeminal mesencephalic nucleus in rat whisker pad proprioception. Behavioral and Brain Functions *6*, 69.

Mameli, O., Stanzani, S., Russo, A., Romeo, R., Pellitteri, R., Spatuzza, M., Caria, M.A., and De Riu, P.L. (2008). Hypoglossal nuclei participation in rat mystacial pad control. Pflügers Archiv-European Journal of Physiology *456*, 1189-1198.

Masri, R., Bezdudnaya, T., Trageser, J., and Keller, A. (2008a). Reply to Ahissar et al. Journal of Neurophysiology *100*, 1155-1157.

Masri, R., Bezdudnaya, T., Trageser, J.C., and Keller, A. (2008b). Encoding of stimulus frequency and sensor motion in the posterior medial thalamic nucleus. Journal of Neurophysiology *100*, 681–689.

Matthews, D.W. (2012). The Architecture of the Mouse Trigeminal-facial Brainstem: Disynaptic Circuitry, Genomic Organization, and Follicle Mechanics (University of California, San Diego).

Mehta, S.B., Whitmer, D., Figueroa, R., Williams, B.A., and Kleinfeld, D. (2007). Active spatial perception in the vibrissa scanning sensorimotor system. Public Library of Science Biology *5*, 309-322.

Mitchinson, B., Grant, R.A., Arkley, K., Rankov, V., Perkn, I., and Prescott, T.J. (2011). Active vibrissal sensing in rodents and marsupials. Philosophical

Transaction of the Royal Society of London B - Biological Science *366*, 3037-3048.

Moore, J.D., Deschênes, M., Furuta, T., Huber, D., Smear, M.C., Demers, M., and Kleinfeld, D. (2013). Hierarchy of orofacial rhythms revealed through whisking and breathing. Nature *497*, 205-210.

Nakamura, S., Narumi, T., Tsutsui, K.-I., and Iijima, T. (2009). Difference in the functional significance between the lemniscal and paralemniscal pathways in the perception of direction of single-whisker stimulation examined by muscimol microinjection. Neuroscience research *64*, 323-329.

Nakamura, Y., and Katakura, N. (1995). Generation of masticatory rhythm in the brainstem. Neuroscience Research *23*, 1-19.

O'Connor, D.H., Clack, N.G., Huber, D., Komiyama, T., Myers, E.W., and Svoboda, K. (2010a). Vibrissa-based object localization in head-fixed mice. Journal of Neuroscience *30*, 1947-1967.

O'Connor, D.H., Hires, S.A., Guo, Z.V., Li, N., Yu, J., Sun, Q.-Q., Huber, D., and Svoboda, K. (2013). Neural coding during active somatosensation revealed using illusory touch. Nature neuroscience.

O'Connor, D.H., Peron, S.P., Huber, D., and Svoboda, K. (2010b). Neural activity in barrel cortex underlying vibrissa-based object localization in mice. Neuron *67*, 10481061.

Olszewski, J. (1950). On the anatomical and functional organization of the spinal trigeminal nucleus. Journal of Comparative Neurology *92*, 401-413.

Ölveczky, B.P., Baccus, S.A., and Meister, M. (2003). Segregation of object and background motion in the retina. Nature *423*, 401-408.

Onimaru, H., Kumagawa, Y., and Homma, I. (2006). Respiration-related rhythmic activity in the rostral medulla of newborn rats. Journal of Neurophysiology *96*, 55-61.

Ono, T., Ishiwata, Y., Inaba, N., Kuroda, T., and Nakamura, Y. (1998). Modulation of the inspiratory-related activity of hypoglossal premotor neurons during ingestion and rejection in the decerebrate cat. Journal of Neurophysiology *80*, 48-58.

Pagliardini, S., Janczewski, W.A., Tan, W., Dickson, C.T., Deisseroth, K., and Feldman, J.L. (2011). Active expiration induced by excitation of ventral medulla in adult anesthetized rats. Journal of Neuroscience *31*, 2895-2905.

Paxinos, G., and Watson, C. (1986). The Rat Brain in Stereotaxic Coordinates (San Diego: Academic Press).

Paxinos, G., Watson, C., Pennisi, M., and Topple, A. (1985). Bregma, lambda and the interaural midpoint in stereotaxic surgery with rats of different sex, strain and weight. Journal of Neuroscience Methods *13*, 139-143.

Petersen, R.S., Brambilla, M., Bale, M.R., Alenda, A., Panzeri, S., Montemurro, M.A., and Maravall, M. (2008). Diverse and temporally precise kinetic feature selectivity in the VPm thalamic nucleus. Neuron *60*, 890-903.

Petreanu, L., Gutnisky, D.A., Huber, D., Xu, N.-l., O'Connor, D.H., Tian, L., Looger, L., and Svoboda, K. (2012). Activity in motor-sensory projections reveals distributed coding in somatosensation. Nature *489*, 299-303.

Pierret, T., Lavallee, P., and Deschênes, M. (2000). Parallel streams for the relay of vibrissal information through thalamic barreloids. Journal of Neuroscience *20*, 7455-7462.

Pietr, M.D., Knutsen, P.M., Shore, D.I., Ahissar, E., and Vogel, Z. (2010). Cannabinoids reveal separate controls for whisking amplitude and timing in rats. Journal of Neurophysiology *104*, 2532-2542.

Poulet, J.F., Fernandez, L.M., Crochet, S., and Petersen, C.C. (2012). Thalamic control of cortical states. Nature neuroscience *15*, 370-372.

Poulet, J.F., and Petersen, C.C. (2008). Internal brain state regulates membrane potential synchrony in barrel cortex of behaving mice. Nature *454*, 881-885.

Ranade, S., Hangya, B., and Kepecs, A. (2013). Multiple Modes of Phase Locking between Sniffing and Whisking during Active Exploration. The Journal of Neuroscience *33*, 8250-8256.

Rice, F.L., Fundin, B.T., Arvidsson, J., Aldskogius, H., and Johansson, O. (1997). Comprehensive immunofluorescence and lectin binding analysis of vibrissal follicle sinus complex innervation in the mystacial pad of the rat. Journal of Comparative Neurology *385*, 149-184.

Rice, F.L., Kinnman, E., Aldskogius, H., Johansson, O., and Arvidsson, J. (1993). The innervation of the mystacial pad of the rat as revealed by PGP 9.5 immunofluorescence. Journal of Comparative Neurology *337*, 366-385.

Richard Waranch, H., and Terman, M. (1975). Control of the rat's sniffing behavior by response-independent and dependent schedules of reinforcing brain stimulation. Physiology & Behavior *15*, 365-372.

Roy, J.E., and Cullen, K.E. (2001). Selective processing of vestibular reafference during self-generated head motion. The Journal of Neuroscience *21*, 2131-2142.

Saito, Y., Ezure, K., Tanaka, I., and Osawa, M. (2003). Activity of neurons in ventrolateral respiratory groups during swallowing in decerebrate rats. Brain Development *25*, 338-345.

Semba, K., and Egger, M.D. (1986). The facial “motor” nerve of the rat: control of vibrissal movement and examination of motor and sensory components. Journal of Comparative Neurology *247*, 144-158.

Semba, K., and Komisaruk, B.R. (1984). Neural substrates of two different rhythmical vibrissal movements in the rat. Neuroscience *12*, 761-774.

Sherrey, J.H., and Megirian, D. (1977). State dependence of upper airway respiratory motoneurons: Functions of the cricothyroid and nasolabial muscles of the unanesthetized rat. Electroencephalography and Clinical Neurophysiology *43*, 218-228.

Shusterman, R., Smear, M.C., Koulakov, A.A., and Rinberg, D. (2011). Precise olfactory responses tile the sniff cycle. Nature Neuroscience *14*, 1039-1044.

Smear, M., Shusterman, R., O'Connor, R., Bozza, T., and Rinberg, D. (2011). Perception of sniff phase in mouse olfaction. Nature *479*, 397-400.

Smith, J.C., Abdala, A.P.L., Rybak, I.A., and Paton, J.F.R. (2009). Structural and functional architecture of respiratory networks in the mammalian brainstem. Philosophical Transactions of the Royal Society of London B *364*, 2577-2587.

Smith, J.C., Ellenberger, H.H., Ballanyi, K., Richter, D.W., and Feldman, J.L. (1991). Pre-Botzinger complex: A brainstem region that may generate respiratory rhythm in mammals. Science *254*, 726-729.

Stål, P., Eriksson, P.-O., Eriksson, A., and Thornell, L.-E. (1990). Enzyme-histochemical and morphological characteristics of muscle fibre types in the human buccinator and orbicularis oris. Archives of oral biology *35*, 449-458.

Sugitani, M., Yano, J., Sugai, T., and Ooyama, H. (1990). Somatopic organization and columnar structure of the vibrissae representation in the rat ventrobasal complex. Experimental Brain Research *81*, 346-351.

Szwed, M., Bagdasarian, K., and Ahissar, E. (2003). Coding of vibrissal active touch. Neuron *40*, 621-630.

Takatoh, J., Nelson, A., Zhou, X., Bolton, M.M., Ehlers, M.D., Arenkiel, B.R., Mooney, R., and Wang, F. (2013). New modules are added to vibrissal premotor circuitry with the emergence of exploratory whisking. Neuron *77*, 346-360.

Tan, W., Janczewski, W.A., Yang, P., Shao, X.M., Callaway, E.M., and Feldman, J.L. (2008). Silencing preBötzinger Complex somatostatin-expressing neurons induces persistent apnea in awake rat. Nature Neuroscience *11*, 538 - 540.

Timofeeva, E., Merette, C., Emond, C., Lavallee, P., and Deschênes, M. (2003). A map of angular tuning preference in thalamic barreloids. Journal of Neuroscience *23*, 10717-10723.

Travers, J.B., DiNardo, L.A., and H., K. (2000). Medullary reticular formation activity during ingestion and rejection in the awake rat. Experimental Brain Research *130*, 78-92.

Travers, J.B., Dinardo, L.A., and Karimnamazi, H. (1997). Motor and premotor mechanisms of licking. Neuroscience and Biobehavioral Reviews *21*, 631-647.

Uchida, N., and Mainen, Z.F. (2003). Speed and accuracy of olfactory discrimination in the rat. Nature Neuroscience *6*, 1224-1229.

Urbain, N., and Deschênes, M. (2007a). Motor cortex gates vibrissal responses in a thalamocortical projection pathway. Neuron *56*, 714-725.

Urbain, N., and Deschênes, M. (2007b). A new thalamic pathway of vibrissal information modulated by the motor cortex. Journal of Neuroscience *27*, 12407-12412.

Van der Maelen, C.P., and Aghajanian, G.K. (1980). Intracellular studies showing modulation of facial motoneurone excitability by serotonin. Nature *287*, 346-347.

Veinante, P., and Deschênes, M. (1999). Single- and multi-whisker channels in the ascending projections from the principal trigeminal nucleus in the rat. Journal of Neuroscience *19*, 5085-5095.

Veinante, P., Jacquin, M.F., and Deschênes, M. (2000). Thalamic projections from the whisker-sensitive regions of the spinal trigeminal complex in the rat. Journal of Comparative Neurology *420*, 233-243.

Vincent, S.B. (1912). The function of the vibrissae in the behavior of the white rat. Behavior Monographs *1*, 7-81.

Vincent, S.B. (1913). The tactile hair of the white rat. Journal of Comparative Neurology *23*, 1-23.

von Holst, E. (1954). Relations between the central nervous system and the peripheral organ. British Journal of Animal Behavior *2*, 89-94.

von Holst, E., and Mittelstaedt, H. (1950). Das reafferenzprinzip. Naturwissenschaften *37*, 464-476.

Wachowiak, M. (2011). All in a sniff: Olfaction as a model for active sensing. Neuron *71*, 962-973.

Waite, P.M.E. (1973). The responses of cells in the rat thalamus to mechanical movements of the whiskers. Journal of Physiology *228*, 541-561.

Welker, W.I. (1964). Analysis of sniffing of the albino rat. Behaviour *12*, 223-244.

Welt, C., and Abbs, J.H. (1990). Musculotopic organization of the facial motor nucleus in macaca fascicularis: A morphometric and retrograde tracing study with cholera toxin B-HRP. Journal of Comparative Neurology *291*, 621-636.

Welzl, H., and Bures, J. (1977). Lick-synchronized breathing in rats. Physiological Behavior *18*, 751-753.

Wesson, D.W., Verhagen, J.V., and Wachowiak, M. (2009). Why sniff fast? The relationship between sniff frequency, odor discrimination, and receptor neuron activation in the rat. Journal of neurophysiology *101*, 1089-1102.

Wolfe, J., Mende, C., and Brecht, M. (2011). Social facial touch in rats. Behavior Neuroscience, in press.

Woolsey, T.A., and Van Der Loos, H. (1970). The structural organization of layer IV in the somatosensory region (SI) of mouse cerebral cortex. Brain Research *17*, 205-242.

Youngentob, S.L., Mozell, M.M., Sheehe, P.R., and Hornung, D.E. (1987). A quantitative analysis of sniffing strategies in rats performing odor detection tasks. Physiology & Behavior *41*, 59-69.

Yu, C., Derdikman, D., Haidarliu, S., and Ahissar, E. (2006). Parallel thalamic pathways for whisking and touch signals in the rat. Public Library of Science Biology *4*, e124.

Zucker, E., and Welker, W.I. (1969). Coding of somatic sensory input by vibrissae neurons in the rat's trigeminal ganglion. Brain Research *12*, 134-156.